SAPIENZA
UNIVERSITÀ DI ROMA

Development of a steady state simulation code for klystrons

Sapienza Università di Roma
Facoltà di Ingegneria
Dottorato di Ricerca in Elettromagnetismo - XXIII ciclo

Chiara Marrelli

Coordinatore:
Prof. P. Lampariello

Docente guida:
Prof. L. Palumbo

Contents

Chapter 1

Introduction

The detection of elementary particles predicted by the theoretical models leads to the conception of always more powerful particles accelerators. The next generation of electron-positron colliders will allow to explore a new energy region in the multi TeV range beyond the capabilities of today's particle accelerators. It would provide significant fundamental physics information complementary to the LHC and to lower-energy linear e+/e- collider, as a result of its unique combination of high energy and experimental precision. These can be reached only with linear acceleration, since the high synchrotron radiation emission limits the maximum energy achievable for electron positron circular colliders. In order to reach this energies in a realistic and cost efficient scenario with linear acceleration (i.e. in a single beam passage), the accelerating gradient has to be very high and, by consequence, the RF power production for this high gradient has to be optimized.

In addition to colliders, next generation of linear particle accelerators based light sources, such as Free Electron Lasers, represents a key instrument to extend the limited range of conventional coherent light sources. Up to date FEL sources can cover a wide range of wavelenghts, with remarkable power and brightness. Such light sources would open new possibilities in pure research fields, and in technological applications. A FEL driven by a photoinjector is able to generate very short light pulses in the picosecond region at a repetition rate that normally extends up to tens of Hertz. The quality of

the light produced by these devices strictly depends on the parameters of the electron beam, in terms of emittance, brightness, energy and energy spread, produced by the linear accelerator and injected in the undulator.

Both the next generation of linear colliders and Free Electron Lasers need an accurate study and optimization of the high power, high efficiency, low cost RF power sources, and this means, at the required frequencies (UHF and above), basically klystrons.

The klystron fundamental working principles are well known since tens of years. Nevertheless, the design of a klystron, expecially at the level of power and efficiency required by accelerator physics, is still a very complicated and expensive process, and it is then privilege of a few laboratories and companies around the world. The high output powers require high beam currents, at the expense of efficiency and of a greater cathode complexity. The high frequency devices (such as X-Band devices) present further issues due to the small dimensions of the structures. In order to partially solve these problems, new typologies of klystrons, like the *sheet beam* or the *multibeam* klystron, have been proposed in the last years.

The design of always more elaborated klystrons lies on the intensive utilization of simulation codes in both the phases of design and analysis and optimization of the device. The main simulation codes can be basically divided in two main categories: the so called 1-D disk codes, that use a combination of analytical formulae and electron dynamics and are used for a quick assessment of the power and efficiency of the new klystron design in steady state. The electron beam is divided in charged disks which can move only in the longitudinal direction. They have the advantage of being extremely simple to use and very fast to run, and are then widely used in the first phase of the klystron "electronic design". At the same time, they represent the klystron cavities through their impedence, and so they don't give accurate electromagnetic information on the fields inside the structure, information that are very useful while simulating a complicated device such as a multibeam klystron.

The other category of klystron simulation codes includes Particle In Cell

2-D and 3-D codes, that simulate klystron performances using first principles (electron dynamics and Maxwell's equations). They give complete electromagnetic information both during the transient and after, and are increasingly more accurate as they proceed from 2-D to 3-D. In the process, they also become more time-consuming, and are then expecially used to simulate the already designed device and verify its behaviour.

In the present work, we will present the development of a new simulation code that is a compromise between the two typologies of codes. It is a 2-D code based on the search of a steady state solution for the interaction between the electron beam and the klystron cavities; the transient evolution is not considered, but information on the steady state cavity fields and on the beam focusing is given.

Chapter 2 is dedicated to a brief recall regarding the fundamental physics at the base of the klystron's operation. The first section is dedicated to the fundamental equations that describe the velocity modulation process in absence of space charge effects (the so called kinematic theory). These are considered in section 2.4. Finally, a short overview on the main klystron simulation code is presented.

In Chapter 3 the algorithm used to simulate the interaction between the beam and the klystron RF cavities is described. It is based on the iterative solution of the power balance equation in the structures and allows to determine the amplitude and phase of the electromagnetic field starting from the cavity mode field. This leads to a *steady state* 2-D code that can self-consistently simulate the contribution of the cavity electromagnetic field on the particles, and the action of the particles back to the field, giving electromagnetic information on the device without the complexity of a PIC code.

Chapter 4 is dedicated to the numerical methods to be used to integrate the particle equations of motion in the algorithm, and chapter 5 presents some results of the application of the method to simple cylindrical klystron cavities and to a two cavity klystron in absence of space charge effects. These are finally taken in account in chapter 6.

Chapter 2

The klystron amplifier

2.1 The klystron: general principles

The idea of using of an high fequency electric field parallel to the direction of an electron beam in order to group the particles in bunches can be dated around the middle of the 30's, when Mr. and Mrs. Heil were studying the effect of the electron transit in the spaces between the electrodes of high frequencies triods [1]. These devices had already some of the charateristics of many longitudinal interaction tubes, like the two cavity klystron.

The klystron amplifier was invented by Bill Hansen and the Varian brothers at Stanford in 1939 [2] [3]; it is a longitudinal interaction device composed by:

1. an electron gun that generates and accelerates a continuous electron beam;

2. a focusing system avoiding the beam spreading due to electron repulsion;

3. some RF cavities made to work on the TM_{010} resonant mode;

4. some drift tubes connecting the cavities and made in such a way that the cavities electric fields do not propagate inside them;

5. a collector where the electrons can dissipate their remaining energy after the interaction with the last cavity.

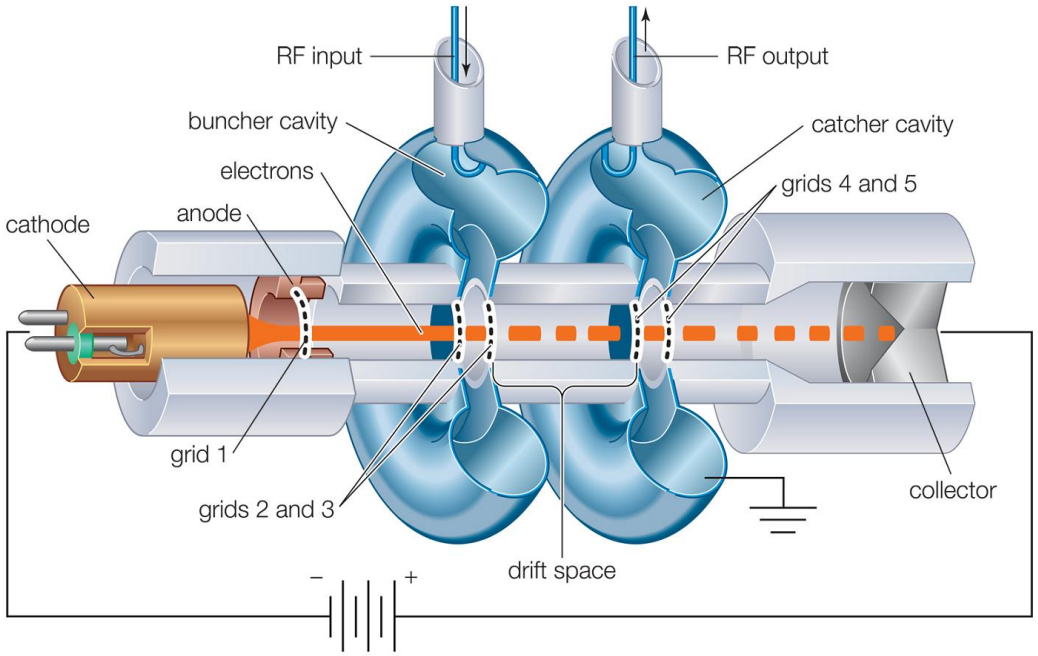

Figure 2.1: Two cavity klystron amplifier.

The radiofrequency signal to be amplified is injected in the first cavity, where it excites the TM_{010} mode and so it generates a longitudinal electric field on the tube axis. This field produces a velocity modulation in the electron beam: the electrons entering the cavity in different times leave the cavity with different velocities depending on the phase of the electric field. In the drift tube after the cavity this velocity modulation gives rise to a grouping opposed by the Coulombian repulsion forces. The intensity of these forces determines the speed by which the faster electrons reach the lowest ones of the same RF cycle or the previous one. The resulting density modulation is then a current modulation who can excite an electromagnetic field inside the second cavity. This field can modulate again the particles velocity and then the beam current. This modulation process repeats in each cavity. The

gain for each cavity and the bunching quality strongly depend on the cavity parameters, as the resonant frequency, the quality factor Q, the R/Q, etc. In a high power klystron the intermediate cavities can be two, three or four. In a klystron with three intermediate cavities, the two cavities immediately after the first one are commonly called *gain cavities* because they contribuite the most to the klystron total amplification. The penultimate cavities are usually named as the *bunching cavities*, because they can significantly enhance the electron grouping. The last cavity (*output cavity*) is designed in such a way that the voltage induced inside can demodulate the beam and extract the power that is then transferred to one or more waveguides.

The multicavity klystron usually has a gain of 10 or 15 dB for each cavity in the saturation mode, while the maximum efficiency rarely exceed the 65 dB.

2.2 Klystron main parameters[20]

The design of a klystron usually starts from the choice of two important parameters, the continuous voltage V_0, that is the voltage who accelerates the electrons emitted from the gun, and the *perveance* P_μ, that is related to the beam current I_0 by the equation:

$$P_\mu = \frac{I_0}{V_o^{\frac{3}{2}}} \tag{2.1}$$

The perveance is strongly tied to the klystron electronic efficiency η_{el}, given by:

$$\eta_{el} = \frac{P_{out}}{P_\mu V_0^{\frac{5}{2}}} \tag{2.2}$$

It is clear that one of the consequences of increasing the perveance for a fixed frequency is the decaying of this efficiency. For the most part of klystrons, the longitudinal magnetic focusing field is chosen in order to approach a confined flux regime, and is then of the order of two or three times the Brillouin field

[4]. The power needed by the electromagnets grows then with the perveance. This is another reason for chosing a low perveance. Another reason is tied to the working frequency and the drift tube radius. This has to be small enough so that the cavity field, excited by the beam, cannot propagate. This gives a constraint on the maximum drift tube radius, once that the cavity frequency has been fixed. Furthermore, there is an optimal interaction between the beam and the cavities when the beam *filling factor* b/a (where b is the medium beam radius and a is the pipe radius) is of the order of 0.6 - 0.8. Since the beam radius b is then fixed from the frequency, we can then determinate the diameter of the cathod and the medium current density that can be obtained. These quantities are related to the *gun convengence factor* C_c, defined by the ratio between the cathod surface and the beam surface at the drift tube entrance, and expressed as a function of the beam current I_0 and the perveance P_μ:

$$C_c = \frac{P_\mu V_0^{\frac{3}{2}}}{\pi b^2 J_c} \tag{2.3}$$

For a given average current density J_c, radius b and voltage V_0 the convergence grows then with the perveance. This corresponds to an increasing of the cathode surface and requires a particular attention while designing a klystron in order to avoid possible interceptions of the beam with the drift tube before the first cavity.

2.2.1 Main electrical parameters

The electrical parameters of a klystrons include all the quantities related to the interaction between the electron beam and the resonant cavities. These quantities can be divided in two categories: the ones related to the RF cavities, and the ones who characterize the not modulated electron beam.

2.2.1.1 RF cavities parameters

The cavity mode who interacts with the beam in a klystron is the TM_{010}. If there is no external coupling, an RF cavity, whose working frequency is

close to the resonant frequency of this mode, is characterized by the following parameters:

- the resonant angolar frequency ω_0;
- the quality factor Q_0, defined by:

$$Q_0 = \frac{\omega U}{P_d} \tag{2.4}$$

  where U is the electromagnetic energy stored inside the cavity and P_d is the average power loss on the walls;

- the R/Q ratio, defined by:

$$\frac{R}{Q} = \frac{V_c^2}{2\omega U} \tag{2.5}$$

where V_c is the peak voltage at the cavity gap, and it is in general defined by the integral of the longitudinal electric field along the axis of the cavity:

$$\frac{R}{Q} = \frac{V_c^2}{2\omega U} \tag{2.6}$$

The cavity can be modeled, if we are close to the resonant frequency, with an equivalent RLC parallel circuit. The impedence Z_c of a not coupled cavity, in absence of the electron beam (*cold impedence*) can be expressed as a function of the three quantities ω_0, Q_0 and R/Q_0:

$$Z_c(\omega) = \frac{R}{Q_0} \frac{Q_0}{1 + jQ_0\left(\frac{\omega}{\omega_0} - \frac{\omega_0}{\omega}\right)} \tag{2.7}$$

with:

- $\omega_0 = \frac{1}{\sqrt{LC}}$,
- $Q_0 = \frac{R}{\omega_0 L} = \omega_0 RC$,
- $\frac{R}{Q_0} = \sqrt{\frac{L}{C}} = \frac{1}{\omega_0 C}$.

These quantities characterize the intermediate cavities of a klystron.

The input and the output cavities of a klystron are coupled to an external waveguide or to a coaxial line. This coupling is characterized by an external merit factor Q_{ext}, defined by:

$$Q_{ext} = \frac{\omega U}{P_{ext}} \tag{2.8}$$

where P_{ext} is the RF power who enters or exits from the cavity. It is possible also to define a *coupling coefficient* β as:

$$\beta = \frac{P_{ext}}{P_d} = \frac{Q_0}{Q_{ext}} \tag{2.9}$$

$$P_L = P_l + P_{ext} = (1 + \beta) P_d \tag{2.10}$$

The total Q is then given by:

$$Q = \frac{\omega U}{P_L} \tag{2.11}$$

So that we have the well known expression:

$$\frac{1}{Q} = \frac{1}{Q_0} + \frac{1}{Q_{ext}} = \frac{1 + \beta}{Q_0} \tag{2.12}$$

The impedence Z_c of a resonant cavity can then be expressed as a function of Q:

$$Z_c(\omega) = \frac{R}{Q} \frac{Q}{1 + jQ\left(\frac{\omega}{\omega_0} - \frac{\omega_0}{\omega}\right)} \tag{2.13}$$

2.2.1.2 Beam parameters

The following parameters tie the angular frequency of the signal to be amplified and the electronic characteristics of the RF cavities to the beam features.

- The *electronic longitudinal propagation constant* β_e is defined as:

$$\beta_e = \frac{\omega}{v_0} \tag{2.14}$$

where v_0 is the initial particles velocity. The length of a interaction gap d, multiplied by β_e is the *transit angle* $\beta_e d$;

- the *electronic radial propagation constant* γ_e is related to β_e by the relation: $\gamma_e = \sqrt{\beta_e^2 - k_0^2}$, with $k_0 = \omega/c$ and where c is the speed of light. We have:

$$\gamma_e = \frac{\beta_e}{\gamma_0} \tag{2.15}$$

where γ_0 is the relativistic factor:

$$\gamma_0 = \left[1 - \left(\frac{v_0}{c}\right)^2\right]^{-\frac{1}{2}} \tag{2.16}$$

and it is related to the beam voltage V_0 by the energy conservation:

$$\gamma_0 = 1 - \frac{q_e V_0}{m_0 c^2} \tag{2.17}$$

where m_e and q_e are respectively the electron mass and charge;

- the *longitudinal coupling coefficient* between the beam and the cavity M_l depends on the longitudinal electric field profile, on the interaction gap length, on the working frequency and on the beam velocity;

- the *radial coupling coefficient* between the beam and the cavity M_r depends on the radial electric field distribution. It is function of the pipe radius a, the beam radius b, the working frequency and the beam velocity;

- the *total coupling coefficient* is defined by the product of the longitudinal and the radial coupling coefficients:

$$M = M_l M_r \tag{2.18}$$

These coupling coefficients characterize the effectiveness of the interaction between the electron beam and the cavity fields, and they are usually calculated for simple field profiles;

- the *plasma angular frequency* ω_p is defined as:

$$\omega_p = \sqrt{\frac{q_e \rho_0}{m_0 \epsilon_0}} \tag{2.19}$$

where ρ_0 is the electronic volume density. We also have, if we substitute $I_0 = (\pi b^2) |\rho_0| v_0$:

$$\omega_p = \frac{1}{b} \sqrt{\frac{|q_e| I_0}{\pi m_0 \epsilon_0 v_0}} \tag{2.20}$$

- the *plasma reduction factor* R_q is a corrective factor which takes in account the presence of the beam pipe in the beam confinement. It is a function of the pipe radius a, the beam radius b, the beam velocity v_0 and the working frequency ω;

- the reduced plasma angular frequency ω_q is then given by the product of the plasma angular frequency and the plasma reduction factor:

$$\omega_q = R_q \omega_p \tag{2.21}$$

- from these quantity it is also possible to define the reduced plasma wavelength:

$$\lambda_q = \frac{2\pi}{\beta_q} \tag{2.22}$$

In a small signal analysis, where the modulation voltages induced by the beam are small with respect to the beam accelerating voltage V_0, the previous quantities allow to calculate the voltages and currents induced by the beam in every cavity on the klystron axis. On the other hand, an analytic study of the large signal regime is very complicated and the utilization of simulation codes becomes indispensable.

2.3 The kinematic theory of velocity modulation

In this section and in the next one we will present the main formulae used in the design of klystron amplifiers [5]. The kinematic analysis does not take in account the presence of the space charge forces between particles, and it is the only large signal analytical treatment of klystrons. This means that the small-signal approximation, which considers the RF components of the electrons velocities and current densities much smaller with respect to the DC components, is not employed beyond the first cavity. This theory will lead to an expression of the current harmonics coefficients which contains Bessel functions and to a calculation of two-cavity amplifier efficiency.

Let's consider a simple klystron consisting of only two cavities, a "buncher" and a "catcher". Let a beam of electrons, which has been accelerated by a potential V_0 to a velocity v_0 traverse the first pair of grids, where it is acted upon by an RF voltage $V_1 \sin(\omega t)$, reduced by a "coupling coefficient" M.

The electrons in the beam enter the gridded gap with energy:

$$\frac{1}{2} m_e v_0^2 = q_e V_0 \tag{2.23}$$

The electron energy is modified by the RF field at the gap and the following relationship can be written for the exit velocity v:

$$\frac{1}{2} m_e v^2 - \frac{1}{2} m_e v_0^2 = q_e m_e V_1 \sin(\omega t) \tag{2.24}$$

From the above it follows that:

$$v = v_0\sqrt{1 + \frac{MV_1}{V_0}\sin(\omega t)} \tag{2.25}$$

If one assumes that $V_1 << V_0$ (which is a good assumption for the first cavity of a two-cavity klystron), then:

$$v \cong v_0\left(1 + \frac{MV_1}{2V_0}\sin(\omega t)\right) \tag{2.26}$$

Let's consider first the case for which the first interaction gap is very narrow, such that the finite transit time of the entering electrons can be neglected. The electrons then enter, and leave the first gap at time t_1, then drift for a distance l, and arrive at the center of the second gap at time t_2. Then (invoking the small-signal assumption $\frac{V_1}{V_0} << 1$):

$$t_2 = t_1 + \frac{l}{v} = t_1 + \frac{l}{v_0\left(1 + \frac{MV_1}{2V_0}\sin(\omega t_1)\right)} \cong t_1 + \frac{l}{v_0} - \frac{lMV_1}{2v_0V_0}\sin(\omega t_1) \tag{2.27}$$

or, in terms of phase:

$$\omega t_2 = \omega t_1 + \theta_0 - X\sin(\omega t_1) \tag{2.28}$$

where $\theta_0 = \frac{\omega l}{v_0}$, and the dimensionless quantity $X = \frac{MV_1\theta_0}{2V_0}$ is called the "*bunching parameter*". When $X > 1$, ωt_2 is a multivalued function of ωt_1 and there is electron overtaking, as it can be seen from figure (2.2).

The quantity of charge leaving the buncher in the time interval t_1 to $t_1 + dt_1$ is $I_0 dt_1$, at $t_1 = 0$, where I_0 is the beam DC current entering the buncher. This charge, after drifting, enters the catcher in the interval t_2 to $t_2 + dt_2$. If I_t (total current, DC and RF) is the current transported by the beam to the entrance to the catcher, then through conservation of charge:

$$I_0 dt_1 = I_t dt_2 \tag{2.29}$$

Differentiating eq. (2.28) yields:

$$\frac{dt_2}{dt_1} = 1 - X\cos(\omega t_1) \tag{2.30}$$

which can be combined with eq. (2.29) to give:

$$I_t = \frac{I_0}{(1 - X\cos(\omega t_1))} \tag{2.31}$$

For $X = 1$ the current at the catcher becomes infinite (fig. 2.2), since the finite charge transported from the buncher at $t_1 = 0$ arrives at the catcher in a zero time interval ($\frac{dt_2}{dt_1} = 0$).

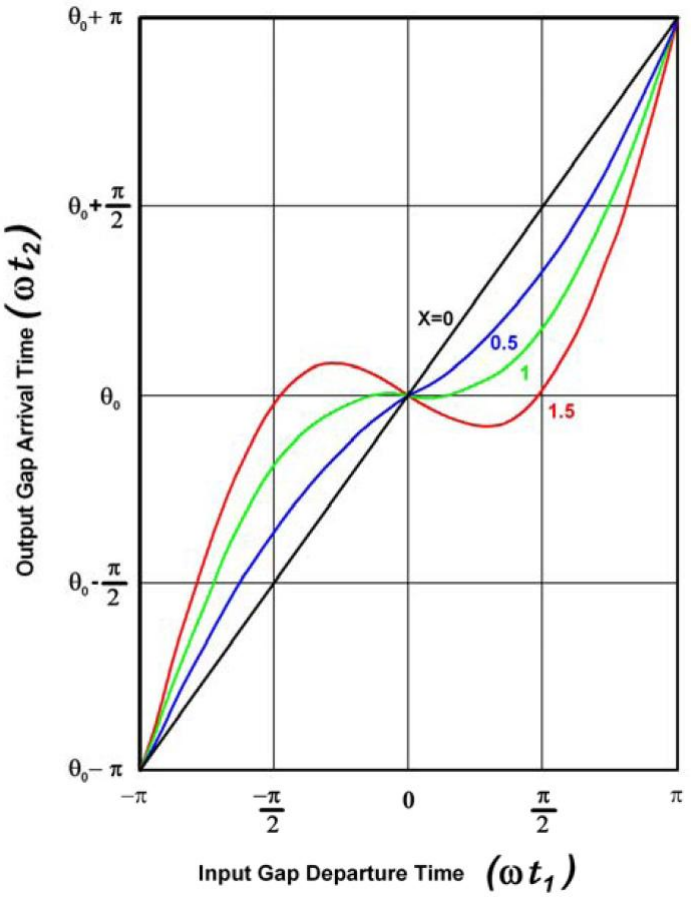

Figure 2.2: Electron arrival vs departure phase in a two cavity klystron, as a function of the bunching parameter X.

To calculate I_t, one must then sum the absolute values of all current contributions to I_t from time segments t_{11}, t_{12}, etc, at the buncher, as follows:

$$I_t = I_0 \left[\frac{1}{|1 - X\cos(\omega t_{11})|} + \frac{1}{|1 - X\cos(\omega t_{12})|} + ... \right] \tag{2.32}$$

The current waveforms at the buncher are shown in fig. 2.3. Note that at the lower values of X they are almost sinusoidal, but they become rich in harmonics at $X = 1$ and above.

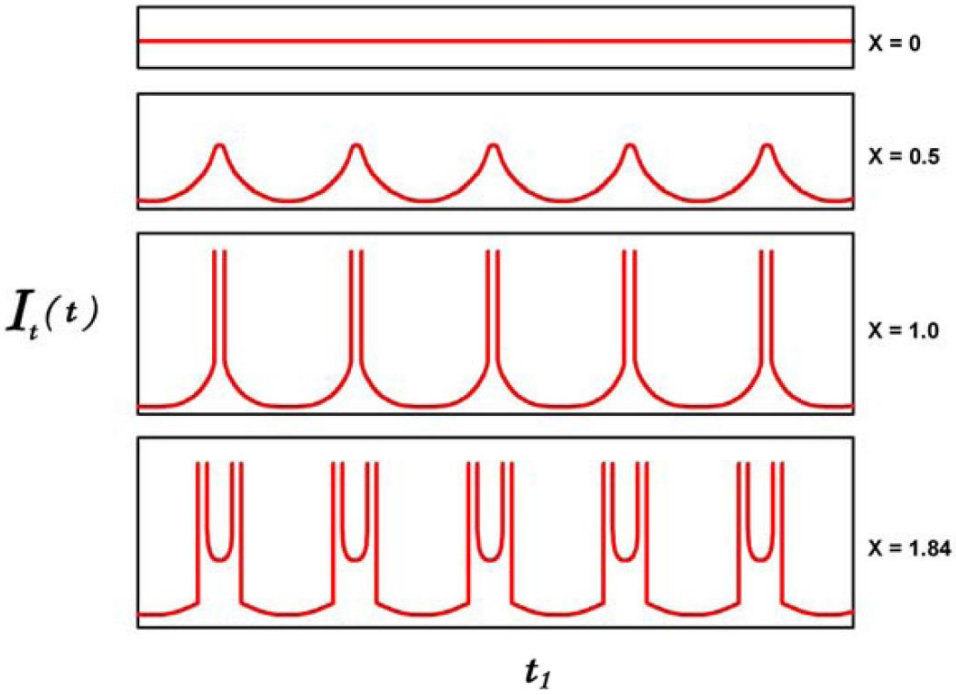

Figure 2.3: Bunching waveforms as a function of X.

Since I_t is clearly a periodic function of ωt_2, it can be expanded in a Fourier series, as follows:

$$I_t = I_0 + \sum_{n=1}^{\infty} \left[a_n \cos\left[n\left(\omega t_2 - \theta_0\right)\right] + b_n \sin\left[n\left(\omega t_2 - \theta_0\right)\right] \right] \tag{2.33}$$

with coefficients given by:

$$a_n = \frac{1}{\pi}\int_{\theta_0-\pi}^{\theta_0+\pi} I_t \cos\left[n\left(\omega t_2 - \theta_0\right)\right] d\left(\omega t_2\right) \tag{2.34}$$

and:

$$b_n = \frac{1}{\pi}\int_{\theta_0-\pi}^{\theta_0+\pi} I_t \sin\left[n\left(\omega t_2 - \theta_0\right)\right] d\left(\omega t_2\right) \tag{2.35}$$

Substituting eq. (2.28) and eq. (2.29) into eq. (2.34) and eq. (2.35) above, these become:

$$a_n = \frac{I_0}{\pi}\int_{-\pi}^{\pi} \cos\left[n\left(\omega t_1 - X\sin\left(\omega t_1\right)\right)\right] d\left(\omega t_1\right) \tag{2.36}$$

and:

$$b_n = \frac{I_0}{\pi}\int_{-\pi}^{\pi} \sin\left[n\left(\omega t_1 - X\sin\left(\omega t_1\right)\right)\right] d\left(\omega t_1\right) \tag{2.37}$$

We can note that b_n is identically equal to zero, since the integrand is an odd function of ωt_1. It turns out that the expression eq. (2.36) for the a_n coefficients is also a representation of the Bessel functions of the first kind and n$^{\text{th}}$ order as in:

$$a_n = 2I_0 J_n\left(nX\right) \tag{2.38}$$

Therefore, the catcher RF current I_t can be written as the following series:

$$I_t = I_0 + 2I_0\sum_{n=1}^{\infty} J_n\left(nX\right)\cos\left[n\left(\omega t_1 - \theta_0\right)\right] \tag{2.39}$$

The $n = 1$ harmonic (the fundamental) is simply:

$$I_1 = 2I_0 J_1\left(X\right)\cos\left(\omega t_1 - \theta_0\right) = \Re\left[2I_0 J_1\left(X\right)e^{j(\omega t - \theta_0)}\right] \tag{2.40}$$

When $X < 1$, the series in eq. (2.39) converges for all values of t_2. For $X = 1$, and $X > 1$, there are discontinuities at various t_2 values as shown in fig. 2.3 (which would disappear if space charge were taken into account).

The harmonic amplitudes correspond to the peaks of the Bessel functions (fig 2.4).

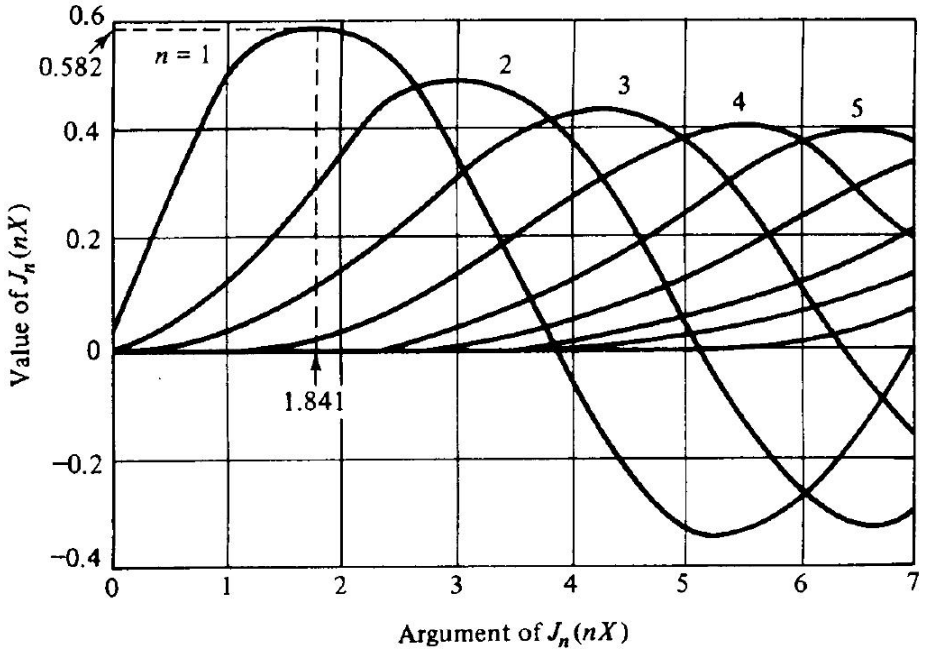

Figure 2.4: The first 5 Bessel functions of the first kind.

One can now calculate the output power from the fundamental ($n = 1$), using eq. (2.40) and the maximum value of $J_1(X)$, which is 0.582 and occurs at $X = 1.84$. The output power is the product of the RF current I_1 and the maximum voltage that can be developed across the output gap without reflecting electrons, which is the beam voltage V_0. Both are peak values, so:

$$P_{out} = \frac{1.16 I_0}{\sqrt{2}} \frac{V_0}{\sqrt{2}} = 0.58 I_0 V_0 = 0.58 P_{in} \tag{2.41}$$

Consequently, for the two-cavity klystron, without space charge and with sinusoidal voltage modulation, the maximum efficiency is 58%.

The above derivation is completely valid, even when there is electron overtaking. In order to arrive to the above result, the small-signal approximation has been used only to formulate the expressions to launch the velocity-

modulated beam into the drift space, but it is not employed beyond the buncher cavity.

However, the effects of space charge and a number of other issues force a much lower efficiency in the two-cavity klystron case. On the other hand, it has been shown by simulations and experiments in multiple cavity klystrons that the use of higher harmonics cavities [6] [7], or multiple cavities properly arranged [8] [9], can produce I_1/I_0 ratios as high as 1.8, and then, higher efficiencies.

The velocity modulation kinematic treatment above was first published (in the US) by D. L. Webster [10], a collaborator of Hansen and the Varians at Stanford. His 1939 *Journal of Applied Physics* article included, in addition to the "bunching" theory, a brief theory of "debunching" (i.e. - accounting of the effects of space charge on the velocity modulation process). Eugene Feenberg, a member of the wartime Sperry Gyroscope "Tube Development Laboratory", developed the Webster theory into a considerably more detailed mathematical treatise [11], which included the addition of a third cavity to the original two-cavity klystron, and the first formulae for coupling coefficients and beam-loading in gridded and ungridded klystron cavity gaps.

2.4 The space-charge wave theory

In kinematic theory, which was the earliest mathematical treatment describing beam interaction with microwave fields, the fields due to the beam's space charge were ignored and calculations were based only on the effects of the fields in the interaction gap. Energy between cavities was transmitted through ballistic electron motion. Kinematic theory does not provide the tools necessary for a satisfactory analysis of multicavity klystrons. For this, a small-signal space-charge wave theory is necessary. This was first developed by Webster [12] and extended by Hahn [13] [14] and Ramo [15]. This theory was later developed by Wessel Berg [16] [17] [18] for space charge waves in extended interaction klystrons for not relativistic beams. In the following section we will expose this theory with particular focusing on multicavity

structures [20]; as a first step, we will write the electronic equations inside a drift tube. Then the interaction with a RF field will be taken in account, and finally, we will study the particular case of a chain of coupled cavities. The following basic assumptions will be made [19][1]:

1. We assume that the magnetic focusing field is strong enough so that no electron motion or current is assumed to exist along any dimension, other than the longitudinal one (z).

2. The transverse beam section is small with respect to the drift tube radius. The electric cavity fields and the space charge fields are supposed to be purely longitudinal and uniform over the beam section. In this way the particles velocity and density fields depend only on the z coordinate.

3. The emitted electron beam is mono-energetic: the initial velocity distribution is neglected (cold beam). This means that, if there is no modulation (i.e. no input RF signal is injected in the first cavity), the electron velocity and density are constant over all the tube length.

4. The electrons can be relativistic and the magnetic field generated by the beam is negligible with respect to the focusing field. The electron plasma frequency is small with respect to the working frequency.

5. The RF components of the velocities and the electron densities, denoted by $\tilde{v}$ and $\tilde{\rho}$ are considered as perturbations of the not-modulated beam. The initial modulation is the result of the interaction between the continuous beam and the RF field in the first cavity. The modulating voltage is small with respect to the accelerating voltage V_0, and this hypothesis is conserved inside the intermediate and the output cavities. This small signal approximation allows to linearize the equations of the velocity and density fields, which are always the superposition of a DC and an RF component.

[1]The following, as well as sections 2.4.1, 2.4.2, 2.4.3, are based on [20]

2.4.1 The electronic equations in the drift tubes

The fields evolution in the drift tubes region is governed only by the space charge fields. The beam can be characterized by the velocity field, the electrons density field and the convection current density field, which can be found with the relativistic dynamic equation, the charge conservation equation and the Gauss law. With the previous hypothesis (hip. 5), the electrons velocity and the charge density can be written as:

$$v_z(z,t) = v_0 + \Re\left(\tilde{v}(z)\, e^{j\omega t}\right) \tag{2.42}$$

$$\rho(z,t) = \rho_0 + \Re\left(\tilde{\rho}(z)\, e^{j\omega t}\right) \tag{2.43}$$

And, for the current density:

$$J_z(z,t) = J_0 + \Re\left(\tilde{J}(z)\, e^{j\omega t}\right) \tag{2.44}$$

where:

$$J_0 = \rho_0 v_0, \qquad \tilde{J}(z) = \tilde{\rho}(z)\, v_0 + \rho_0 \tilde{v}(z) \tag{2.45}$$

2.4.1.1 Dynamic equation linearization

Particles travelling inside the pipe are subject to two fields: the space charge fields $\vec{E}_{sc}$ and $\vec{B}_{sc}$ due the other electrons, and the static focusing magnetic field $\vec{B}_0$. The dynamic equation for a particle inside the drift tube can be then written as:

$$\frac{d\vec{p}}{dt} = q_e\left(\vec{E}_{sc} + \vec{v} \times \left(\vec{B}_{sc} + \vec{B}_0\right)\right) \tag{2.46}$$

where $\vec{p}$ is the momentum:

$$\vec{p} = \gamma m_0 \vec{v} \tag{2.47}$$

We have:

$$\frac{d\left(\gamma\vec{v}\right)}{dt} = \frac{q_e}{m_0}\left(\vec{E}_{sc} + \vec{v} \times \left(\vec{B}_{sc} + \vec{B}_0\right)\right) \tag{2.48}$$

It can be easily shown that the energy conservation can be written as:

$$\frac{d\left(\gamma m_0 c^2\right)}{dt} = \vec{v} \cdot \frac{d\vec{p}}{dt} \tag{2.49}$$

And so, by utilizing eq. (2.46):

$$\frac{d\left(\gamma\right)}{dt} = \frac{q_e}{m_0 c^2}\vec{v} \cdot \vec{E}_{sc} \tag{2.50}$$

By developing the first member of eq. (2.48) we have that this can be written as:

$$\frac{d\left(\vec{v}\right)}{dt} = \frac{q_e}{m_0\gamma}\left(\vec{E}_{sc} + \vec{v} \times \left(\vec{B}_{sc} + \vec{B}_0\right) - \frac{1}{c^2}\left(\vec{v} \cdot \vec{E}_{sc}\right)\vec{v}\right) \tag{2.51}$$

Eq. (2.51) can be projected on the z-axis:

$$\frac{d\left(v_z\right)}{dt} = \frac{q_e}{m_0\gamma}\left(E_{sc,z} + \vec{v_\perp} \times \left(\vec{B}_{sc,\perp}\right) - \frac{1}{c^2}\left(\vec{v} \cdot \vec{E}_{sc}\right)v_z\right) \tag{2.52}$$

We can then neglect the transverse space charge fields and velocities and obtain:

$$\frac{dv_z}{dt} = \frac{q_e}{m_0\gamma^3}E_{sc,z} \tag{2.53}$$

where:

$$\gamma \cong \left[1 - \left(\frac{v_z}{c}\right)^2\right]^{-\frac{1}{2}} \tag{2.54}$$

Since we are performing an Eulerian description of the particles motion, it is convenient to express the derivatives as the sum of a partial time derivative plus a convective term:

$$\frac{d}{dt} = \frac{\partial}{\partial t} + \vec{v} \cdot \vec{\nabla} \tag{2.55}$$

Eq. (2.53) becomes:

$$\left(\frac{\partial}{\partial t}+v_z\frac{\partial}{\partial z}\right)v_z=\frac{q_e}{m_0\gamma^3}E_{sc,z} \tag{2.56}$$

If we linearize the last equation, by using, for the RF quantities:

$$E_{sc,z}\left(z,t\right)=\Re\left[\tilde{E}_{sc}\left(z\right)e^{j\omega t}\right] \tag{2.57}$$

we get:

$$\left(j\omega+v_0\frac{\partial}{\partial z}\right)\tilde{v}\left(z\right)=\frac{q_e}{m_0\gamma_0^3}\tilde{E}_{sc}\left(z\right) \tag{2.58}$$

where γ_0 is a function of the longitudinal velocity v_0. By using the longitudinal electronic propagation constant β_e we have that the velocity modulation satisfies the following first order partial differential equation:

$$\left(\frac{\partial}{\partial z}+j\beta_e\right)\tilde{v}\left(z\right)=\frac{q_e}{m_0v_0\gamma_0^3}\tilde{E}_{sc}\left(z\right) \tag{2.59}$$

2.4.1.2 Continuity equation linearization

The continuity equation ties the local variation of the convection current to the local temporal variation of the charge density:

$$\nabla\cdot\vec{J}=-\frac{\partial\rho}{\partial t} \tag{2.60}$$

By neglecting the transverse current:

$$\frac{\partial J_z}{\partial z}=-\frac{\partial\rho}{\partial t} \tag{2.61}$$

And, after linearization we have, for the RF components $\tilde{J}\left(z\right)$ and $\tilde{\rho}\left(z\right)$:

$$\frac{\partial\tilde{J}}{\partial z}=-j\omega\tilde{\rho}\left(z\right) \tag{2.62}$$

2.4.1.3 Gauss law

The Gauss law relates the space charge field to the electron density:

$$\nabla \cdot \vec{E}_{sc} = \frac{\rho}{\epsilon_0} \tag{2.63}$$

So, in our case:

$$\frac{\partial E_{sc,z}}{\partial z} = \frac{\rho}{\epsilon_0} \tag{2.64}$$

And, linearizing:

$$\frac{\partial \tilde{E}_{sc,z}}{\partial z} = \frac{\tilde{\rho}\left(z\right)}{\epsilon_0} \tag{2.65}$$

The previous equation does not take in account the finite transverse dimensions of the beam and the boundary condition that the space charge field has to satisfy due to the presence of the metallic pipe. Eq. (2.64) is then modified by the plasma reduction factor R_q [21]:

$$\frac{\partial \tilde{E}_{sc,z}}{\partial z} = R_q^2 \frac{\tilde{\rho}\left(z\right)}{\epsilon_0} \tag{2.66}$$

2.4.1.4 Space charge waves in the drift tubes

By utilizing eq. (2.61) and eq. (2.64) we arrive to the following equation for $\tilde{J}(z)$ and $\tilde{E}_{sc}(z)$:

$$\frac{\partial}{\partial z}\left(\tilde{J}\left(z\right) + j\omega \frac{\epsilon_0}{R_q^2} \tilde{E}_{sc}\left(z\right)\right) = 0 \tag{2.67}$$

And so:

$$\tilde{E}_{sc}\left(z\right) = \frac{j}{\omega} \frac{R_q^2}{\epsilon_0} \tilde{J}\left(z\right) \tag{2.68}$$

From the last relation, and from eq. (2.59) we have then the equation relating $\tilde{v}(z)$ and $\tilde{J}(z)$:

$$\left(\frac{\partial}{\partial z} + j\beta_e\right) \tilde{v}\left(z\right) = \frac{j}{\omega} \frac{q_e R_q^2}{m_0 \epsilon_0 v_0 \gamma_0^3} \tilde{J}\left(z\right) \tag{2.69}$$

The plasma reduced angular frequency ω_p is given by:

$$\omega_p = \sqrt{\frac{q_e \rho_0}{m_0 \epsilon_0 \gamma_0^3}} \tag{2.70}$$

and the longitudinal propagation constant:

$$\beta_p = \frac{\omega_p}{v_0} = \sqrt{\frac{q_e \rho_0}{m_0 \epsilon_0 v_0^2 \gamma_0^3}} \tag{2.71}$$

In the same way we can define the reduced quantities:

$$\omega_q = R_q \omega_p \tag{2.72}$$

$$\beta_q = \frac{\omega_q}{v_0} \tag{2.73}$$

Eq. (2.67) can then be expressed by using these quantities:

$$\left(\frac{\partial}{\partial z} + j\beta_e\right) \tilde{v}\,(z) = j \frac{\beta_q^2}{\beta_e \rho_0} \tilde{J}\,(z) \tag{2.74}$$

We can obtain the relationship between $\tilde{v}(z)$ and $\tilde{J}(z)$ also by multiplying eq. (2.45) for $j\beta_e$ and by using eq. (2.62):

$$\left(\frac{\partial}{\partial z} + j\beta_e\right) \tilde{J}\,(z) = j\beta_e \rho_0 \tilde{v}(z) \tag{2.75}$$

Let's now define the differential operator $\mathcal{L}_z$ as:

$$\mathcal{L}_z = \frac{\partial^2}{\partial z^2} + 2j\beta_e \frac{\partial}{\partial z} - \left(\beta_e^2 - \beta_q^2\right) \tag{2.76}$$

This can be factorized as:

$$\mathcal{L}_z = \left(\frac{\partial}{\partial z} + j\beta_s\right)\left(\frac{\partial}{\partial z} + j\beta_f\right) \tag{2.77}$$

where β_s and β_f are defined by:

$$\beta_s = \beta_e + \beta_q \tag{2.78}$$

$$\beta_f = \beta_e - \beta_q \tag{2.79}$$

The modulations $\tilde{v}(z)$ and $\tilde{J}(z)$ satisfy the homogenous equations:

$$\mathcal{L}_z\left(\tilde{v}(z)\right) = 0 \tag{2.80}$$

$$\mathcal{L}_z\left(\tilde{J}(z)\right) = 0 \tag{2.81}$$

where the solutions are linear combinations of the functions $e^{-j\beta_s z}$ and $e^{-j\beta_f z}$. We than have two plasma waves propagating in the electron beam with propagation velocities above the beam velocity (*fast wave*, with propagating constant β_f), and below the beam velocity (*slow wave*, with propagating constant β_s).

Equations (2.74) and (2.75) form a linear system of two first order differential equations whose solutions are:

$$\begin{aligned}\tilde{v}_z(z) &= \frac{1}{2}\left(e^{-j\beta_f(z-x_0)} + e^{-j\beta_s(z-x_0)}\right)\tilde{v}\left(x_0\right) + \\ &+ \left(\frac{\beta_q}{2\beta_e\rho_0}\right)\left(e^{-j\beta_f(z-x_0)} - e^{-j\beta_s(z-x_0)}\right)\tilde{J}\left(x_0\right)\end{aligned} \tag{2.82}$$

$$\begin{aligned}\tilde{J}_z(z) &= \frac{\beta_e\rho_0}{2\beta_q}\left(e^{-j\beta_f(z-x_0)} - e^{-j\beta_s(z-x_0)}\right)\tilde{v}\left(x_0\right) + \\ &+ \left(\frac{1}{2}\right)\left(e^{-j\beta_f(z-x_0)} + e^{-j\beta_s(z-x_0)}\right)\tilde{J}\left(x_0\right)\end{aligned} \tag{2.83}$$

or, in matrix form:

$$\begin{pmatrix} \tilde{v}(z) \\ \tilde{J}(z) \end{pmatrix} = e^{-j\beta_e(z-x_0)} \begin{pmatrix} \cos\left(\beta_q\left(z-x_0\right)\right) & j\frac{\beta_q}{\beta_e\rho_0}\sin\left(\beta_q\left(z-x_0\right)\right) \\ j\frac{\beta_e\rho_0}{\beta_q}\sin\left(\beta_q\left(z-x_0\right)\right) & \cos\left(\beta_q\left(z-x_0\right)\right) \end{pmatrix} \begin{pmatrix} \tilde{v}(x_0) \\ \tilde{J}(x_0) \end{pmatrix} \tag{2.84}$$

where $\tilde{v}(x_0)$ and $\tilde{J}(x_0)$ are the initial velocity and current density modulations in the point x_0, longitudinal arbitrary coordinate along the z-axis of the drift tube.

2.4.2 The electronic equations in presence of a RF field

Let's now consider the modification of the electronic equations inside a klystron cavity. The presence of a longitudinal RF field produces the addition of a new term in the dynamic equation. Eq. (2.59) becomes then:

$$\left(\frac{\partial}{\partial z} + j\beta_e\right)\tilde{v}\left(z\right) = \frac{q_e}{m_0 v_0 \gamma_0^3}\left(\tilde{E}_{sc}\left(z\right) + \tilde{E}_c\left(z\right)\right) \tag{2.85}$$

where $\tilde{E}_c$ is the complex amplitude of the longitudinal projection of the RF cavity field.

Since equations (2.68) and (2.75) are not directly affected from the presence of the RF field, the new first order differential equation satisfied by $\tilde{v}(z)$ as a function of $\tilde{J}(z)$ and $\tilde{E}_{sc}(z)$ can be obtained by replacing the space charge field $\tilde{E}_{sc}(z)$ in equation (2.85) with its expression as a function of $\tilde{J}(z)$ (eq. (2.68)):

$$\left(\frac{\partial}{\partial z} + j\beta_e\right)\tilde{v}\left(z\right) = j\frac{\beta_q^2}{\beta_e \rho_0}\tilde{J}\left(z\right) + \frac{q_e}{m_0 v_0 \gamma_0^3}\tilde{E}_c(z) \tag{2.86}$$

This expression is analogue to eq. (2.74).

Then second order partial differential equation for $\tilde{v}(z)$ can be obtained by applying the operator $\left(\frac{\partial}{\partial z} + j\beta_e\right)$ to equation (2.86) and utilizing eq. (2.75):

$$\mathcal{L}_z\left(\tilde{v}\left(z\right)\right) = \frac{q_e}{m_0 v_0 \gamma_0^3}\left(\frac{\partial}{\partial z} + j\beta_e\right)\tilde{E}_c(z) \tag{2.87}$$

In the same way, it is possible to obtain the equation for $\tilde{J}(z)$:

$$\mathcal{L}_z\left(\tilde{J}\left(z\right)\right) = j\frac{q_e \beta_e \rho_0}{m_0 v_0 \gamma_0^3}\tilde{E}_c(z) \tag{2.88}$$

We can now express the constants on the right of the previous equations as a function of the beam voltage V_0 (defined positive). By applying the

kinetic energy theorem to the emitted electrons we have (if we assume that the electrons are emitted with zero velocity):

$$\gamma_0 = 1 - \frac{q_e V_0}{m_0 c^2} \tag{2.89}$$

and so:

$$\frac{1}{2} m_0 v_0^2 = -\frac{q_e V_0}{\gamma_0^3 \Gamma_0} \tag{2.90}$$

where:

$$\Gamma_0 = \frac{2}{\gamma_0 (\gamma_0 + 1)} \tag{2.91}$$

Equations (2.87) and (2.88) can then be rewritten as:

$$\mathcal{L}_z (\tilde{v}(z)) = -\frac{v_0 \Gamma_0}{2V_0} \left(\frac{\partial}{\partial z} + j\beta_e \right) \tilde{E}_c(z) \tag{2.92}$$

$$\mathcal{L}_z \left(\tilde{J}(z) \right) = -j \frac{\beta_e J_0 \Gamma_0}{2V_0} \tilde{E}_c(z) \tag{2.93}$$

These second order inhomogeneous differential equations constitute a system that can be solved with the method of the variation of constants or with the spatial Laplace transform method. We have, in matrix form:

$$\begin{aligned} \begin{pmatrix} \tilde{v}(z) \\ \tilde{J}(z) \end{pmatrix} &= e^{-j\beta_e (z - x_1)} \\ &\begin{pmatrix} \cos(\beta_q (z - x_1)) & j \frac{\beta_q}{\beta_e \rho_0} \sin(\beta_q (z - x_1)) \\ j \frac{\beta_e \rho_0}{\beta_q} \sin(\beta_q (z - x_1)) & \cos(\beta_q (z - x_1)) \end{pmatrix} \begin{pmatrix} \tilde{v}(x_1) \\ \tilde{J}(x_1) \end{pmatrix} + \\ &- \frac{\Gamma_0}{2V_0} \begin{pmatrix} v_0 \mathcal{C}(z) \\ j \frac{\beta_e J_0}{\beta_q} \mathcal{S}(z) \end{pmatrix} \end{aligned} \tag{2.94}$$

where x_1 is a longitudinal position on the axis before the first cavity so that the circuit electric field is zero and the functions $\mathcal{C}(z)$ and $\mathcal{S}(z)$ determinate the modulations due to the cavity field $\tilde{E}_c$ and are defined as:

$$\mathcal{C}(z) = \frac{1}{2}\left(\int_{x_1}^{z} e^{-j\beta_f(z-y)}\tilde{E}_c(y)\,dy + \int_{x_1}^{z} e^{-j\beta_s(z-y)}\tilde{E}_c(y)\,dy\right) \tag{2.95}$$

$$\mathcal{S}(z) = \frac{1}{2j}\left(\int_{x_1}^{z} e^{-j\beta_f(z-y)}\tilde{E}_c(y)\,dy - \int_{x_1}^{z} e^{-j\beta_s(z-y)}\tilde{E}_c(y)\,dy\right) \tag{2.96}$$

or:

$$\mathcal{C}(z) = \int_{x_1}^{z} \cos(\beta_q(z-y))\, e^{-j\beta_e(z-y)}\tilde{E}_c(y)\,dy \tag{2.97}$$

$$\mathcal{S}(z) = \int_{x_1}^{z} \sin(\beta_q(z-y))\, e^{-j\beta_e(z-y)}\tilde{E}_c(y)\,dy \tag{2.98}$$

A useful rapresentation of the previous solutions can be done by using the voltage and current modulation; the *normalized kinetic potential* is defined as:

$$\tilde{V}_{kin}(z) = \frac{m_0 v_0 \gamma_0^3}{q_e}\tilde{v}(z) \tag{2.99}$$

while the current modulation is:

$$\tilde{I}(z) = S\tilde{J}(z) \tag{2.100}$$

where S is the beam section. We can also define the *beam dynamic impedence* as:

$$Z_f = \frac{2\beta_q}{\Gamma_0\beta_e}\frac{V_0}{I_0} \tag{2.101}$$

where the beam current is defined positive as $I_0 = S\,|J_0|$. We finally obtain:

$$\begin{pmatrix} \tilde{V}_{kin}(z) \\ \tilde{I}(z) \end{pmatrix} = e^{-j\beta_e(z-x_1)} \begin{pmatrix} \cos(\beta_q(z-x_1)) & jZ_f\sin(\beta_q(z-x_1)) \\ \frac{j}{Z_f}\sin(\beta_q(z-x_1)) & \cos(\beta_q(z-x_1)) \end{pmatrix} \begin{pmatrix} \tilde{V}_{kin}(x_1) \\ \tilde{I}(x_1) \end{pmatrix} + + \begin{pmatrix} \mathcal{C}(z) \\ \frac{j}{Z_f}\mathcal{S}(z) \end{pmatrix} \tag{2.102}$$

The kinetic potential and the current modulation are the sum of two contributions: the first is due to the initial modulations, the other one is made by the cavity field.

2.4.3 The electronic equations in presence of a discrete RF field

We will consider now the more complicated case of an extended interaction structure. This can be represented by a sequence of coupled cylindric cavities. We suppose that the coupling of these cavities across the drift spaces is equal to zero, and the cavities resonate only on the TM_{010} mode. The discretization and the linearization of the interaction between the fields and the beam allow us to express the modulations in a position z inside one of the cavities (cavity j) gap as a sum of the contributions due to the initial modulation (i.e. the modulation produced by the cavities before the considered structure), plus the ones due to the modulations produced in the cavities of the structure before cavity j and to the modulation inside cavity j.

The current induced from the beam inside the cavity j is given by [20]:

$$I_{ind,j} = -\frac{1}{\alpha_j} \int_{V_j} \vec{\tilde{J}}\left(\vec{r}\right) \cdot \vec{E}_j\left(\vec{r}\right) dV \tag{2.103}$$

where $\vec{E}_j\left(\vec{r}\right)$ is the normalized electric field and α_j is a coefficient related to the voltage definition. Since we made the hypothesis that the electric field is uniform on the beam transverse section, we have that the previous expression for induced current reduces to an integral of the field on the longitudinal axis:

$$I_{ind,j} = -\frac{1}{\alpha_j} \int_{x_j}^{x_{j+1}} \tilde{I}\left(z\right) \cdot E_j\left(z\right) dz \tag{2.104}$$

where E_j is the normalized longitudinal electric field and x_j and x_{j+1} are the coordinates between which we have this field. The complex amplitude of the electric field in the cavity j is a function of the normalized field and of the RF voltage:

$$\tilde{E}_j(z) = \frac{V_j}{\alpha_j} E_j(z) \tag{2.105}$$

where the RF voltage in the cavity gap is given by:

$$V_j = -e_j \int_{x_j}^{x_{j+1}} E_j(z)\, dz \tag{2.106}$$

and:

$$\alpha_j = -\int_{x_j}^{x_{j+1}} E_j(z)\, dz \tag{2.107}$$

2.4.3.1 Calculation of voltage and current modulations

From the previous paragraphs we have that the kinetic potential in a position z inside the cavity j is given by:

$$\tilde{V}_{kin}(z) = e^{-j\beta_e(z-x_1)} \left[\cos\left(\beta_q(z-x_1)\right) \tilde{V}_{kin}(x_1) + jZ_f \sin\left(\beta_q(z-x_1)\right) \tilde{I}(x_1)\right] + \\ + \mathcal{C}(z) \tag{2.108}$$

And, for the current modulation:

$$\tilde{I}(z) = e^{-j\beta_e(z-x_1)} \left[\cos\left(\beta_q(z-x_1)\right) \tilde{I}(x_1) + \frac{j}{Z_f} \sin\left(\beta_q(z-x_1)\right) \tilde{V}_{kin}(x_1)\right] + \\ + \frac{j}{Z_f} \mathcal{S}(z) \tag{2.109}$$

where the integrals $\mathcal{C}(z)$ and $\mathcal{S}(z)$ are given respectively from equations (2.97) and (2.98). Since we discretized the problem and we made the hypothesis of linearity, the modulations of current and kinetic potential in one position z inside the cavity j can be expressed as the sum of the contributions of every cavity. Let's suppose that the interaction gaps before the cavity j are all short-circuited, except the one of cavity m. We have that the integrals $\mathcal{C}(z)$ and $\mathcal{S}(z)$ can be written as:

$$\mathcal{C}(z) = V_m \mathcal{C}_{m,m+1}(z) + V_j \mathcal{C}_j(z) \tag{2.110}$$

$$\mathcal{S}(z) = V_m \mathcal{S}_{m,m+1}(z) + V_j \mathcal{S}_j(z) \tag{2.111}$$

where the functions $\mathcal{C}_{m,m+1}(z)$ and $\mathcal{S}_{m,m+1}(z)$ are defined by:

$$\mathcal{C}_{m,m+1}(z) = \frac{1}{\alpha_m} \int_{x_m}^{x_{m+1}} \cos\left(\beta_q \left(z-y\right)\right) e^{-j\beta_e(z-y)} E_m\left(y\right) dy \tag{2.112}$$

$$\mathcal{S}_{m,m+1}(z) = \frac{1}{\alpha_m} \int_{x_m}^{x_{m+1}} \sin\left(\beta_q \left(z-y\right)\right) e^{-j\beta_e(z-y)} E_m\left(y\right) dy \tag{2.113}$$

and so:

$$\mathcal{C}_{m,m+1}(z) = \frac{1}{2\alpha_m} \left(e^{-j\beta_f z} + e^{-j\beta_s z}\right) * E_m(z) \tag{2.114}$$

$$\mathcal{S}_{m,m+1}(z) = \frac{1}{2\alpha_m} \left(e^{-j\beta_f z} - e^{-j\beta_s z}\right) * E_m(z) \tag{2.115}$$

The symbol $*$ represents the convolution product. The functions $\mathcal{C}_j(z)$ and $\mathcal{S}_j(z)$ are defined by:

$$\mathcal{C}_j(z) = \frac{1}{\alpha_j} \int_{x_j}^{z} \cos\left(\beta_q \left(z-y\right)\right) e^{-j\beta_e(z-y)} E_j\left(y\right) dy \tag{2.116}$$

$$\mathcal{S}_j(z) = \frac{1}{\alpha_j} \int_{x_j}^{z} \sin\left(\beta_q \left(z-y\right)\right) e^{-j\beta_e(z-y)} E_j\left(y\right) dy \tag{2.117}$$

If we now take in account the action on the beam of all the cavities before cavity j, we have, for a coordinate z inside the considered cavity:

$$\mathcal{C}(z) = \sum_{m=1}^{j-1} V_m \mathcal{C}_{m,m+1}\left(z\right) + V_j \mathcal{C}_j(z) \tag{2.118}$$

$$\mathcal{S}(z) = \sum_{m=1}^{j-1} V_m \mathcal{S}_{m,m+1}\left(z\right) + V_j \mathcal{S}_j(z) \tag{2.119}$$

We can see that:

$$\frac{1}{\alpha_m} e^{-j\beta_\sigma z} * E_m(z) = \frac{1}{\alpha_m} \int_{x_m}^{x_{m+1}} e^{-j\beta_\sigma (z-y)} E_m(y)\, dy \tag{2.120}$$

where $\sigma = s$ or f. We can then define the *longitudinal coupling coefficient* of the cavity m as the spatial Fourier transform of the longitudinal normalized electric field:

$$M_m(\beta_\sigma) = -\frac{1}{\alpha_m} e^{-j\beta_\sigma z_m} \int_{x_m}^{x_{m+1}} e^{j\beta_\sigma y} E_m(y)\, dy \tag{2.121}$$

If d_m is the interaction gap length we have that, for a cavity with the center in the position z_m, $x_m = z_m - \frac{d_m}{2}$ and $x_{m+1} = z_m + \frac{d_m}{2}$; if the electric field is uniform, we then find the well-known expression:

$$M_m(\beta_\sigma) = \frac{\sin\left(\beta_\sigma \frac{d_m}{2}\right)}{\left(\beta_\sigma \frac{d_m}{2}\right)} \tag{2.122}$$

The definition of the coupling coefficient allows us to write:

$$\frac{1}{\alpha_m} e^{-j\beta_\sigma z} * E_m(z) = -e^{-j\beta_\sigma (z-z_m)} M_m(\beta_\sigma) \tag{2.123}$$

so that the integrals (2.112) and (2.113) can be rewritten as:

$$\mathcal{C}_{m,m+1}(z) = -\frac{1}{2}\left(e^{-j\beta_f (z-z_m)} M_m(\beta_f) + e^{-j\beta_s (z-z_m)} M_m(\beta_s)\right) \tag{2.124}$$

$$\mathcal{S}_{m,m+1}(z) = -\frac{1}{2j}\left(e^{-j\beta_f (z-z_m)} M_m(\beta_f) - e^{-j\beta_s (z-z_m)} M_m(\beta_s)\right) \tag{2.125}$$

And, introducing:

$$\mathcal{N}_{\sigma,j}(z) = -\frac{1}{\alpha_j} e^{-j\beta_\sigma \left(z - \frac{d_j}{2}\right)} \int_{x_j}^{z} e^{j\beta_\sigma y} E_j(y)\, dy \tag{2.126}$$

the functions $\mathcal{C}_j(z)$ and $\mathcal{S}_j(z)$ become:

$$\mathcal{C}_j(z) = -\frac{1}{2}\left(e^{-j\beta_f \frac{d_j}{2}} \mathcal{N}_{f,j}(z) + e^{-j\beta_s \frac{d_j}{2}} \mathcal{N}_{s,j}(z)\right) \tag{2.127}$$

$$\mathcal{S}_j(z) = -\frac{1}{2j}\left(e^{-j\beta_f \frac{d_j}{2}}\mathcal{N}_{f,j}(z) - e^{-j\beta_s \frac{d_j}{2}}\mathcal{N}_{s,j}(z)\right) \tag{2.128}$$

The modulations of the kinetic potential and RF current can be expressed as functions of the coupling coefficients and RF voltages:

$$\begin{aligned}\tilde{V}_{kin}(z) = e^{-j\beta_e(z-x_1)}\left[\cos\left(\beta_q\left(z-x_1\right)\right)\tilde{V}_{kin}\left(x_1\right) + jZ_f\sin\left(\beta_q\left(z-x_1\right)\right)\tilde{I}\left(x_1\right)\right] + \\ - \sum_{m=1}^{j-1}\frac{V_m}{2}\left[e^{-j\beta_f(z-z_m)}M_m\left(\beta_f\right) + e^{-j\beta_s(z-z_m)}M_m\left(\beta_s\right)\right] + \\ - \frac{V_j}{2}\left[e^{-j\beta_f \frac{d_j}{2}}\mathcal{N}_{f,j}(z) + e^{-j\beta_s \frac{d_j}{2}}\mathcal{N}_{s,j}(z)\right]\end{aligned} \tag{2.129}$$

We can write:

$$\tilde{V}_{kin}(z) = \tilde{V}_{kin,init}(z) + \sum_{m=1}^{j-1}\tilde{V}_{kin,inj,m}(z) + \tilde{V}_{kin,el}(z) \tag{2.130}$$

where:

$$\tilde{V}_{kin,init}(z) = e^{-j\beta_e(z-x_1)}\left[\cos\left(\beta_q\left(z-x_1\right)\right)\tilde{V}_{kin}\left(x_1\right) + jZ_f\sin\left(\beta_q\left(z-x_1\right)\right)\tilde{I}\left(x_1\right)\right] \tag{2.131}$$

$$\tilde{V}_{kin,inj,m}(z) = -\frac{V_m}{2}\left[e^{-j\beta_f(z-z_m)}M_m\left(\beta_f\right) + e^{-j\beta_s(z-z_m)}M_m\left(\beta_s\right)\right] \tag{2.132}$$

$$\tilde{V}_{kin,inj,m}(z) = -\frac{V_j}{2}\left[e^{-j\beta_f \frac{d_j}{2}}\mathcal{N}_{f,j}(z) + e^{-j\beta_s \frac{d_j}{2}}\mathcal{N}_{s,j}(z)\right] \tag{2.133}$$

and:

$$\tilde{I}(z) = \tilde{I}_{init}(z) + \sum_{m=1}^{j-1}\tilde{I}_{inj,m}(z) + \tilde{I}_{el}(z) \tag{2.134}$$

where:

$$\tilde{I}_{init}(z) = e^{-j\beta_e(z-x_1)}\left[\cos\left(\beta_q\left(z-x_1\right)\right)\tilde{I}\left(x_1\right) + \frac{j}{Z_f}\sin\left(\beta_q\left(z-x_1\right)\right)\tilde{V}_{kin}\left(x_1\right)\right] \tag{2.135}$$

$$\tilde{I}_{inj,m}(z) = -\frac{V_m}{2Z_f}\left[e^{-j\beta_f(z-z_m)}M_m\left(\beta_f\right) - e^{-j\beta_s(z-z_m)}M_m\left(\beta_s\right)\right] \tag{2.136}$$

$$\tilde{I}_{el}(z) = -\frac{V_j}{2Z_f}\left[e^{-j\beta_f\frac{d_j}{2}}\mathcal{N}_{f,j}(z) - e^{-j\beta_s\frac{d_j}{2}}\mathcal{N}_{s,j}(z)\right] \tag{2.137}$$

The modulations of the kinetic potential and of the current at the position z are the sum of three contributions:

- one term (with subscript *init*) associated to the potential and current modulations who take place before the considered cavity;
- a sum of terms (with subscript *inj*) coming from the modulations produced by the electric fields of the cavities m of the structure, before cavity j;
- one term (with subscript *el*) who represents the re-modulation of the kinetic potential or of the current inside the considered cavity j.

2.4.3.2 Induced current from the beam in cavity j

In order to calculate the current induced by the beam in cavity j, given by:

$$\tilde{I}_{ind,j}(z) = -\frac{1}{\alpha_j}\int_{x_j}^{x_{j+1}}\tilde{I}(z)E_j(z)dz \tag{2.138}$$

we just need to integrate the three different terms of expression (2.134). Let's then define:

$$I_{init,j}(z) = -\frac{1}{\alpha_j}\int_{x_j}^{x_{j+1}}\tilde{I}_{init}(z)E_j(z)dz \tag{2.139}$$

$$I_{inj,j}(z) = -\frac{1}{\alpha_j}\int_{x_j}^{x_{j+1}} \tilde{I}_{inj}(z)E_j(z)dz \tag{2.140}$$

$$I_{el,j}(z) = -\frac{1}{\alpha_j}\int_{x_j}^{x_{j+1}} \tilde{I}_{el}(z)E_j(z)dz \tag{2.141}$$

where $\tilde{I}_{init,j}(z)$, $\tilde{I}_{inj,j}(z)$ and $\tilde{I}_{el,j}(z)$ are given respectively from equations (2.135),(2.136) and (2.137).

The first contribution $I_{init,j}(z)$ can be written as:

$$\begin{aligned} I_{init,j}(z) = &-\left(\frac{1}{\alpha_j}\int_{x_j}^{x_{j+1}} \cos\left(\beta_q\left(z-x_1\right)\right)e^{-j\beta_e(z-x_1)}E_j(z)dz\right)\tilde{I}\left(x_1\right) + \\ &+\frac{j}{Z_f}\left(-\frac{1}{\alpha_j}\int_{x_j}^{x_{j+1}} \sin\left(\beta_q\left(z-x_1\right)\right)e^{-j\beta_e(z-x_1)}E_j(z)dz\right)\tilde{V}_{kin}\left(x_1\right) \end{aligned} \tag{2.142}$$

The two integrals on the right of eq. (2.142) are respectively $\left[\mathcal{C}_{j,j+1}\left(x_1\right)\right]^*$ and $\left[\mathcal{S}_{j,j+1}\left(x_1\right)\right]^*$ and can be expressed as functions of the coupling coefficients of cavity j, like in equations (2.124) and (2.125). We get:

$$I_{init,j}(z) = \lambda_{j,1}^I\tilde{I}\left(x_1\right) + \lambda_{j,1}^V\tilde{V}_{kin}\left(x_1\right) \tag{2.143}$$

where:

$$\lambda_{j,1}^I = \frac{1}{2}\left(e^{-j\beta_f(z_j-x_1)}\left[M_j\left(\beta_f\right)\right]^* + e^{-j\beta_s(z_j-x_1)}\left[M_j\left(\beta_s\right)\right]^*\right) \tag{2.144}$$

$$\lambda_{j,1}^V = \frac{1}{2Z_f}\left(e^{-j\beta_f(z_j-x_1)}\left[M_j\left(\beta_f\right)\right]^* - e^{-j\beta_s(z_j-x_1)}\left[M_j\left(\beta_s\right)\right]^*\right) \tag{2.145}$$

The second contribution $I_{inj,j}$ to the induced current is given by the integration of the $\tilde{I}_{inj,j,m}(z)$:

$$I_{inj,j,m} = -\frac{1}{\alpha_j}\int_{x_j}^{x_{j+1}} \tilde{I}_{inj,m}(z)E_j(z)dz \tag{2.146}$$

we have:

$$I_{inj,j} = \sum_{m=1}^{j-1} I_{inj,j,m} \tag{2.147}$$

For eq. (2.146) we get:

$$\begin{aligned} I_{inj,j,m} = \frac{V_m}{2Z_f} \Bigg[& M_m(\beta_f)\, e^{j\beta_f z_m} \left(\frac{1}{\alpha_j} \int_{x_j}^{x_{j+1}} e^{j\beta_f z} E_j(z) dz \right) + \\ & - M_m(\beta_s)\, e^{j\beta_s z_m} \left(\frac{1}{\alpha_j} \int_{x_j}^{x_{j+1}} e^{j\beta_s z} E_j(z) dz \right) \Bigg] \end{aligned} \tag{2.148}$$

These two integrals are, with the exception of a phase factor, the conjugates of $M_j(\beta_f)$ and $M_j(\beta_s)$, so:

$$I_{inj,j,m} = -Y_{trans,j,m} V_m \tag{2.149}$$

where the transadmittance $Y_{trans,j,m}$ associated to cavity m for cavity j is defined by:

$$\begin{aligned} Y_{trans,j,m} = \frac{1}{2Z_f} \Big[& M_m(\beta_f)\, e^{-j\beta_f (z_j - z_m)} \left[M_j(\beta_f) \right]^* + \\ & - M_m(\beta_s)\, e^{-j\beta_s (z_j - z_m)} \left[M_j(\beta_s) \right]^* \Big] \end{aligned} \tag{2.150}$$

We then obtain:

$$I_{inj,j} = -\sum_{m=1}^{j-1} Y_{trans,j,m} V_m \tag{2.151}$$

The last contribution to the induced current inside cavity j is given by:

$$I_{el,j} = -\frac{1}{\alpha_j} \int_{x_j}^{x_{j+1}} \tilde{I}_{el}(z) E_j(z) dz \tag{2.152}$$

or:

$$I_{el,j} = \frac{V_j}{2Z_f}\left[e^{-j\beta_f\frac{d_j}{2}}\left(\frac{1}{\alpha_j}\int_{x_j}^{x_{j+1}}\mathcal{N}_{f,j}E_j(z)dz\right) + \right. \\ \left. - e^{-j\beta_s\frac{d_j}{2}}\left(\frac{1}{\alpha_j}\int_{x_j}^{x_{j+1}}\mathcal{N}_{s,j}E_j(z)dz\right)\right] \tag{2.153}$$

where the coefficient $\mathcal{N}_j(\beta_\sigma)$ is defined by:

$$\mathcal{N}_j(\beta_\sigma) = \frac{1}{\alpha_j^2}\int_{x_j}^{x_{j+1}}\int_{x_j}^{z} e^{-j\beta_\sigma(z-y)}E_j(z)E_j(y)dzdy \tag{2.154}$$

We have:

$$I_{el,j} = -Y_{el,j}V_j \tag{2.155}$$

where the *electronic charge admittance* is defined by:

$$Y_{el,j} = \frac{1}{2Z_f}\left(\mathcal{N}_j(\beta_f) - \mathcal{N}_j(\beta_s)\right) \tag{2.156}$$

It is now possible to express the electronic charge conductance $G_{el,j} = \Re\left[Y_{el,j}\right]$ as a function of the coupling coefficients associated to cavity j. In order to do this, let's integrate by part expression (2.154):

$$\mathcal{N}_j(\beta_\sigma) = \frac{1}{\alpha_j^2}\left(\int_{x_j}^{x_{j+1}} e^{j\beta_\sigma z}E_j(z)dz\right)\left(\int_{x_j}^{x_{j+1}} e^{-j\beta_\sigma z}E_j(y)dz\right) - \left[\mathcal{N}_j(\beta_\sigma)\right]^* \tag{2.157}$$

By comparing with eq. (2.121), and separating the real and the imaginary part we get:

$$\Re\left[\mathcal{N}_j(\beta_\sigma)\right] = \frac{1}{2}\left|M_j(\beta_\sigma)\right|^2 \tag{2.158}$$

$$\Im\left[\mathcal{N}_j(\beta_\sigma)\right] = \frac{1}{\alpha_j^2}\int_{x_j}^{x_{j+1}}\int_{x_j}^{z}\sin\left(\beta_\sigma(y-z)\right)E_j(z)E_j(y)\,dzdy \tag{2.159}$$

and we obtain the following expression for the electronic charge conductance:

$$G_{el,j} = \frac{1}{4Z_f}\left(\left|M_j\left(\beta_f\right)\right|^2 - \left|M_j\left(\beta_s\right)\right|^2\right) \tag{2.160}$$

While, for the susceptance $B_{el,j} = \Im\left[Y_{el,j}\right]$:

$$\begin{aligned} B_{el,j} = \frac{1}{2\alpha_j^2 Z_f}\Bigg[&\int_{x_j}^{x_{j+1}}\int_{x_j}^{z}\cos\left(\beta_f\left(y-z\right)\right)E_j(z)E_j\left(y\right)dzdy + \\ &- \int_{x_j}^{x_{j+1}}\int_{x_j}^{z}\sin\left(\beta_s\left(y-z\right)\right)E_j(z)E_j\left(y\right)dzdy\Bigg] \end{aligned} \tag{2.161}$$

The RF current induced in cavity j is then the sum of three contributions:

$$I_{ind,j} = I_{init,j} + I_{inj,j} + I_{el,j} \tag{2.162}$$

The first one $I_{init,j}$ is the result of the kinetic potential and RF current modulations produced before the multicavity structure:

$$I_{init,j} = \lambda_{j,1}^{I}\tilde{I}\left(x_1\right) + \lambda_{j,1}^{V}\tilde{V}_{kin}\left(x_1\right) \tag{2.163}$$

The second $I_{inj,j}$ is due to the modulations of cavities before cavity j:

$$I_{inj,j} = -\sum_{m=1}^{j-1} Y_{trans,j,m}V_m \tag{2.164}$$

And the third $I_{el,j}$ is due to the modulations inside cavity j:

$$I_{el,j} = -Y_{el,j}V_j. \tag{2.165}$$

This space charge theory is a small signal, one-dimensional theory. It can be used to study the interaction between a modulated beam and a sequence of cylindrical resonators by taking in account, at every longitudinal position in a considered cavity, the different contributions to the beam modulations given by the previous structures and by the considered one. The combination of the electronic equations and the circuit equations can also be used to study the oscillation conditions and the stability of the system [20].

2.5 Klystron design and simulation

The kinematic and the space charge theory exposed in the previous sections are not sufficient to give a complete description of the interaction between the electromagnetic structure and the beam. The first one because it does not take in account the effect of the Coulombian repulsion between particles; and the second because it is a one-dimensional, small signal theory. In a klystron, and in general in all the devices based on the interaction between an electron beam and a RF circuit, the full analysis of the device behaviour requires the use of simulation programs.

The design of klystrons lies then on an intensive utilization of simulation codes which allow to evaluate the complete interaction in the large signals hypothesis. The tools used in klystron design are several, but they can be divided in two main categories:

- the 1-D *Disk codes*;
- the *particle in cell* (PIC) codes.

In the so called "disk codes" the beam is discretized along its axis, and the non-linear dynamics of disks with identical mass and charge is evaluated. The most used of these codes is probably AJDisk, who is the more advanced and modern version of the DOS/FORTRAN based code JPNDisk [22], written in 1982 at the Stanford Linear Accelerator Center and inspired to the works of T. Kageyama [23] and P.J. Tallerico [8]. The equations of motion of every disk are solved at every time step by taking in account the interaction with both the cavities RF fields and the space charge field [24]. Every cavity is modelized by a RLC parallel circuit who is excited by the disks transit at the interaction gap level. The result is an RF voltage across this gap. For every disk, the Coulombian repulsion field is expressed in his own reference system and it is then Lorentz transformed in order to obtain an analytical expression of the space charge field. The calculation of currents and voltages induced in the cavities is iterated to obtain a self-consistent solution of the

problem. The code is then a *steady state* code, and it does not give information about the system transient evolution. AJDisk is capable to simulate also multigap and higher harmonics cavities, but it does not give any information on the reflected fields from the input and output cavities. It is then not very appropriate to simulate devices with more complicated shape cavities, such as multibeam klystrons. The other limitation is that the transverse motion is not taken into account, since the code is 1-D, and the focusing field can not be simulated. Even with these limitations, it is one of the most important simulation codes used in the klystron design phase, thanks to its reliability and fast exacution time.

The PIC codes are a more complex class of codes, widely used for plasma physics numerical simulations. They can use a wide range of algorithms, but they usually includes some standard steps:

- the integration of the equations of motion ;
- the interpolation of charge and current source terms to the field mesh;
- the computation of the fields on mesh points;
- the interpolation of the fields from the mesh to the particle locations.

PIC codes represent the particles with a bunch of test particles or *macroparticles* and solve simultaneously the Maxwell equations and the relativistic dynamic equations on a mesh interval. The macroparticles have an assigned mass and charge and they are characterized by their positions and velocities. The number of real particles corresponding to a super-particle must be chosen such that sufficient statistics can be collected on the particle motion. The number of simulated particles is then usually very large ($> 10^5$), and often the particle mover is the most time consuming part of a PIC code. Thus, it is required to be of high accuracy and speed and much effort is spent on optimizing the traking routine, which can be either implicit or explicit. The Maxwell equations are solved with numerical methods that are usually Finite Difference Methods (FDM), Finite Element Methods (FEM), or spectral methods, like the Fast Fourier Transform (FFT).

With the FDM, the continuous domain is replaced with a discrete grid of points, on which the electric and magnetic fields are calculated. Derivatives are then approximated with differences between neighboring grid-point values and thus partial differential equations are turned into algebraic equations.

Using FEM, the continuous domain is divided into a discrete mesh of elements. The partial differential equations are treated as an eigenvalue problem and initially a trial solution is calculated using basis functions that are localized in each element. The final solution is then obtained by optimization until the required accuracy is reached.

Also spectral methods transform the partial differential equations into an eigenvalue problem, but this time the basis functions are high order and defined globally over the whole domain. The domain itself is not discretized in this case, it remains continuous. Again, a trial solution is found by inserting the basis functions into the eigenvalue equation and then optimized to determine the best values of the initial trial parameters.

PIC codes, like MAGIC [25] or CST Particle Studio [26], are the most important simulation tools used to simulate complete klystron devices with high accuracy. They are normally used after that the "electric project" has been done with the faster Disk codes. The PIC codes goal is to mimic nature, in order to *verify* that the designed device behaves as desired. Diagnostics allow the researcher to observe the system, and interpret what is happening in a physical sense: they give a 2-D or 3-D descriprion of the system and complete information on the cavity fields, including the transient evolution. At the same time they require the complete electromagnetic project of the device to be simulated and also a considerable computational time, expecially if we want to perform start-to-end simulations.

Among PIC codes, a particular mention has to go to the so called *gun codes*, like the code MICHELLE: this is a general purpose two-dimensional and three-dimensional charged particle beam optics code [27]. MICHELLE has models for both equilibrium flow particle trajectories and initial-value time-dependent beam trajectories. It self-consistently computes the emis-

sion and transport of charged particles in the presence of electrostatic and magnetostatic fields. The charged particles contribute to the static fields, and the static fields act on the charged particles. The equilibrium flow particle model is also known as a steady-state static PIC code or a gun code. The time-dependent model is an electrostatic time-domain particle-in-cell code.

The finite-element field solver computes the electrostatic and magnetostatic potentials, the latter a full vector potential in 3-D. The field solver works with both multiblock structured grids and unstructured grids and it is coupled with particle trackers for both mesh types.

The basic algorithm starts off by solving Laplace's equation for the electrostatic potential, since no particles exist in the problem on the very first cycle [28]. Once the fields are solved to some accuracy, the Particle Tracking Algorithm begins. In this algorithm, particles are tracked in fixed fields, and they are advanced at every time step. The system is then queried for remaining particles. If particles remain in the system, those particles are advanced another time step. This continues until no particles remain, signaling that the particle advance loop is completed. At this time, one complete cycle (field solver followed by a complete particle tracking through the system) has been completed, and a convergence test is done to determine if the calculation should continue. If convergence has not been met, then the algorithm returns to the field solution and starts another cycle, where the accumulated particle sources are now used to solve Poisson's equation. Then, in these updated fields, the particles are traced once again, and a test for convergence done once again. This cycle continues until convergence is met. The converged solution will represent the equilibrium, steady-state self-consistent solution of the system being modeled.

2.6 Subject of the present work

In the previous section we described the working algorithm implemented in the code MICHELLE in order to obtain a steady-state self-consistent solution for the system in presence of static fields. In the present work, we

will develop a steady state and self-consistent algorithm valid also for RF fields who can be applied to the case of klystron cavities, feeded or not. This will be implemented to write a klystron simulation code who finds a steady state solution for the device. The simulation algorithm is based on the search of the steady state solution inside the RF cavities by iteratively solving the power balance equation inside the resonator. The solution allows to determine the amplitude and phase of the electromagnetic field inside the structure starting from the fundamental cavity mode. The latter can be the analytical pillbox field (as a first approximation), or can be imported by 2-D electromagnetic simulation codes such as SUPERFISH [29], or from the Finite Element Method based code developed at the Stanford Linear Accelerator Center by Prof. Sami Tantawi [30]. The fundamental theory necessary to obtain the formulae used to develop the simulation algorithm is exposed in chapter 3.

Chapter 4 is dedicated to the numerical method to be used to integrate the particles equations of motion in the algorithm. It is known that numerical methods such as the ordinary Runge-Kutta methods are not ideal for integrating Hamiltonian systems, because the numerical approximation to a Hamiltonian system obtained from an ordinary numerical method does introduce a non-Hamiltonian perturbation. This problem has led to the introduction of methods of symplectic integration for Hamiltonian systems, which do preserve the features of the Hamiltonian structure by arranging that each step of the integration be a canonical or symplectic transformation.

The application of the algorithm to simple examples in absence of space charge effects and the check of the self-consistency of the method is treated in Chapter 5, together with a comparison with the results obtained with the kinematic theory and with the code AJDisk.

Chapter 6 is finally dedicated to the problem of the introduction in the code of the effects of the space charge fields inside the drift tubes and an iterative method for the steady state solution is presented.

Chapter 3

The cavity simulation algorithm

The first stage when writing a klystron simulation code is the study of the non linear interaction between the electron beam and the electromagnetic field inside an RF cavity.

In the following sections we will derive the self-consistent algorithm which finds a steady state solution for the system composed by the electron beam plus an electromagnetic resonator, either feeded (as it is for the klystron input cavity), or not.

This will be done by using the complex power balance inside the resonator in order to determine the electromagnetic field taking in account also the beam loading. We will then obtain an equation which expresses the amplitude and phase of the field as a function of the beam current density and that can be solved iteratively in order to obtain a complete description of the mutual interaction between the electron beam and the klystron resonators.

3.1 Cavity balance equation

Let's consider a generic electromagnetic resonator, fed from a RF driver and with an electron beam going through it.

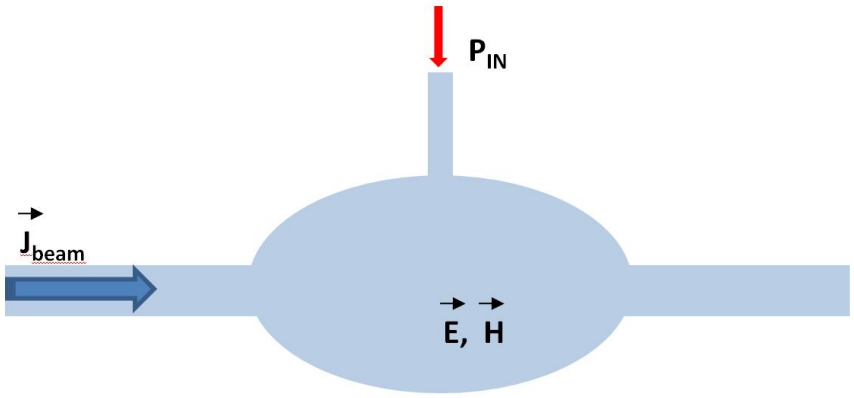

Figure 3.1: Generic klystron input cavity.

The field in the cavity is governed by Maxwell equations:

$$\nabla \times \vec{E} = -j\omega\mu\vec{H} \tag{3.1}$$

$$\nabla \times \vec{H} = j\omega\epsilon\vec{E} + \vec{J} \tag{3.2}$$

where $\vec{J}$ is the fundamental harmonic of the current density produced by the electron beam inside the cavity and ω is the frequency of the cavity field. Since the natural modes of a resonator form a complete and orthogonal set, the cavity field can be expanded in terms of these natural modes:

$$\vec{E} = \sum_i \alpha_i \vec{e_i} \tag{3.3}$$

$$\vec{H} = \sum_i \beta_i \vec{h_i} \tag{3.4}$$

where $\vec{e_i}$ and $\vec{h_i}$ satisfy Maxwell equations with the absence of the excitation term $\vec{J}$:

$$\nabla \times \vec{e_i} = -j\omega_i\mu\vec{h_i} \tag{3.5}$$

$$\nabla \times \vec{h_i} = j\omega_i\epsilon\vec{e_i} \tag{3.6}$$

By substituting the expansions (3.3) and (3.4) in equation (3.1) we get:

$$\nabla \times \sum_i \alpha_i \vec{e_i} = -j\omega\mu \sum_i \beta_i \vec{h_i} \tag{3.7}$$

Then, inverting the curl with the sum, and by using the (3.5) and (3.6):

$$\sum_i \alpha_i (-j\omega_i \mu \vec{e_i}) = -j\omega\mu \sum_i \beta_i \vec{h_i} \tag{3.8}$$

Finally, multiplying by $\vec{h_i}$ and integrating over the volume of the cavity, due to mode orthogonality we get:

$$\beta_i = \frac{\omega_i}{\omega} \alpha_i \tag{3.9}$$

The last relation is true, in general, only if the cavity is ideal, because in this case it is right to invert the sum and the curl in equation (3.7); if the cavity has losses, the series (3.3) and (3.4) are not uniformly convergent on the cavity walls and we are not allowed to write eq. (3.8). Anyway, if the cavity is driven at a frequency that is close to the resonant frequency of a particular mode (i.e. the fundamental), and if the quality factor of that mode is high enough, the amplitude of that mode will be large with respect to all others. This case is very common for klystron cavities, so we can consider only one mode in the expansions (3.3) and (3.4), and we can also use relation (3.9). We have then:

$$\vec{E} \cong \alpha \vec{e_0} \tag{3.10}$$

$$\vec{H} \cong \beta \vec{h_0} \tag{3.11}$$

The field in the cavity is equal to the natural field of the design mode of the structure, multiplied by a complex coefficient, α, to be determined in amplitude and phase. To get an expression for this coefficient α, we can apply the Poynting theorem [31]: the cavity has a volume V, and it is delimited by a surface S, as in fig.(3.2):

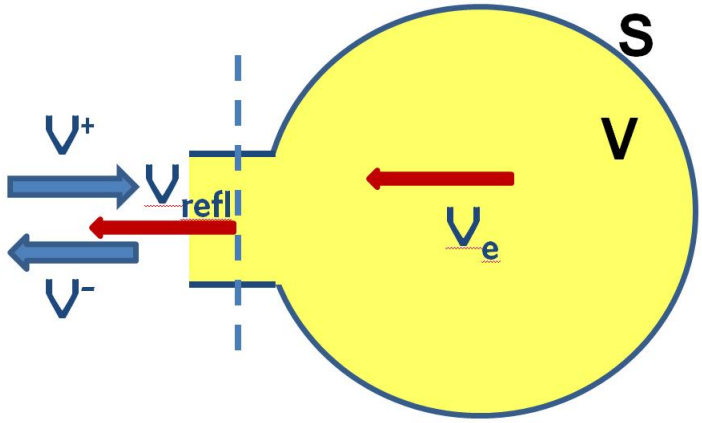

Figure 3.2: Generic coupled cavity.

$$\frac{1}{2}\int_S \left(\vec{E}\times\vec{H}^*\right)\cdot\hat{n}dS = j\omega\left(\frac{1}{2}\epsilon\int_V \vec{E}\cdot\vec{E}^*dV - \frac{1}{2}\mu\int_V \vec{H}\cdot\vec{H}^*dV\right) + \\ -\frac{1}{2}\int_V \vec{E}\cdot\vec{J}^*_{beam}dV$$

The surface S is just inside the cavity walls so that in the expression of the current density we don't have to consider the current flow on the metal, but only the beam contribute. Let's now consider each term of equation (3.12) separately.

The first integral can be written as:

$$\frac{1}{2}\int_S \left(\vec{E}\times\vec{H}^*\right)\cdot\hat{n}dS = \frac{1}{2}\int_{S_1} \left(\vec{E}\times\vec{H}^*\right)\cdot\hat{n}dS + \frac{1}{2}\int_{S_2} \left(\vec{E}\times\vec{H}^*\right)\cdot\hat{n}dS \tag{3.12}$$

The last term in eq. (3.12) represents the total power flux across the waveguide aperture, and it can be written by using the transmission line formalism [32]; so we have:

$$\frac{1}{2}\int_S \left(\vec{E}\times\vec{H}^*\right)\cdot\hat{n}dS = -\frac{1}{2}\left(V^+ + V^-\right)\left(I^+ + I^-\right)^* + \int_{S_2} \left(\vec{E}\times\vec{H}^*\right)\cdot\hat{n}dS \tag{3.13}$$

The integral on the surface S_2 is not zero for a lossy cavity; we can then use the Leontovich-Schelkunoff condition for a good conductor [33] [34]:

$$\widehat{n} \times \vec{E} = \frac{1+j}{\sigma d}\left(\widehat{n} \times \vec{H}\right) \times \widehat{E} \tag{3.14}$$

where σ is the conductivity and d is the skin depth; we are assuming that, in the good conductor, the fields are parallel to the surface, and propagate normally to it, with magnitudes that depend only on the tangential magnetic field that exist just outside the surface. So we have that just outside the surface there is a small tangential electric field given by eq. (3.14). In this approximation there is also a small normal component of $\vec{H}$ just outside the surface. The existence of a small tangential component of $\vec{E}$ outside the surface (in addiction to the normal $\vec{E}$ and tangential $\vec{H}$) means that there is power flowing into the conductor.

The last integral in equation (3.13) becomes then:

$$\frac{1}{2}\int_{S_2}\left(\vec{E} \times \vec{H}^*\right) \cdot \widehat{n} dS = \frac{1}{2}\int_{S_2} \vec{H}^* \cdot \left(\widehat{n} \times \vec{E}\right) dS = \frac{1}{2}\frac{1+j}{\sigma d}\int_{S_2}\left|\widehat{n} \times \vec{H}\right|^2 dS \tag{3.15}$$

On the surface S_2 we can assume that the magnetic field is purely tangential and approximate [35]:

$$\widehat{n} \times \vec{H} \cong \beta \vec{H_0} \tag{3.16}$$

Eq.(3.15) becomes then:

$$\frac{1}{2}\int_{S_2}\left(\vec{E} \times \vec{H}^*\right) \cdot \widehat{n} dS = \frac{1}{2}\frac{1+j}{\sigma d}\int_{S_2}\left|\beta \vec{h_0}\right|^2 dS \tag{3.17}$$

We can now express the right member of the last equation by using the definition of the quality factor Q_0 of the cavity:

$$\frac{1}{2\sigma d}\int_{S_2}\left|\beta \vec{h_0}\right|^2 dS = \frac{\omega_0}{Q_0}\left|\beta\right|^2 u \tag{3.18}$$

where $u = \frac{1}{2}\epsilon_0 \int_V \left|\vec{e_0}\right|^2 dV$. The integral over the surface S_2 becomes then:

$$\frac{1}{2}\int_{S_2}\left(\vec{E}\times\vec{H}^*\right)\cdot\widehat{n}dS=(1+j)\,\frac{\omega_0}{Q_0}\,|\beta|^2\,u \tag{3.19}$$

Substituting equations (3.13) and (3.19) in eq. (3.12) we have that the power balance equation for the cavity is :

$$-\frac{1}{2}\left(V^+ + V^-\right)\left(I^+ + I^-\right)^* = -\,(1+j)\,\frac{\omega_0}{Q_0}\,|\beta|^2\,u + j\omega_0\,|\alpha|^2\,u\delta + \\ -\,\frac{1}{2}\alpha\int_V \vec{e_0}\cdot\vec{J}^*_{beam}dV$$

where $\delta=\frac{\omega}{\omega_0}-\frac{\omega_0}{\omega}$.

The left side of equation (3.20) contains the power flowing across the waveguide aperture surface; the incoming wave V^+ is given by:

$$V^+=\sqrt{2Z_0P_{IN}}e^{j\Phi^+} \tag{3.20}$$

while V^- is the outcoming wave, i.e. the wave that comes back toward the generator from the cavity aperture, and it is given by the superposition of a reflected wave and an emitted wave:

$$V^-=V_{refl}+V_e=\Gamma V_+ + V_e \tag{3.21}$$

If the cavity aperture is small enough we can assume that the reflection coefficient Γ is equal to -1, and obtain:

$$V^-=\Gamma V_+ + V_e=-V^+ + V_e \tag{3.22}$$

We then have that the first member of the balance equation becomes:

$$-\frac{1}{2}\left(V^+ + V^-\right)\left(I^+ + I^-\right)^* = \frac{1}{2Z_0}V_eV_e^* - \frac{V_eV^{+*}}{Z_0} \tag{3.23}$$

with:

$$P_e=\frac{\omega_0U}{Q_{ext}}=\frac{\omega_0\,|\alpha|^2\,u}{Q_{ext}} \tag{3.24}$$

By substituting the previous expression in eq.(3.20) we have:

$$\frac{\omega_0 |\alpha|^2 u}{Q_{ext}} - \frac{V_e V^{+*}}{Z_0} = -(1+j)\frac{\omega_0}{Q_0}|\beta|^2 u + j\omega_0 |\alpha|^2 u\delta - \frac{1}{2}\alpha \int_V \vec{e_0} \cdot \vec{J}^*_{beam} dV \tag{3.25}$$

To get an equation for the complex coefficient α we need now an expression for the emitted wave V_e. In order to do this, we can observe that the amplitude of the emitted wave from the cavity depends only on the stored energy, while, if there is no beam, its phase can be expressed as a function of the phase of the incoming field V^+; if there is also the beam, it depends also on the phase of the field inside the cavity (i.e., on the phase of α) [36]. We can then start by getting V_e from equation (3.25) for $J_{beam} = 0$.

$$V_e = \frac{\omega_0 |\alpha|^2 u Z_0}{|V^+|}\left(\frac{1}{Q_{ext}} + \frac{x^2}{Q_0} + j\left(\frac{x^2}{Q_0} - \delta\right)\right) e^{j\Phi^+} \tag{3.26}$$

where $x = \frac{\omega_0}{\omega}$ and Φ^+ is the phase of the incoming wave. Since from the definition of the external Q we also have:

$$|V_e| = \sqrt{\frac{2\omega_0 |\alpha|^2 u Z_0}{Q_{ext}}} \tag{3.27}$$

we can write (without the beam):

$$V_e = \sqrt{\frac{2\omega_0 |\alpha|^2 u Z_0}{Q_{ext}}} e^{j\left(\Phi^+ + \arctan\left(\frac{x^2 - Q_0\delta}{Q_0 - Q_{ext}x^2}\right)\right)} \tag{3.28}$$

And finally, if the beam is in the cavity, we have to take in account also the phase of the field inside the cavity (phase of the coefficient α):

$$V_e = \alpha\sqrt{\frac{2\omega_0 |\alpha|^2 u Z_0}{Q_{ext}}} e^{j\left(\Phi^+ + \arctan\left(\frac{x^2 - Q_0\delta}{Q_0 - Q_{ext}x^2}\right)\right)} \tag{3.29}$$

By substituting expression (3.29) in eq. (3.25) we have the final equation for the coefficient α:

$$\alpha^* = \frac{2\sqrt{\frac{\omega_0 u P_{IN}}{Q_{ext}}} e^{j\left(\Phi^+ + \arctan\left(\frac{x^2 - Q_0\delta}{Q_0 - Q_{ext}x^2}\right)\right)} - \frac{1}{2}\int_V \vec{e_0}\cdot\vec{J}^*_{beam}dV}{\omega_0 u\left(\frac{1}{Q_{ext}} + \frac{x^2}{Q_0} + j\left(\frac{x^2}{Q_0} - \delta\right)\right)} \tag{3.30}$$

We now have a complex expression for the amplitude and phase of the electric field inside the klystron cavity. The magnetic field coefficient can then be obtained from eq. (3.9).

The first term in eq.(3.30) is due to the input power coming from the waveguide (P_{IN}), while the last integral represents the interaction between the cavity field and the current density due to the electron beam. This current density can be represented by the sum of N individual electron currents:

$$\vec{J}_{Btot} = \sum_{i=1}^{N} q_i \vec{v_i} \delta\left(\vec{r} - \vec{r_i}\right) \tag{3.31}$$

where q_i is the charge of particle i. The fundamental harmonic of this current is given by:

$$\begin{aligned} \vec{J}_{beam} &= \frac{2}{T}\left(\int_0^T \vec{J}_{Btot} e^{-j\omega\tau} d\tau\right) e^{j\omega t} = \\ &= \frac{2}{T}\left(\sum_{i=1}^{N} q_i \int_0^T \vec{v_i}\left(\tau\right)\delta\left(\vec{r} - \vec{r_i}\right) e^{-j\omega\tau} d\tau\right) e^{j\omega t} \end{aligned} \tag{3.32}$$

The term representing the interaction between the electron beam and the electric field in eq. (3.30) becomes then:

$$\begin{aligned} \int_V \vec{e_0}^* \cdot \vec{J}_{beam} = \frac{2}{T}\sum_{i=1}^{N} q_i \int_0^L \int_0^R \int_0^{2\pi} e^{j\omega t}\vec{e_0}^*\left(\rho, z, t\right)\cdot \\ \cdot \int_0^T \vec{v_i}\left(\tau\right)\frac{\delta\left(\rho - \rho_i\right)\delta\left(z - z_i\right)\delta\left(\phi - \phi_i\right)}{\rho_i} e^{-j\omega\tau} d\tau \rho d\rho d\phi dz \end{aligned} \tag{3.33}$$

where $\vec{e_0^*} = \widehat{e}_0 e^{-j\omega t}$.

Since we don't know *when* an electron will leave the interaction region (particles with different initial conditions spend different times inside the cavity gap), but we know *where* it will leave, it is more suitable to evaluate the velocities and positions of the electrons in terms of the longitudinal position z. To this end we change the variables inside the δ function appearing in equation (3.33) from t to z according to:

$$\delta\left(z-z_i\right)=\frac{\delta\left(t-t_i\right)}{\frac{dz}{dt}} \tag{3.34}$$

Substituting into (3.33) we get:

$$\begin{aligned}\int_V \vec{e_0}^* \cdot \vec{J}_{beam} &= \frac{2}{T}\sum_{i=1}^{N} q_i \int_0^L \widehat{e}_0\left(\rho_i, z\right) \cdot \int_0^T \frac{\vec{v_i}\left(\tau\right)}{v_{zi}\left(\tau\right)} \delta\left(\tau-\tau_i\right) e^{-j\omega\tau} d\tau dz = \\ &= \frac{2}{T}\sum_{i=1}^{N} q_i \int_0^L \widehat{e}_0\left(\rho_i\left(z\right), z\right) e^{-j\omega t(z)} \cdot \frac{\vec{v_i}\left(t_i\left(z\right)\right)}{v_{zi}\left(t_i\left(z\right)\right)} dz = \\ &= \frac{2}{T}\sum_{i=1}^{N} q_i \int_0^L \vec{e_0}^*\left(\rho_i\left(z\right), t_i\left(z\right), z\right) \cdot \frac{\vec{v_i}\left(t_i\left(z\right)\right)}{v_{zi}\left(t_i\left(z\right)\right)} dz\end{aligned} \tag{3.35}$$

Equation (3.30) becomes then:

$$\begin{aligned}\alpha^* = &\frac{2\sqrt{\frac{\omega_0 u P_{IN}}{Q_{ext}}} e^{j\left(\Phi^+ + \arctan\left(\frac{x^2 - Q_0\delta}{Q_0 - Q_{ext}x^2}\right)\right)}}{\omega_0 u\left(\frac{1}{Q_{ext}} + \frac{x^2}{Q_0} + j\left(\frac{x^2}{Q_0} - \delta\right)\right)} + \\ &- \frac{\frac{1}{T}\left(\sum_{i=1}^{N} q_i \int_0^L \vec{e_0}^*\left(\rho_i\left(z\right), t_i\left(z\right), z\right) \cdot \frac{\vec{v_i}(t_i(z))}{v_{zi}(t_i(z))} dz\right)^*}{\omega_0 u\left(\frac{1}{Q_{ext}} + \frac{x^2}{Q_0} + j\left(\frac{x^2}{Q_0} - \delta\right)\right)}\end{aligned} \tag{3.36}$$

3.2 The simulation algorithm

Let's now analyze equation (3.36): in order to get the value of the field coefficient α we need to know the positions and the velocities of all the

particles along all the cavity. This means that we have to solve the relativistic equations of motion for all the N particles in presence of the electromagnetic field given by eq (3.10) and (3.11). We can procede with the following steps:

1. assume an initial value α_1 for the field coefficient;
2. integrate the equations of motion for each particle through the lenght of the cavity ;
3. calculate the new value α_2 of the field coefficient through eq. (3.36);
4. if $\alpha_2 = \alpha_1$ (within a certain tolerance) go to the next step; otherwise assume a new value for α_1 and go to step 2;
5. calculate the steady state solution for the electromagnetic field by eq.(3.9), (3.10) and (3.11).

The next step is then to write the relativistic equations of motion in a form suitable for numerical integration. This is done in the following chapter.

Chapter 4

The equations of motion

4.1 Hamiltonian systems

A dynamical system consists of an abstract phase space or state space, whose coordinates describe the state at any instant, and a dynamical rule that specifies the immediate future of all state variables, given only the present values of those same state variables. Mathematically, a dynamical system is described by an initial value problem. The implication is that there is a notion of time and that a state at one time evolves to a state or possibly a collection of states at a later time.

A dynamical system described by the following ordinary differential equations:

$$\frac{dq_i}{dt} = \frac{\partial H}{\partial P_i} \tag{4.1}$$

$$\frac{dP_i}{dt} = -\frac{\partial H}{\partial q_i} \tag{4.2}$$

or, in a more compact form:

$$\frac{d\mathbf{z}}{dt} = \mathbf{J}\nabla_z H\left(\mathbf{z}, t\right) \tag{4.3}$$

where the Hamiltonian H is a smooth scalar function of the extended phase space variables $\mathbf{z} := \{\vec{q}, \vec{P}\}$ and time t, and $\mathbf{J}$ is the $2d \times 2d$ *canonical structure matrix*:

$$\mathbf{J} := \begin{bmatrix} 0 & +I_d \\ -I_d & 0 \end{bmatrix} \tag{4.4}$$

is said to be Hamiltonian. If H does not depend on time (i.e. only time-independent forces are acting), it is a constant of motion and the system is *autonomous*. Similarly if the Hamiltonian is independent of one of the configuration variables (the variable is ignorable), then the corresponding canonical momentum is an invariant, or a *first integral* of motion.

Let's now denote the solution of any differential equation $\dot{\mathbf{z}} = \mathbf{f}(\mathbf{z})$ through a given initial condition $\mathbf{z}^0$ by $\mathbf{z}(t, \mathbf{z}^0)$; assuming that this solution is globally defined, we have that its value at any given point on the trajectory determines the value at all later points on the trajectories; in effect, the solution defines a mapping which take initial data to later points along the trajectories:

$$\mathbf{\Phi}_t(\mathbf{z}^0) = \mathbf{z}(t, \mathbf{z}^0) \qquad\qquad \mathbf{z}^0 \in \mathbb{R}^k \tag{4.5}$$

The map $\mathbf{\Phi}_t$ is the *flow map* of the given system: in general, the flow map cannot be written down explicitly but can only be approximated numerically. Each Hamiltonian system gives then rise to a family of flow maps parametrized by time t; we have that, if we solve the differential equations from a given point $\mathbf{z}^0$ up to a time t_1, then we solve from the resulting point forward t_2 units of time, the effect is the same as solving the equations with initial value $\mathbf{z}^0$ up to time $t_1 + t_2$. In terms of the mapping, $\mathbf{\Phi}_{t_1} \circ \mathbf{\Phi}_{t_2} = \mathbf{\Phi}_{t_1+t_2}$, and we say that the family of flow maps is closed under the composition operation. The flow map $\mathbf{\Phi}_0$ at $t = 0$ is the identity map, and every flow map has evidently an inverse in the family:

$$\mathbf{\Phi}_{-t} \circ \mathbf{\Phi}_t = \mathbf{\Phi}_0 = \mathbf{id} \tag{4.6}$$

Much of the elegance of the Hamiltonian formulation stems from its geometric structure, and in particular from the concept of *symplecticness* of its flow maps and its implications for the solution behavior of an Hamiltonian

system: we say that a smooth map $\mathbf{\Psi_z}$ on the phase space $\mathbb{R}^{2d}$ is a *symplectic map* with respect to the structure matrix $\mathbf{J}$ if its Jacobian $\mathbf{\Psi_z}(\mathbf{z})$ satisfies:

$$[\mathbf{\Psi_z}(\mathbf{z})]^T \mathbf{J}^{-1} \mathbf{\Psi_z}(\mathbf{z}) = \mathbf{J}^{-1} \tag{4.7}$$

for all $\mathbf{z}$ in the domain of definition of $\mathbf{\Psi}$.

It can be shown that the flow map $\mathbf{\Phi}_t$ of any Hamiltonian system is symplectic [37].

The symplecticness of the flow map implies the existence of certain global conservation laws or *integral invariants* related to the evolution of subsets of phase space. In particular, it can be shown that symplecticness implies preservation of volume ($d > 1$). This fact follows from Liouville's theorem and it implies severe and important restrictions on the possible solution behavior of Hamiltonian dynamical systems; in particular preservation of the symplectic structure under numerical discratization is a very desirable property for long term approximate integration of Hamiltonian systems.

4.2 The symplectic structure of phase space

The definition (4.7) is not always the most convenient approach to check the symplecticness of a given map Ψ. This is true in particular if the map is given implicitely, or of the definition involves additional variables that could, in principle, be eliminated. In those cases, it is best to use implicit differentiation combined with a definition of symplecticness in terms of differential one- and two-forms.

Recall from differential geometry that a *two-form* on $\mathbb{R}^{2d}$ is a skew-symmetric bilinear function $\Omega(\xi, \eta)$ with arguments ξ and η in $\mathbb{R}^{2d}$. The symplectic structure matrix:

$$\mathbf{J} := \begin{bmatrix} 0 & +I_d \\ -I_d & 0 \end{bmatrix} \tag{4.8}$$

introduce the *symplectic two-form* Ω on the phase space $\mathbb{R}^{2d}$:

$$\Omega(\xi,\eta) := \xi^T \mathbf{J}^{-1}\eta \qquad\qquad \xi,\eta \in \mathbb{R}^{2d} \tag{4.9}$$

From a geometric point of view, if we denote by $\xi^{(i)}$ and $\eta^{(i)}$ the projections of $\xi \in \mathbb{R}^{2d}$ and $\eta \in \mathbb{R}^{2d}$ on the (q_i, p_i) coordinate planes, the two-form $\Omega(\xi,\eta)$, for $d > 1$, is equivalent to the sum of the oriented areas of the parallelograms spanned by the pair of vectors $\xi^{(i)}$ and $\eta^{(i)}$.

As we know from calculus, if $f : \mathbb{R}^m \to \mathbb{R}$ is a smooth function, then its *directional derivative* along a vector $\xi \in \mathbb{R}^m$, denoted here by $df(\xi)$, is given by:

$$df(\xi) = \frac{\partial f}{\partial z_1}\xi_1 + \frac{\partial f}{\partial z_2}\xi_2 + ... + \frac{\partial f}{\partial z_m}\xi_m \tag{4.10}$$

where the partial derivatives of f are computed at a fixed location $\mathbf{z} \in \mathbb{R}^m$. The linear functional $df(.)$ is called the *differential* of f at $\mathbf{z}$ and is an example of a differential one-form. A particularly simple class of differentials is provided by the coordinate functions $f(\mathbf{z}) = z_i$ and we have:

$$dz_i(\xi) = \xi_i, \tag{4.11}$$

$i = 1, .., m$.

Since:

$$df(\xi) = \frac{\partial f}{\partial z_1}dz_1(\xi) + \frac{\partial f}{\partial z_2}dz_2(\xi) + ... + \frac{\partial f}{\partial z_m}dz_m(\xi), \tag{4.12}$$

the set of al differentials at a point $\mathbf{z} \in \mathbb{R}^m$ forms a linear space with the differentials dz_i as a basis. We now apply a coordinate transformation $\mathbf{\Psi} : \mathbb{R}^{\mathbf{m}} \to \mathbb{R}^{\mathbf{m}}$ and define:

$$\hat{\mathbf{z}} = \mathbf{\Psi}(\mathbf{z}) \tag{4.13}$$

as well as the transformed function:

$$\hat{f}(\mathbf{z}) = f(\hat{\mathbf{z}}) = f(\mathbf{\Psi}(\mathbf{z})) \tag{4.14}$$

Differentiating we obtain:

$$d\hat{f} = \frac{\partial f}{\partial \hat{z}_1} d\hat{z}_1 + \frac{\partial f}{\partial \hat{z}_2} d\hat{z}_2 + ... + \frac{\partial f}{\partial \hat{z}_m} d\hat{z}_m \tag{4.15}$$

in the new basis:

$$d\hat{z}_j = \sum_i \frac{\partial \Psi^j}{\partial z_i} dz_i \tag{4.16}$$

where Ψ^i is the ith component of the transformation $\mathbf{\Psi}$.

To compactify the notation, we introduce the column vector of differential one-forms:

$$d\mathbf{z} = (dz_1, dz_2, ..., dz_m)^T \tag{4.17}$$

with the property that $d\mathbf{z}(\xi) = \xi$ and hence:

$$df = f_z \cdot d\mathbf{z} \tag{4.18}$$

The transformation rule becomes:

$$d\hat{\mathbf{z}} = \mathbf{\Psi}_z(\mathbf{z})\, d\mathbf{z} \tag{4.19}$$

and, consequentely:

$$d\hat{\mathbf{z}}(\xi) = \mathbf{\Psi}_z(\mathbf{z})\, d\mathbf{z}(\xi) = \mathbf{\Psi}_z(\mathbf{z})\, \xi. \tag{4.20}$$

Let us now coming back to symplectic transformations and a splitting of variables $z = (\xi, \eta) \in \mathbb{R}^{2d}$ with associated one-forms dq_i, dp_i, $i = 1, ..., d$. Using the ordering of the two vectors ξ and η into a sequence of projections down on to the (q_i, p_i) coordinate planes, the symplectic two-form defined by (4.9) can be written as:

$$\Omega(\xi, \eta) = \sum_i \left[dp_i(\xi), dq_i(\eta) - dq_i(\xi)\, dp_i(\eta) \right]. \tag{4.21}$$

This suggest to introduce the wedge product of two differentials df and dg via:

$$(df \wedge dg)(\xi, \eta) := dg(\xi)\, df(\eta) - df(\xi)\, dg(\eta) \tag{4.22}$$

and, in particular, to write, using vector notation:

$$\Omega = d\mathbf{q} \wedge d\mathbf{p} \tag{4.23}$$

Conservation of symplecticness, under a transformation:

$$\hat{\mathbf{q}} = \mathbf{\Psi}^1(\mathbf{q}, \mathbf{p}) \tag{4.24}$$

$$\hat{\mathbf{p}} = \mathbf{\Psi}^2(\mathbf{q}, \mathbf{p}) \tag{4.25}$$

reduces now to the statement that:

$$d\hat{\mathbf{q}} \wedge d\hat{\mathbf{p}} = d\mathbf{q} \wedge d\mathbf{p} \tag{4.26}$$

In order to demonstrate (4.26) we first verify that:

$$d\hat{\mathbf{q}} \wedge d\hat{\mathbf{p}} = \frac{1}{2}\left(\mathbf{J}^{-1} d\mathbf{z}\right) \wedge d\mathbf{z} \tag{4.27}$$

Indeed, we have:

$$\begin{aligned} \left(\mathbf{J}^{-1} d\mathbf{z}\right) \wedge d\mathbf{z} &= \sum_{i=1}^{d} \left[dz_i \wedge dz_{d+1} - dz_{d+1} \wedge dz_i\right] \\ &= \sum_{i=1}^{d} \left[dq_i \wedge dp_i - dp_i \wedge dq_i\right] \\ &= 2 d\mathbf{q} \wedge d\mathbf{p} \end{aligned} \tag{4.28}$$

Hence (4.26) is equivalent to:

$$\left(\mathbf{J}^{-1} d\hat{\mathbf{z}}\right) \wedge d\hat{\mathbf{z}} = \left(\mathbf{J}^{-1} d\mathbf{z}\right) \wedge d\mathbf{z} \tag{4.29}$$

where

$$d\hat{\mathbf{z}} = \mathbf{\Psi}_{\mathbf{z}}(\mathbf{z})\, d\mathbf{z}. \tag{4.30}$$

Applying the rule of matrix multiplication, we obtain:

$$\begin{aligned}\left(\mathbf{J}^{-1}d\hat{\mathbf{z}}\right)\wedge d\hat{\mathbf{z}} &= \left(\mathbf{J}^{-1}\boldsymbol{\Psi}_{\mathbf{z}}\left(\mathbf{z}\right)d\mathbf{z}\right)\wedge\left(\boldsymbol{\Psi}_{\mathbf{z}}\left(\mathbf{z}\right)d\mathbf{z}\right)\\ &= \left(\boldsymbol{\Psi}_{\mathbf{z}}\left(\mathbf{z}\right)^{T}\mathbf{J}^{-1}\boldsymbol{\Psi}_{\mathbf{z}}\left(\mathbf{z}\right)d\mathbf{z}\right)\wedge d\mathbf{z}\end{aligned} \tag{4.31}$$

and symplecticness of the map Ψ implies (4.29). The wedge product combined with implicit differentiation is then a powerful tool to verify symplecticness of an implicitely given transformation Ψ.

4.3 Geometric integrators

As we already said in the previous section, in general, the flow map of a given system cannot be written down explicitely and exactly, but can only be approximated numerically. We can say then that a numerical method $\boldsymbol{\Psi}_{\Delta t}$ can be seen as a mapping from one time level to another one which, via iteration, generates discrete approximations $(\mathbf{q}^n, \mathbf{p}^n)$. Standard error analysis can be used to demonstrate that a certain numerical method converges in the limit of a small timestep, but in any simulation the ability to take small timesteps is in direct conflict with the cost of a timestep and the need to perform integrations on time intervals long enough to elicit relevant macroscopic behavior. The typical picture is a locally accurate approximation that gradually drifts further from the true trajectory; the reducing of the stepsize can reduce the rate of drift, but the qualitative picture does not change in any significant way. Anyway it can be observed that certain methods show a strong asymptotic stability property, if the stepsize is below some threshold value [38] [39]. In order to better explain this concept, let's consider a simple harmonic oscillator:

$$\frac{d\mathbf{z}}{dt} = \mathbf{A}\mathbf{z} \tag{4.32}$$

with:

$$\mathbf{A} = \begin{bmatrix} 0 & 1 \\ -\omega^2 & 0 \end{bmatrix} \tag{4.33}$$

The solution at any time can be defined by a matrix (the fundamental solution matrix), $\mathbf{R}(t)$:

$$\mathbf{z}\left(t, \mathbf{z}^0\right) = \mathbf{R}(t)\,\mathbf{z}^0, \qquad \mathbf{R}(t) = \begin{bmatrix} \cos\omega t & \frac{1}{\omega}\sin\omega t \\ -\omega\sin\omega t & \cos\omega t \end{bmatrix} \tag{4.34}$$

which has eigenvalues $\mu_{1,2} = e^{\pm i\omega t}$, both of which lie on the unit circle. It is also easy to verify that the determinant of $\mathbf{R}(t)$ is equal to one. Let's try to solve equations (4.32) by the one-step Eulero numerical method, defined by:

$$\mathbf{z}^{n+1} = \mathbf{z} + \Delta t\mathbf{f}\left(\mathbf{z}^n\right) \tag{4.35}$$

The Euler's method approximation leads to the mapping:

$$\mathbf{z}^{n+1} = \hat{\mathbf{R}}(\Delta t)\,\mathbf{z}^n, \qquad \hat{\mathbf{R}}(\Delta t) = \begin{bmatrix} 1 & \Delta t \\ -\Delta t\omega^2 & 1 \end{bmatrix} \tag{4.36}$$

where the propagation matrix $\hat{\mathbf{R}}(\Delta t)$ has the eigenvalues

$$\hat{\lambda}_{1,2} = 1 \pm i\Delta t\omega \tag{4.37}$$

A numerical method is *asymptotically* stable if the growth of the solution for a linear model problem is asymptotically bounded. A sufficient condition for asymptotic stability is that the eigenvalues of the method are (i) in the unit disk in the complex plane, and (ii) simple (not repeated) if in the unit circle. The Euler's method eigenvalues are both on modulus greater than one and their powers grow exponentially fast; since the error is determined by the powers of the eigenvalues of the matrix, this means that Euler's method is unstable. One manifestation of this is that the determinant of the Jacobian of the transformation for one time step differs slightly from unity, and thus the system will be damped or excited artificially. The most important physical consequence of this fact is that the system Hamiltonian is not preserved during the integration. The asymptotic stability does not contradict the convergence of the method, since, fixing any time interval $[0, T]$ and

simoultaneously driving the number of steps N to infinity as $\Delta t \to 0$ so that $N\Delta t = T$, we have:

$$\lim_{N\to\infty} \left(\hat{\lambda}_{1,2}\right)^N = \lim_{N\to\infty} \left(1 \pm i\Delta t\omega\right)^N = e^{\pm i\omega T} + O\left(\Delta t\right) \tag{4.38}$$

In some cases, it is possible to show that the eigenvalues of a numerical method applied to the harmonic oscillator lie on the unit circle in the complex plane. This is, for example, the case of Störmer-Verlet method, or Euler-B method. A related long-term stability property extends also to nonlinear models, and this is reflected in a qualitative agreement between the numerical and exact solutions. This feature can be explained by making use of the concept of symplecticity: we already seen that the symplectic property of Hamiltonian systems carries with it geometric implications regarding the way in which the flow map acts on sets of initial conditions. By imposing the structural properties of the flow map of a Hamiltonian system on the numerical integrator itself, we can then obtain an improved behavior in simulations.

Recall that a map $\mathbf{\Psi}$ from $\mathbb{R}^{2d}$ to $\mathbb{R}^{2d}$ is symplectic if:

$$\left[\frac{\partial}{\partial \mathbf{z}}\mathbf{\Psi}\left(\mathbf{z}\right)\right]^T \mathbf{J}^{-1} \left[\frac{\partial}{\partial \mathbf{z}}\mathbf{\Psi}\left(\mathbf{z}\right)\right] = \mathbf{J}^{-1} \tag{4.39}$$

Equivalently, if we write

$$\begin{bmatrix} \mathbf{Q} \\ \mathbf{P} \end{bmatrix} = \mathbf{\Psi}\left(\begin{bmatrix} \mathbf{q} \\ \mathbf{p} \end{bmatrix}\right), \tag{4.40}$$

then the symplecticness of the map is summarized by the condition:

$$d\mathbf{Q} \wedge d\mathbf{P} = d\mathbf{q} \wedge d\mathbf{p}, \tag{4.41}$$

in terms of the wedge product od differential one-forms. We can view a numerical method as a mapping from one time level to another which, via iteration, generates discrete approximations $(\mathbf{q}^n, \mathbf{p}^n)$; any reasonable integrator applied to the Hamiltonian system will preserve the symplecticness

relation up to a certain error which is proportional to a power of the stepsize Δt.

We will term a numerical method a *symplectic integrator* if the symplecticess condition:

$$d\mathbf{q}^{n+1} \wedge d\mathbf{p}^{n+1} = d\mathbf{q}^{n} \wedge d\mathbf{p}^{n}, \tag{4.42}$$

is preserved *exactly*. A symplectic integration step with a sufficiently small step size generates a phase space portrait which is close to that of the original system, without introducing artificial damping or excitation in the Hamiltonian. The problem is now to derive such symplectic integrators and to write the equations of motion for the particles in a way suitable for them.

4.4 The integration of the equations of motion

The equations of motion for a particle moving in an electromagnetic field can be derived from the following Hamiltonian [40]:

$$H = \sum_i q_i P_i - \mathcal{L} = \sqrt{c^2 \left| \vec{P} - q_e \vec{A}\left(\vec{q}, t\right) \right|^2 + m^2 c^4} + q_e \Phi\left(\vec{q}, t\right) \tag{4.43}$$

where $\vec{P}$ is the canonical momentum, given by:

$$\vec{P} = \vec{p} - q_e \vec{A}\left(\vec{q}, t\right) \tag{4.44}$$

q_e is the particle charge and $\vec{A}$ and Φ are the vector and the scalar potential that describe the electromagnetic field:

$$\vec{E} = \alpha \vec{e}_0 = -j\omega\mu\vec{A} - \nabla\Phi \tag{4.45}$$

$$\vec{H} = \frac{\omega_0}{\omega} \alpha \vec{h}_0 = \nabla \times \vec{A} \tag{4.46}$$

The equations of motion can be obtained from Hamiltonian (4.43) through equations (4.1) and (4.2). Since the above Hamiltonian is explicitely dependent on time, the system is not autonomous. Anyway it is possible to replace the time-dependent problem with a "pseudo time-independent" one by introducing two more variables, τ and its related canonical momentum P_τ; the new set of variables is given by:

$$\left[\begin{array}{c} \vec{q} \\ \tau \end{array} \right], \left[\begin{array}{c} \vec{P} \\ P_\tau \end{array} \right] \tag{4.47}$$

with $\vec{q} = \{x, y, z\}$ and $\vec{P} = \{P_x, P_y, P_z\}$. We can then consider the following modified Hamiltonian:

$$\tilde{H} = H\left(\vec{q}, \tau, \vec{P}\right) + P_\tau = \sqrt{c^2 \left|\vec{P} - q_e \vec{A}\left(\vec{q}, \tau\right)\right|^2 + m^2 c^4} + q_e \Phi\left(\vec{q}, \tau\right) + P_\tau \tag{4.48}$$

We obtain a set of 8 Hamilton's equations:

$$\frac{dx}{dt} = \frac{\partial \tilde{H}}{\partial P_x} \tag{4.49}$$

$$\frac{dy}{dt} = \frac{\partial \tilde{H}}{\partial P_y} \tag{4.50}$$

$$\frac{dz}{dt} = \frac{\partial \tilde{H}}{\partial P_z} \tag{4.51}$$

$$\frac{d\tau}{dt} = \frac{\partial \tilde{H}}{\partial P_\tau} \tag{4.52}$$

$$\frac{dP_x}{dt} = -\frac{\partial \tilde{H}}{\partial x} \tag{4.53}$$

$$\frac{dP_y}{dt} = -\frac{\partial \tilde{H}}{\partial y} \tag{4.54}$$

$$\frac{dP_z}{dt} = -\frac{\partial \tilde{H}}{\partial z} \tag{4.55}$$

$$\frac{dP_\tau}{dt} = -\frac{\partial \tilde{H}}{\partial \tau} \tag{4.56}$$

where eq. (4.52) yelds obviously $\tau = t$. By using the following normalized variables:

$$\vec{q}_n = \frac{x}{\lambda} \tag{4.57}$$

$$\tau_n = \frac{\tau}{T_0} \tag{4.58}$$

$$\vec{P}_n = \frac{\vec{P}}{mc} \tag{4.59}$$

$$P_{\tau n} = \frac{P_\tau}{mc^2} \tag{4.60}$$

$$t_n = \frac{t}{T_0} \tag{4.61}$$

$$\vec{A}_n = \frac{q_e}{mc}\vec{A} \tag{4.62}$$

$$\Phi_n = \frac{q_e}{mc^2}\Phi \tag{4.63}$$

and omitting the subscript n, we obtain, for the particle in the electromagnetic field:

$$\dot{x} = \frac{P_x - A_x}{\sqrt{1 + \left|\vec{P} - \vec{A}\right|^2}} \tag{4.64}$$

$$\dot{y} = \frac{P_y - A_y}{\sqrt{1 + \left|\vec{P} - \vec{A}\right|^2}} \tag{4.65}$$

$$\dot{z} = \frac{P_z - A_z}{\sqrt{1 + \left|\vec{P} - \vec{A}\right|^2}} \tag{4.66}$$

$$\dot{\tau} = 1 \tag{4.67}$$

$$\dot{P}_x = \frac{\left(\vec{P} - \vec{A}\right)}{\sqrt{1 + \left|\vec{P} - \vec{A}\right|^2}} \cdot \frac{\partial \vec{A}}{\partial x} + \frac{\partial \Phi}{\partial x} \tag{4.68}$$

$$\dot{P}_y = \frac{\left(\vec{P} - \vec{A}\right)}{\sqrt{1 + \left|\vec{P} - \vec{A}\right|^2}} \cdot \frac{\partial \vec{A}}{\partial y} + \frac{\partial \Phi}{\partial y} \tag{4.69}$$

$$\dot{P}_z = \frac{\left(\vec{P} - \vec{A}\right)}{\sqrt{1 + \left|\vec{P} - \vec{A}\right|^2}} \cdot \frac{\partial \vec{A}}{\partial z} + \frac{\partial \Phi}{\partial z} \tag{4.70}$$

$$\dot{P}_\tau = \frac{\left(\vec{P} - \vec{A}\right)}{\sqrt{1 + \left|\vec{P} - \vec{A}\right|^2}} \cdot \frac{\partial \vec{A}}{\partial \tau} + \frac{\partial \Phi}{\partial \tau} \tag{4.71}$$

Another advantage from the introduction of the two new variables is that the integration of equation (4.71) leads to the evaluation of the quantity $\frac{\left(\vec{P}-\vec{A}\right)}{\sqrt{1+\left|\vec{P}-\vec{A}\right|^2}} \cdot \frac{\partial \vec{A}}{\partial \tau}$, that is proportional to the scalar product between the particle momentum and the cavity electric field. This allows us to calculate the integral (3.33) needed to obtain the coefficient (3.30) directly while integrating the equations of motion.

The obtained equations of motion have then to be integrated numerically. The Hamiltonian (4.48) is not separable (i.e. is not possible to write it in the form $H(\vec{q}, \vec{P}, t) = T(\vec{P}) + V(\vec{q}, t)$). Symplectic integration methods for general (not separable) Hamiltonians are implicit: this means that it is not possible to calculate the state of the system at a later time directly from the state of the system at the current time, but we have to find a solution by solving an equation involving both the current state of the system and the later one. A second-order implicit symplectic method is the *implicit midpoint method*, defined as follows:

$$\mathbf{z}^{n+1} = \mathbf{z}^n + \Delta t \mathbf{J} \nabla H \left(\mathbf{z}^{n+\frac{1}{2}} \right) \tag{4.72}$$

with

$$\mathbf{z}^{n+\frac{1}{2}} = \frac{(\mathbf{z}^{n+1} + \mathbf{z}^n)}{2} \tag{4.73}$$

This method is evidently implicit. For implementation purposes, it is useful to write it as a composition of two "half-steps": an *implicit Euler* step

$$\mathbf{z}^{n+\frac{1}{2}} = \mathbf{z} + \frac{1}{2} \Delta t \mathbf{J} \nabla H \left(\mathbf{z}^{n+\frac{1}{2}} \right) \tag{4.74}$$

followed by an *explicit Euler* step

$$\mathbf{z}^{n+1} = \mathbf{z}^{n+\frac{1}{2}} + \frac{1}{2} \Delta t \mathbf{J} \nabla H \left(\mathbf{z}^{n+\frac{1}{2}} \right) \tag{4.75}$$

For implicit midpoint, the equation for $d\mathbf{z}^n$ is equivalent to

$$d\mathbf{z}^{n+1} = d\mathbf{z}^n + \Delta t \mathbf{J} H_{zz} \frac{d\mathbf{z}^n + d\mathbf{z}^{n+1}}{2} \tag{4.76}$$

Taking the wedge product with $\mathbf{J}^{-1} d\mathbf{z}^n$ and $\mathbf{J}^{-1} d\mathbf{z}^{n+1}$, respectively, from the left, we obtain:

$$\begin{aligned} \mathbf{J}^{-1} d\mathbf{z}^{n+1} \wedge d\mathbf{z}^n &= \mathbf{J}^{-1} d\mathbf{z}^n \wedge d\mathbf{z}^n + \Delta t \mathbf{J}^{-1} \mathbf{J} H_{zz} \frac{d\mathbf{z}^n + d\mathbf{z}^{n+1}}{2} \wedge d\mathbf{z}^n \\ &= \mathbf{J}^{-1} d\mathbf{z}^n \wedge d\mathbf{z}^n + \frac{\Delta t}{2} H_{zz} d\mathbf{z}^{n+1} \wedge d\mathbf{z}^n, \end{aligned} \tag{4.77}$$

and

$$\begin{aligned} \mathbf{J}^{-1} d\mathbf{z}^{n+1} \wedge d\mathbf{z}^{n+1} &= \mathbf{J}^{-1} d\mathbf{z}^n \wedge d\mathbf{z}^{n+1} + \Delta t \mathbf{J}^{-1} \mathbf{J} H_{zz} \frac{d\mathbf{z}^n + d\mathbf{z}^{n+1}}{2} \wedge d\mathbf{z}^{n+1} \\ &= \mathbf{J}^{-1} d\mathbf{z}^{n+1} \wedge d\mathbf{z}^n - \frac{\Delta t}{2} H_{zz} d\mathbf{z}^{n+1} \wedge d\mathbf{z}^n. \end{aligned} \tag{4.78}$$

Here we have made use of the property of the wedge product:

$$d\mathbf{z}^n \wedge \mathbf{A} d\mathbf{z}^n = d\mathbf{z}^{n+1} \wedge \mathbf{A} d\mathbf{z}^{n+1} = 0 \tag{4.79}$$

for any symmetric matrix $\mathbf{A} \in \mathbb{R}^{2d\times 2d}$. Summing up, we arrive at the equality:

$$\mathbf{J}^{-1}d\mathbf{z}^{n+1} \wedge d\mathbf{z}^{n+1} = \mathbf{J}^{-1}d\mathbf{z}^{n} \wedge d\mathbf{z}^{n} \tag{4.80}$$

implying symplecticness of the scheme with respect to the sructure matrix $\mathbf{J}$. Observe that this argument required at no point that $\mathbf{J}$ be the canonical structure matrix, but only that it be constant, skew-symmetric and invertible, thus we have shown that the implicit midpoint method preserves any constant symplectic structure.

Chapter 5

The code

The routine described in section 3.2 has been implemented using Mathematica (see Appendix A). In order to check the self-consistency of the algorithm, the first step is to simulate the case of a simple pillbox input cavity with a initially continuous beam flowing through it. In the considered case the macro-particles will interact only with the TM_{010} cavity field, without considering space charge; since we are just interested in a first check on the consistance of the method, we can use an ideal cylindrical cavity without beam pipe, so that we can employ the well-known analytic fields of the TM_{010} mode.

5.1 Cavity parameters

We can start considering a cylindrical cavity driven by an input power of 250 W at 11.424 GHz and crossed by a 100 A - 100 kW continuous electron beam. The main cavity parameters are summarized in table 5.1:

Since we are considering a cavity without beam pipe, we can use the analytic expression of the vector potential for the TM_{010} cavity mode plus the focusing field [32]:

$$\vec{A} = -\frac{B_0}{2} y \vec{x}_0 + \frac{B_0}{2} x \vec{y}_0 + j A_0 J_o \left(\frac{\chi_{0,1} \sqrt{x^2 + y^2}}{a} \right) e^{j\omega t} \vec{z}_0 \qquad (5.1)$$

where $\chi_{0,1}$ is the first zero of the zero-order, first kind Bessel Function J_0.

Table 5.1: Cavity parameters

Driving frequency (GHz)	f	11.424
Lenght (cm)	L	0.5
Radius (cm)	a	1.044
Quality factor (copper)	Q_0	5652
Focusing field (T)	B_0	0.093
Input power (W)	P_{IN}	250
Beam current (A)	I_0	100
Beam voltage (kV)	V_0	100
Beam radius (cm)	Rb	0.375

The vector potential amplitude A_0 is related to the field coefficient α, while the focusing field amplitude B_0 has been chosen equal to the Brillouin field $\sqrt{\frac{\sqrt{2}I_0}{\epsilon_0 \pi a^2 \eta^{\frac{3}{2}} \sqrt{V_0}}}$, with $\eta = \frac{q_e}{m}$.

The particles distribution has to be uniform in time and space to simulate a continuous beam. In order to do this, we can then divide the RF period in m time slots: since we have cylindrical symmetry we can choose, in every time slot, a set of n macro-particles distribuited on the x-axis at decreasing distances x_i from the center:

$$x_i = \frac{R}{2n}(2i-1) \qquad i = 1, ..., n \tag{5.2}$$

and with charge:

$$q_i = \frac{I_0 T}{m\pi R^2}\pi\left(r_i^2 - r_{i-1}^2\right) \qquad i = 1, ..., n \tag{5.3}$$

where:

$$r_i = \frac{R}{n}i \qquad i = 0, ..., n \tag{5.4}$$

and, obviously, $nm = N$ is the total number of macro-particles.

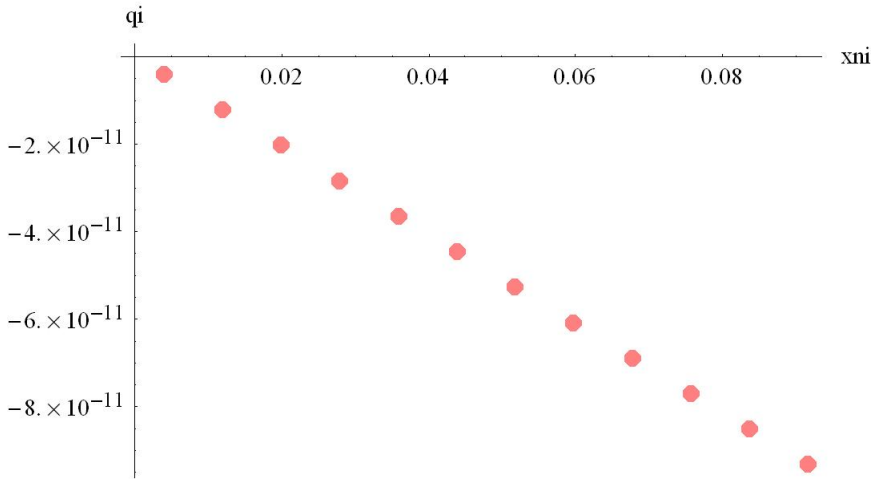

Figure 5.1: Charge of the macroparticles of a time slot as a function of the initial x coordinate.

The two integers n and m have to be big enough so that the particle distribution can be considered uniform. Pictures 5.2 and 5.3 show the variation of the normalized real and imaginary part of the field coefficient α as a function of the number of time slots m, while in pictures 5.4 and 5.5 the normalized real and imaginary part of the field coefficient α as a function of the number of space slots n in shown.

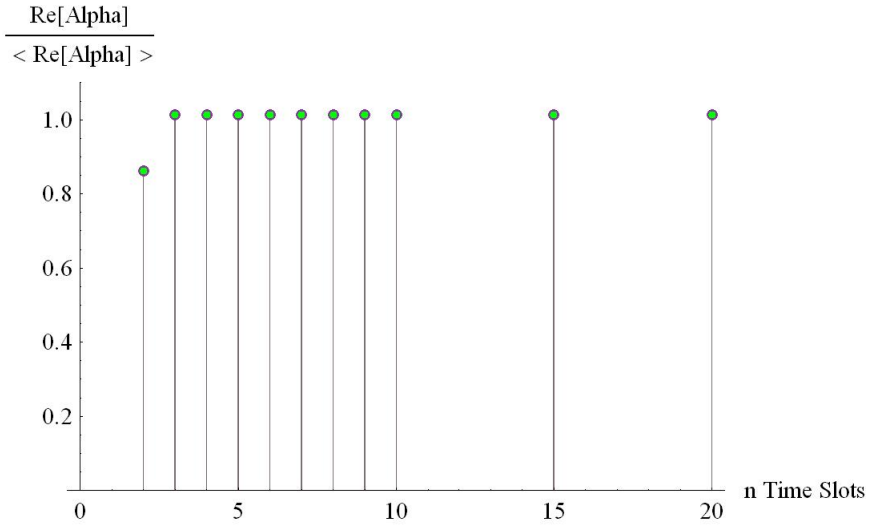

Figure 5.2: Normalized real part of the field coefficient α as a function of the number of time slots m.

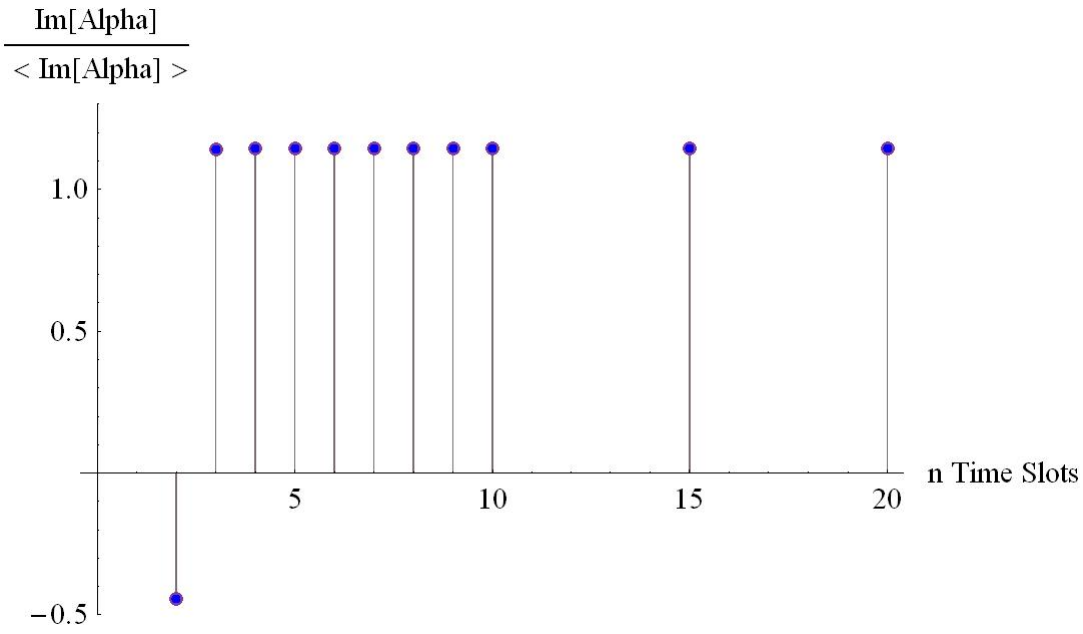

Figure 5.3: Normalized imaginary part of the field coefficient α as a function of the number of time slots m.

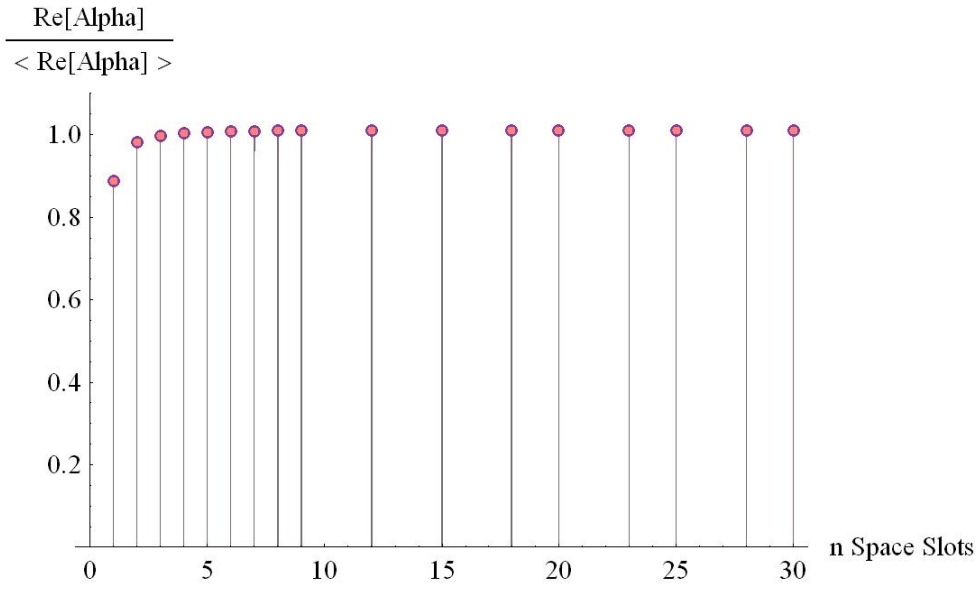

Figure 5.4: Normalized real part of the field coefficient α as a function of the number of space slots n.

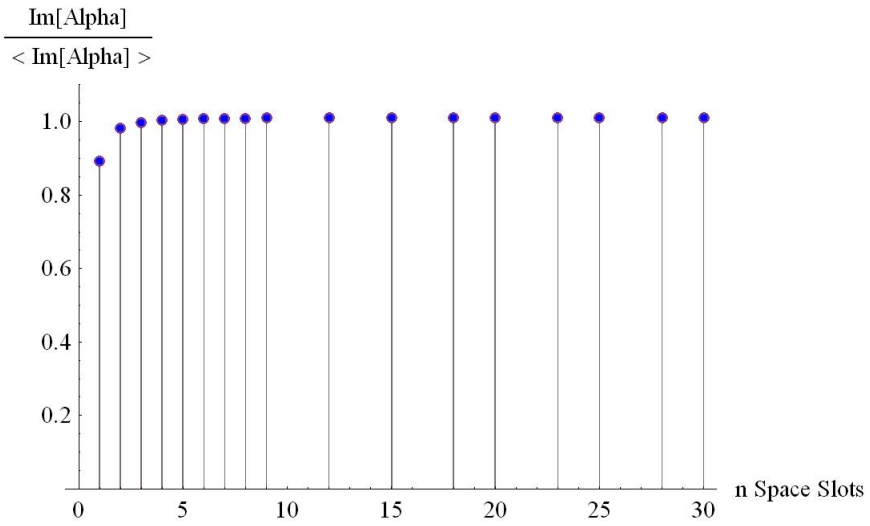

Figure 5.5: Normalized imaginary part of the field coefficient α as a function of the number of space slots n.

In particular, we have that the simulation results have a strong dependence on the number of space slots n (i.e. on the number of macro-particles for every time-slot) if this number is chosen under a minimum value. In order to optimize also the computation time we will set $m = 5$ and $n = 12$ for the future simulations, unless otherwise specified.

We then have to choose a guess value for the field coefficient α to be used as starting point for the algorithm described in section 3.2. A reasonable guess can be obtained from expression (3.30) in the case of no beam current. We obtain:

$$\alpha^* = \frac{2\sqrt{\frac{\omega_0 u P_{IN}}{Q_{ext}}}e^{j\left(\Phi^+ + \arctan\left(\frac{x^2 - Q_0\delta}{Q_0 - Q_{ext}x^2}\right)\right)}}{\omega_0 u\left(\frac{1}{Q_{ext}} + \frac{x^2}{Q_0} + j\left(\frac{x^2}{Q_0} - \delta\right)\right)} \tag{5.5}$$

The input wave phase Φ^+ can be set equal to zero, while the cavity resonant angular frequency ω_0 and the external quality factor Q_{ext}, are parameters that can be chosen in order to minimize the outcoming power at the entrance of the cavity when the beam is inside. The outcoming power is given by:

$$P_{oc} = \frac{1}{2}\left|V_e - V^+\right|^2 \tag{5.6}$$

with:

$$V_e = \sqrt{\frac{2\omega_0 u}{Q_{ext}}}\alpha e^{j\arctan\left(\frac{x^2 - Q_0\delta}{Q_0 + Q_{ext}x^2}\right)} \tag{5.7}$$

and:

$$V^+ = \sqrt{2P_{IN}} \tag{5.8}$$

We can first put $Q_{ext} = Q_0$ and vary the ω_0. The result is shown in fig. 5.6:

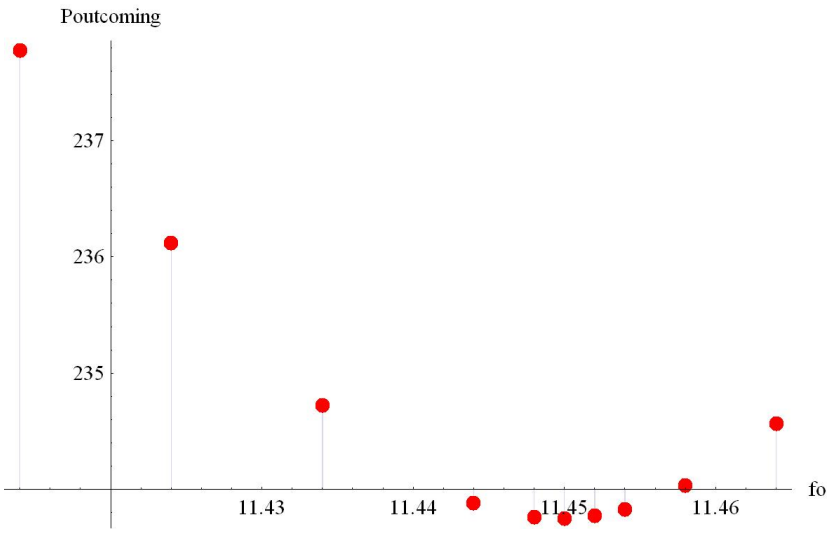

Figure 5.6: Outcoming power at the cavity entrance as a function of the cavity resonant frequency f_0 and for $Q_{ext} = Q_0$.

We have a minimum outcoming power for $f_0 = 11.450$ GHz, corresponding to $P_{oc} \cong 234$ W.

We can then set $f_0 = 11.450$ GHz and vary the external Q: in this way we can determine the optimum value for the coupling coefficient of the klystron input resonator in order to have the mimimum outcoming power in presence of both the beam and the RF power. The resulting curve shows a minimum ($\cong 0.01W$) in the outcoming power for $Q_{ext} = 95$ (fig. 5.7).

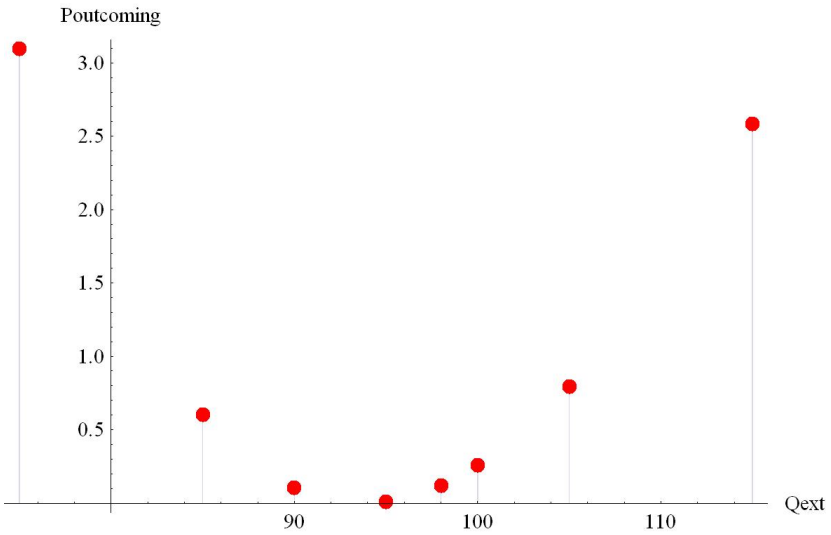

Figure 5.7: Outcoming power at the cavity entrance as a function of the external Q and for $f_0 = 11.445$ GHz

.

5.2 Two cavity klystron

The second step is to verify the self-consistency of the algorithm when it is applied to a cavity with no RF power coming from a driver. We can, for example, simulate the passage of a velocity modulated beam into an output klystron cavity. In this case the input power is set equal to zero and the beam itself is responsible of the field excitation. No space charge field is taken in account. The cavity is coupled with an output waveguide and in this case the resonant frequency and the external Q have to be chosen in order to *maximize* the outcoming power. The modulated beam can be, in the simplest case, the beam coming from the input cavity followed by a drift space. In this situation we have the basic case of a two cavity klystron. The drift tube length is also a free parameter to be optimized.

Let's then consider again the case of an ideal pillbox cavity (i.e. without beam pipe). The main cavity parameters are the same of the input one but this time we have that $P_{IN} = 0$. As we did for the input cavity, we start optimizing the cavity resonant frequency ω_0. The results are summarized in

fig. 5.8 for $Q_{ext} = 100$. The optimum resonant frequency is 11.364 GHz. The beam current density is the one obtained with a drift tube length of 30 cm.

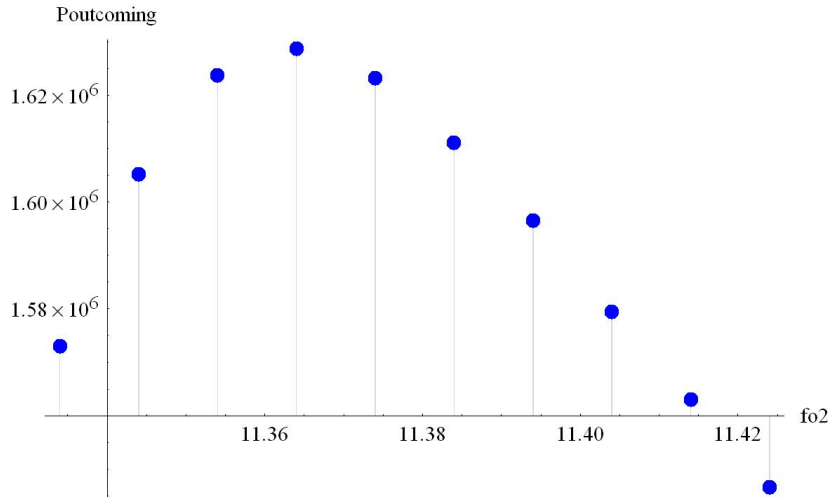

Figure 5.8: Output power from the second cavity as a function of the output cavity resonant frequency f_{02} and for $Q_{ext2} = 100$ GHz

.

In fig. 5.9 is then shown the value of the emitted power as a function of the external Q and for $f_{02} = 11.364$ GHz.

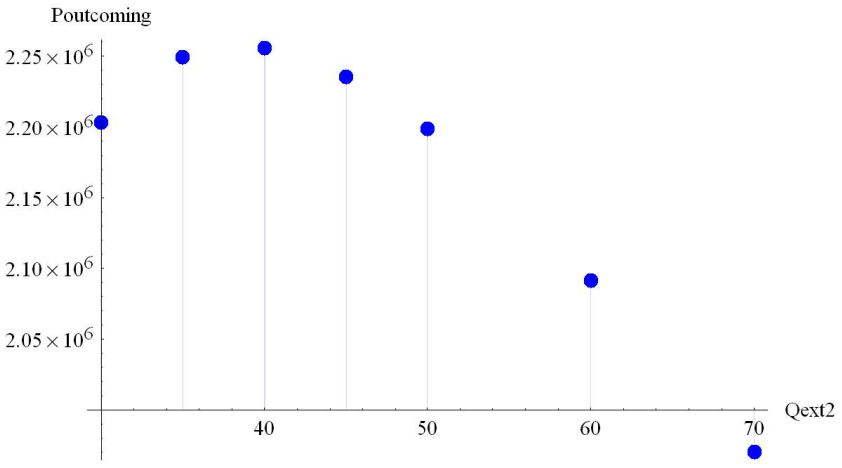

Figure 5.9: Output power from the second cavity as a function of the external Q and for $f_{02} = 11.364$ GHz

.

Finally, the drift tube length can be chosen in order to maximize the output power (i.e. the emitted power from the second cavity) and the total efficiency of the two cavity klystron. We have the maximum for a drift length of 30 cm:

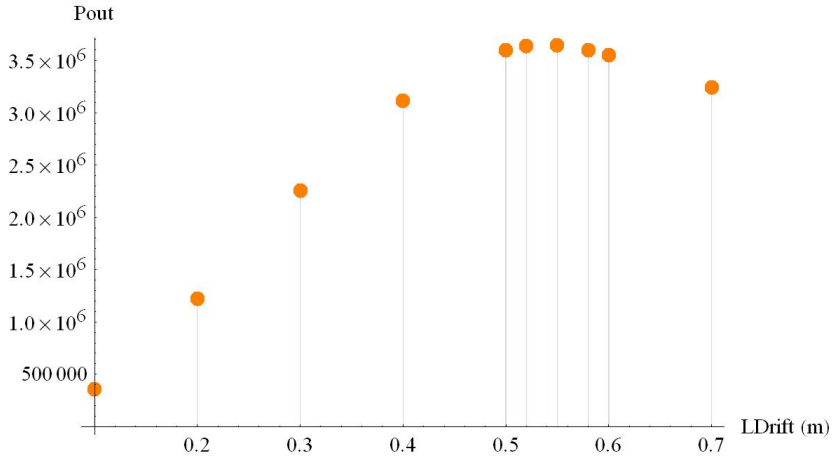

Figure 5.10: Output power from the second cavity as a function of the drift length.

The correnspondingefficiency of the device is given by:

$$\eta = \frac{P_{OUT}}{V_0 I_0} = 30\% \tag{5.9}$$

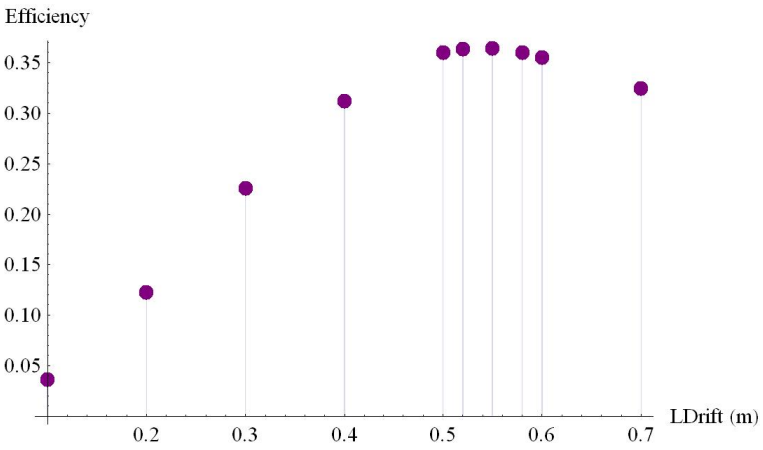

Figure 5.11: Two cavity klystron efficiency as a function of the drift length.

5.3 Comparison with other simulation tools

The previous results are a check of the self-consistency of the algorithm. The simulations can be now compared to the results obtained from other design tools. We will consider two different other methods: the first one is the simple kinematic klystron analysis, which does not include the contribution of the space charge fields. The second one will be the 1-D code AJDisk, a one dimensional simulation tool for round and sheet beam klystrons developed at the Stanford Lineear Accelerator Center and currently used to run fast large signal design simulations with the inclusion of the space charge field.

5.3.1 The klystron kinematic analysis

The kinematic analysis below provides a simple description of the klystron passive cavities by a parallel equivalent circuit. The input cavity is represented by a voltage V_1 which modulates the particles momenta. We consider that the interaction gaps are very narrow, and we neglect the finite transit time of the entering electrons. The beam of electrons, which has been accelerated by a potential V_0 to a momentum p_0, traverses the first gap, where it is acted by an RF voltage $V_1 \cos(\omega t)$, reduced by a "coupling coefficient", M (always less than 1). The latter modifies the gap voltage due to the finite transit time, resulting in a lower effective voltage modulating the beam. The expression for M is given by:

$$M(\beta_e) = \frac{\int_0^d E_z(z)\, e^{j\beta_e z} dz}{\int_0^d E_z(z)\, dz} \tag{5.10}$$

where d is the gap length, and $\beta_e = \frac{\omega m \gamma}{p_0}$ is the *beam propagation factor*. The electrons enter, and leave the first gap at time t_0 with a modified momentum p_1, then drift for a distance l, and arrive at the second gap at time t_1. We have (using normalized variables):

$$t_{0i} = idt \qquad i = 1, ..., N \qquad dt = \frac{1}{N} \tag{5.11}$$

where N is the number of particles in every period,

$$p_{1i} = p_{0i} + M_1 \frac{\sqrt{1+p_{0i}^2}}{p_{0i}} V_1 \cos(\omega t_{0i}) \tag{5.12}$$

$$t_{1i} = t_{0i} + \frac{\sqrt{1+p_{1i}^2}}{p_{1i}} l \tag{5.13}$$

The first harmonic component of the beam current at the second gap is given by:

$$I_1 = -\frac{I_0}{N} \sum_{i=1}^{N} \left(e^{j\omega t_{1i}}\right) e^{i\omega t} \tag{5.14}$$

This current induces a voltage V_2 in the second cavity; the latter has an impedence:

$$Z = \frac{\frac{R}{Q}}{\frac{1}{Q} + j\delta} \tag{5.15}$$

with $\delta = \frac{\omega}{\omega_0} - \frac{\omega_0}{\omega}$. We have then:

$$V_2 = ZI_1 \tag{5.16}$$

This voltage acts back on the beam, resulting in a modified momentum p_2 for all the particles:

$$p_{2i} = p_{1i} + M_2 \frac{\sqrt{1+p_{1i}^2}}{p_{1i}} \Re[ZI_1] \tag{5.17}$$

Similar equations can be written for all the klystron cavities, in order to obtain informations on the beam current and on the induced voltage in every cavity, and on the particles longitudinal phase space. The coupling coefficient M can be easily calculated analitically if we use the ideal pillbox field, or determined with the help of electromagnetic simulation codes like SUPERFISH for more complicated cavity shapes.

5.3.2 AJDisk

AJDisk is a one-dimensional code developed at SLAC during the past 8 years in order to create a robust, user friendly, and accurate version of the already existing DOS/FORTRAN based code JPNDisk [22]. Today, AJDisk is the primary code used for accurate one dimensional simulations of round and sheet beam klystrons in SLAC's klystron department. The code works by splitting the beam into a series of disks (or plates for sheet beam devices) and allowing them to move only in the direction of propagation. The disks can then be acted on by both cavity fields and space charge forces. This approach allows for accurate but simplified modeling of beam dynamics and tube performance. The algorithm of AJDisk is fundamentally simple: a simplified flow chart is shown in fig. 5.12 [24]:

AJDisk starts initializing the data such as beam loading admittance (G_b and B_b), gap quality factors and impedances (Q_n and Z_n), etc. The input voltage is then calculated from the desired input power, while all the other voltages are set to zero. After these steps, the program is ready to move the beam through the tunnel. To do this the electron beam is sliced into a set of charged disks. The motion of each disk is governed by the space charge from other disks and/or the electric field associed with each cavity. The expressions for these fields are:

$$E_s = -\frac{q_{disk}}{\pi b^2 2\epsilon_0} \sum_{d=0}^{N_{disk}} \sum_{i=0}^{\infty} 4 \left[\frac{J_1\left(\mu_i \frac{b}{a}\right)}{\mu_i J_1\left(\mu_i\right)} \right]^2 e^{\left(\frac{-\mu_i |z-z_0|}{\gamma a}\right)} sign\left(z - z_0\right) \tag{5.18}$$

$$E_c = |V_n| \, f\left(z\right) \cos\left(\omega t + \theta\right) \tag{5.19}$$

where E_s is the space charge field from all the other disks and E_c is the circuit field associated with a cavity. It should also be noted that μ_i is the i^{th} zero of the J_0 Bessel function, γ is the radial propagation constant, and a and b are the pipe radius and the beam radius.

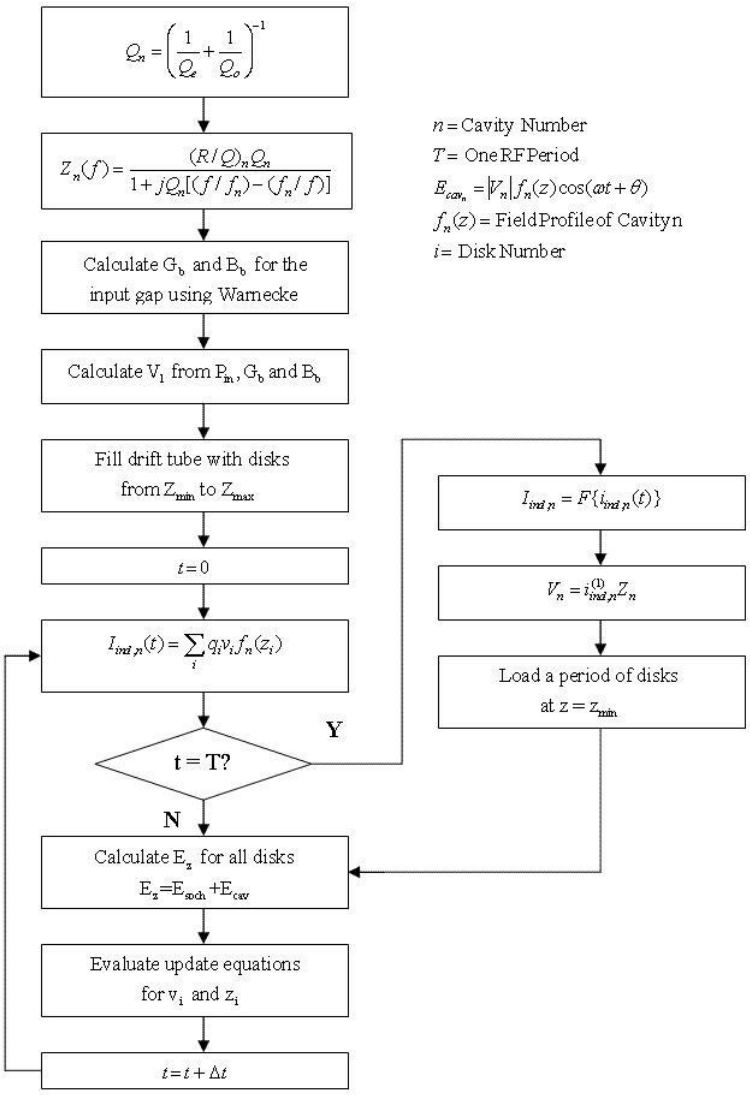

Figure 5.12: Simplified flow chart of AJDisk algorithm.

The space charge field can be broken down: the first part of the equation before the summation corresponds to the magnitude of the space-charge electric field at the location of the disk (the maximum value). The second summation simply corresponds to an exponential decay with axial distance (the magnitude is equal to one at the location of the present disk). The first summation just sums the fields from all the other disks. For further discussion see Rowe [41].

The cavity field is much simpler to understand: the field is described by multiplying the gap voltage by the shape factor of the field $f(z)$ and by an oscillating term. The field oscillation is represented by the cosine term and the field shape is given by the Gaussian approximation:

$$f(z) = \frac{k}{\sqrt{\pi}} e^{-k^2(z-z_{center})^2} \tag{5.20}$$

k can be chosen by fitting the Gaussian profile with the actual field (simulated by SUPERFISH [29]), or it is possible to calculate M for a Gaussian cavity field and then solve for k:

$$k = \frac{1}{2} \frac{\beta_e}{\sqrt{-\ln M}} \tag{5.21}$$

where β is the electron propagation constant.

Returning to the algorithm, AJDisk evaluates for each disk the equation of motion based on the field $E = E_s + E_c$. The induced current for each cavity is then calculated:

$$I_{ind} = \int_{-\infty}^{\infty} \rho \cdot v \cdot f(z) \cdot dz \tag{5.22}$$

where ρ is the one dimensional charge density, v is the velocity found after the evaluation of the equations of motion and $f(z)$ is used to represent the coupling. The fundamental component of this current is calculated using a Fourier expansion, and the induced voltage is then given by the gap impedance times the fundamental component of the induced current. The evaluation of the equations of motion and the calculation of the induced voltage are repeated until the resulting voltage from the last iteration is the voltage from the present iteration to within some predefined percentage error. The next step is then the calculation of the gain and efficiency.

AJDisk evaluates two kind of efficiencies; the kinetic efficiency is:

$$\eta_k = 1 - \frac{\sum_{d=0}^{N_{disk}} \left(1 - \left(\frac{v_{exit,d}}{c}\right)^2\right)^{-1/2} - 1}{\sum_{d=0}^{N_{disk}} \left(1 - \left(\frac{v_{inlet,d}}{c}\right)^2\right)^{-1/2} - 1} \tag{5.23}$$

where v_{exit} is the velocity at the end of the output region and v_{inlet} is the velocity at the beginning of the output region. A simple way to look at this equation is to break it down, into the form $\frac{KE_{inlet}-KE_{outlet}}{KE_{inlet}}$.

The electronic efficiency is:

$$\eta_e = Re\left[\frac{V_N \cdot I^*_{ind,N}}{2 \cdot V_0 \cdot I_0}\right] \tag{5.24}$$

where N refers to the output cavity. This equation finds the percentage of the beam power which is converted to RF power in the output gap.

The final step is to display the results. Fig. 5.14 shows an example of the output plots given by AJDisk.

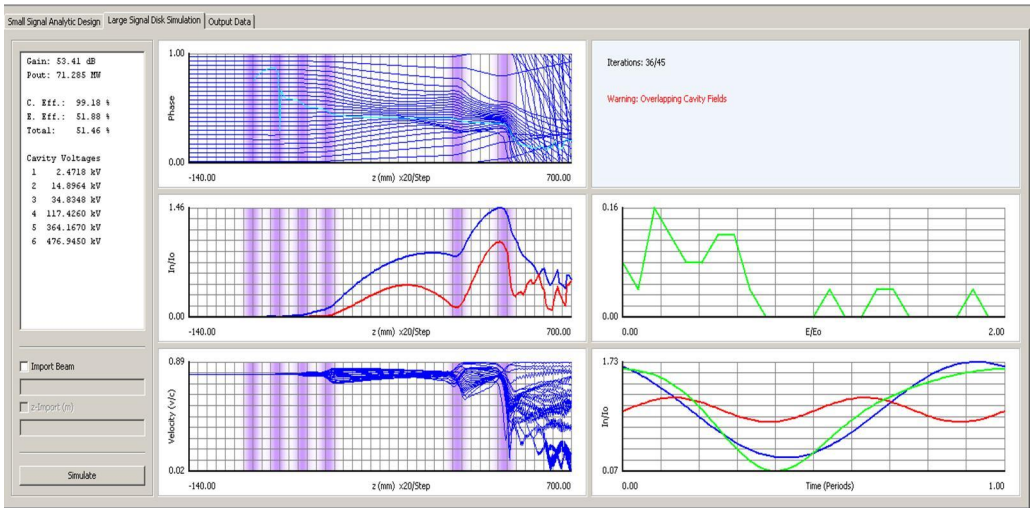

Figure 5.13: Example of the output given by AJDisk after the simulation of the SLAC 5045 S-band klystron.

One of the major restrictions of AJDisk is that it does not allow to obtain "electromagnetic" information: for example, it is not possible to obtain the cavity fields in presence of the beam, or to calculate the reflected power at the entrance of the input and output cavities.

5.3.3 Main results

Let's consider now the case of the first cavity of a klystron working at 11.424 GHz followed by a drift and by a second passive cavity. Since the kinematic analysis does not consider the contribution of the space charge fields, it can be interesting to start the comparison with the new code from here. As a first example let's consider the following parameters:

Table 5.2:

Driving frequency (GHz)	f	11.424
Focusing field (only considered in the new code) (T)	B_0	0.093
Input power (W)	P_{IN}	250
Beam current (A)	I_0	10
Beam voltage (kV)	V_0	100
Beam radius (cm)	R_b	0.375
First cavity lenght (cm)	L_1	0.3
First cavity resonant frequency (GHz)	f_1	11.424
First cavity quality factor	Q_0	3729.66
First cavity external Q	Q_e	95
Drift length (cm)	L_2	10
Second cavity lenght (cm)	$L1$	0.5
Second cavity resonant frequency (GHz)	f_2	11.454
Second cavity quality factor	Q_0	5415.57
Second cavity external Q	Q_e	∞

The following graphics show the value of the particles normalized z-momentum before and after the first cavity, and after the drift space (before the second cavity) obtained with the kinematic analysis (blue dots) and with the new code (pink dots).

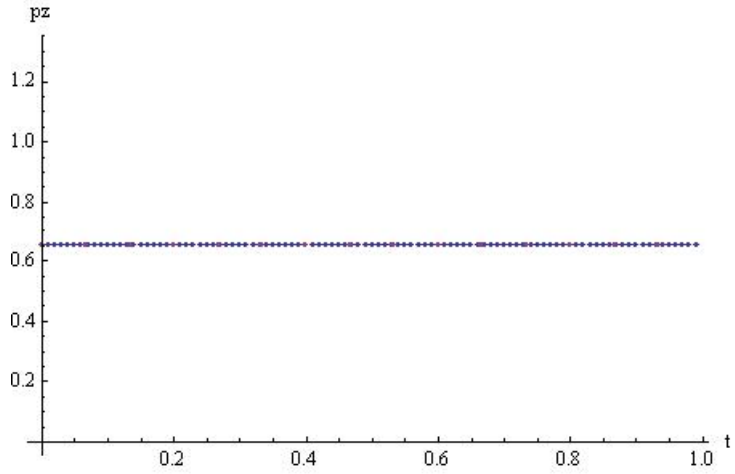

Figure 5.14: Particles normalized z-momentum as a function of the normalized arrival time before the first cavity obtained with the klystron kinematic theory (blue) and with the new code (pink).

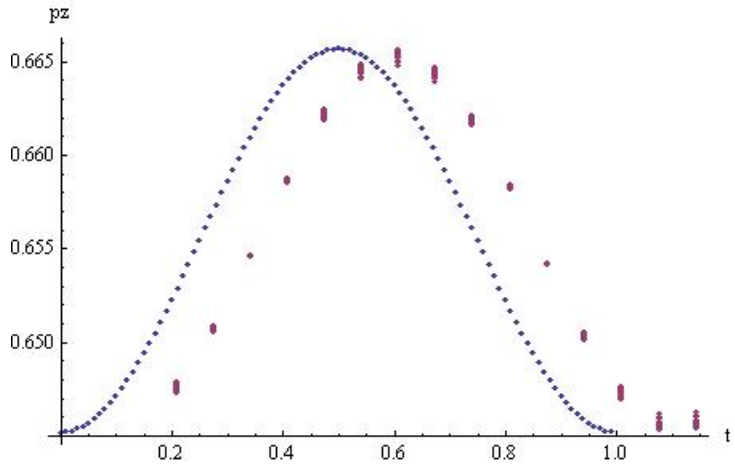

Figure 5.15: Particles normalized z-momentum as a function of the normalized arrival time after the first cavity obtained with the klystron kinematic theory (blue) and with the new code (pink).

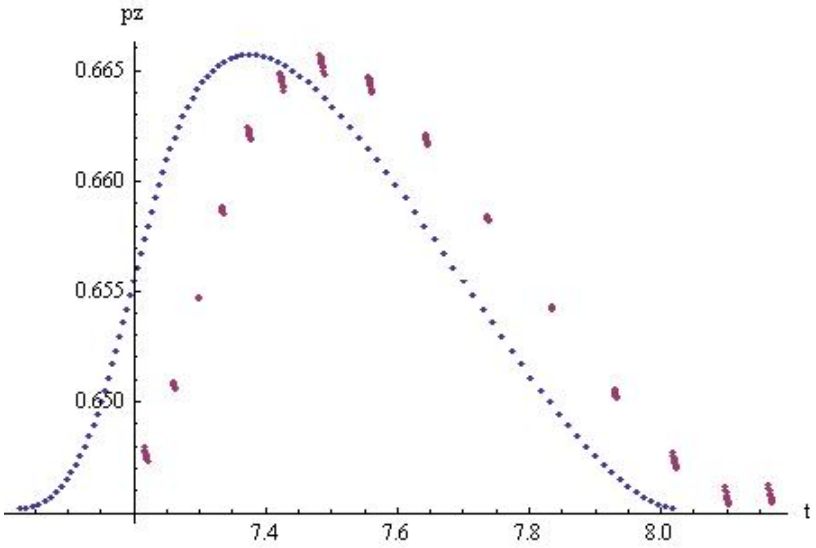

Figure 5.16: Particles normalized z-momentum as a function of the normalized arrival time after the drift space obtained with the klystron kinematic theory (blue) and with the new code (pink).

The two methods show a good agreement if we consider that the klystron kinematic analysis does not take in account the finite cavity length; this explains the displacement between the two graphics on the horizontal axis. Furthermore, the kinematic theory allows to consider only on-axis particles. The other important difference is in the fact that the klystron kinematic analysis calculates only the action of the first cavity field on the particles, but it does not consider the effect of the beam back on the cavity, while in the new code a steady state solution is found. These difference is more evident if we look at the particles normalized z-momentum after the second cavity:

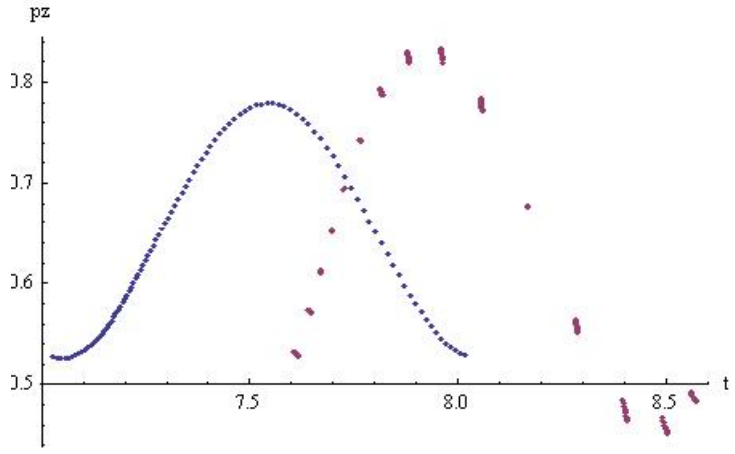

Figure 5.17: Particles normalized z-momentum as a function of the normalized arrival time after the second cavity obtained with the klystron kinematic theory (blue) and with the new code (pink).

In this case the beam current induces a voltage in the second cavity; this voltage acts again on the beam, modifying the current, and so the cavity field itself is again affected. This effect is neglected in the kinematic analysis, in which the voltage induced in the second cavity is calculated by simply multiplying the beam current by the cavity impedence, while it is taken into account in the research of the steady state solution in the new code; the more evident difference is that the momentum spread between all the particles obtained with the mathematica code is greater than the one obtained with the ballistic theory.

Let's now compare the results obtained with the ones from the code AJDisk. Since the new code simulations made so far do not consider the space charge fields contribution, we will consider only very low current cases. The following table shows the main parameters.

Table 5.3:

Driving frequency (GHz)	f	11.424
Focusing field (only considered in the new code) (T)	B_0	0.093
Input power (W)	P_{IN}	250
Beam current (A)	I_0	5
Beam voltage (kV)	V_0	100
Beam radius (cm)	R_b	0.375
First cavity lenght (cm)	L_1	0.3
First cavity resonant frequency (GHz)	f_1	11.424
First cavity quality factor	Q_0	3729.66
First cavity external Q	Q_e	95
Drift length (cm)	L_2	5
Second cavity lenght (cm)	$L1$	0.5
Second cavity resonant frequency (GHz)	f_2	11.454
Second cavity quality factor	Q_0	5415.57
Second cavity external Q	Q_e	∞

The following graphics show the value of the particles longitudinal v/c as a function of z obtained with the new code and with AJDisk respectively.

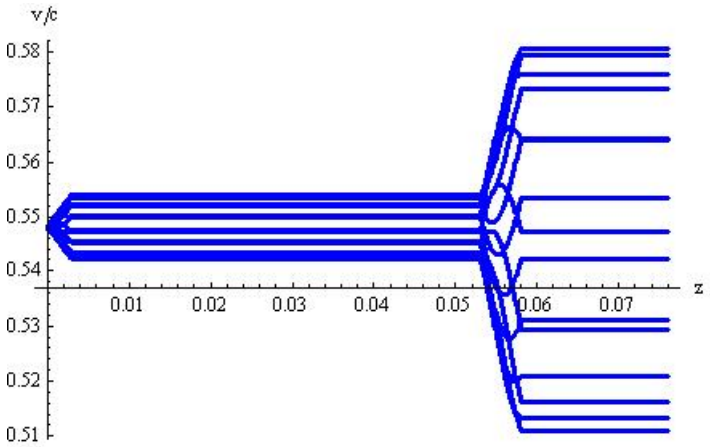

Figure 5.18: Particles v/c as a function of the longitudinal distance z.

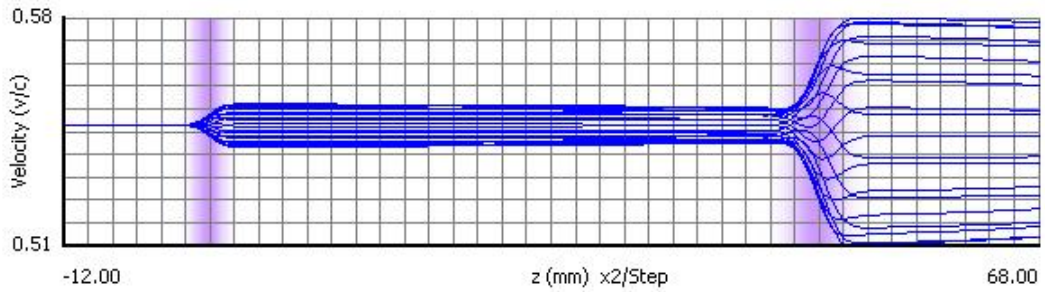

Figure 5.19: Particles v/c as a function of the longitudinal distance z.

Since we considered a low current and a short drift length, the results show a good agreement. This is obviously not true anymore if we consider an higher current, and if we let the particles drift for a longer distance before the second cavity: in this case we have that the space charge fields create oscillations in the beam that modify dramatically the beam dynamics. As an example, we can consider the case of a higher current beam (25 A) drifting for a 10 cm distance after the second cavity:

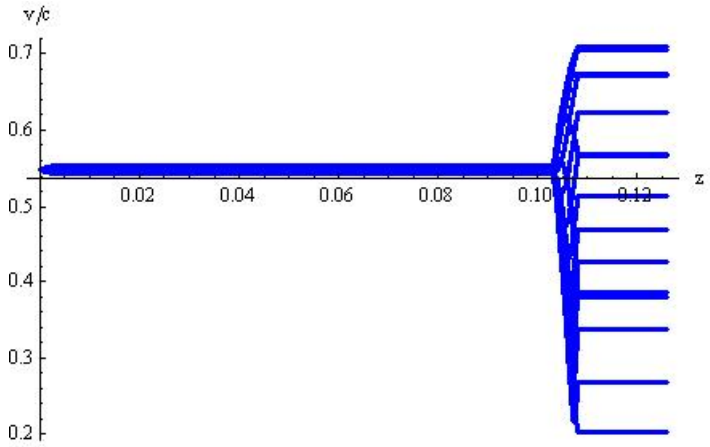

Figure 5.20: Particles v/c as a function of the longitudinal distance z.

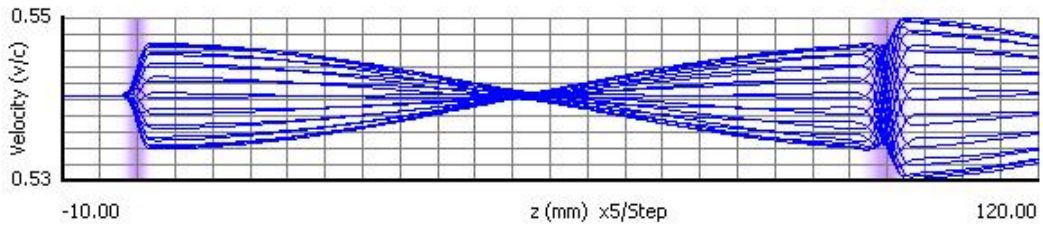

Figure 5.21: Particles v/c as a function of the longitudinal distance z.

As one can see from the AJDisk simulation, the space charge forces strongly contribute to the velocity modulation process and to the maximum velocity spread that can be reached inside the beam. This means, obviously, that also the beam current, and the voltage induced in the second cavity will be affected. The following plots show the maximum v_z/c spread and the normalized induced voltage into the second cavity as a function of the logarithm of the beam current obtained with the three methods: the kinematic klystron theory (green dots), the new code (blue dots) and AJDisk (red dots):

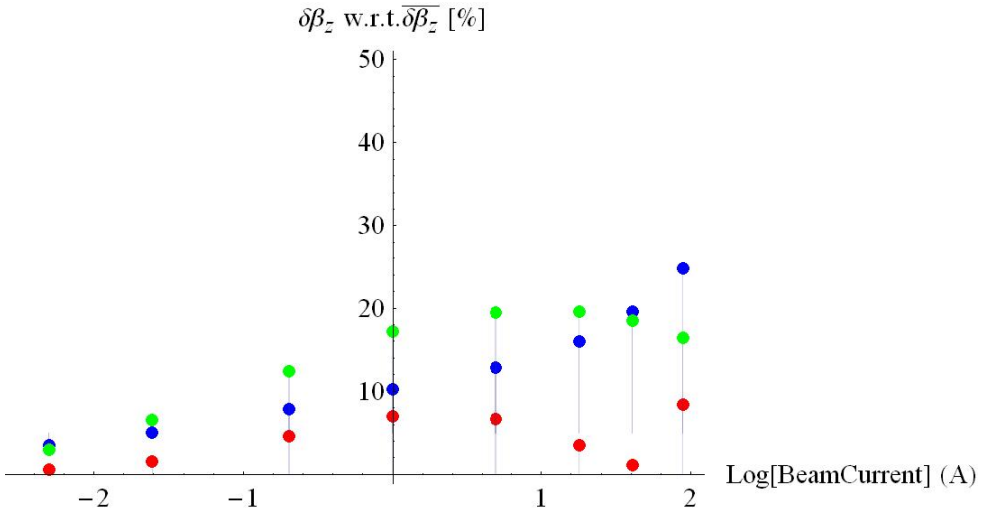

Figure 5.22: Maximum v/c spread after the second cavity as a function of the beam current for a drift length of 10 cm.

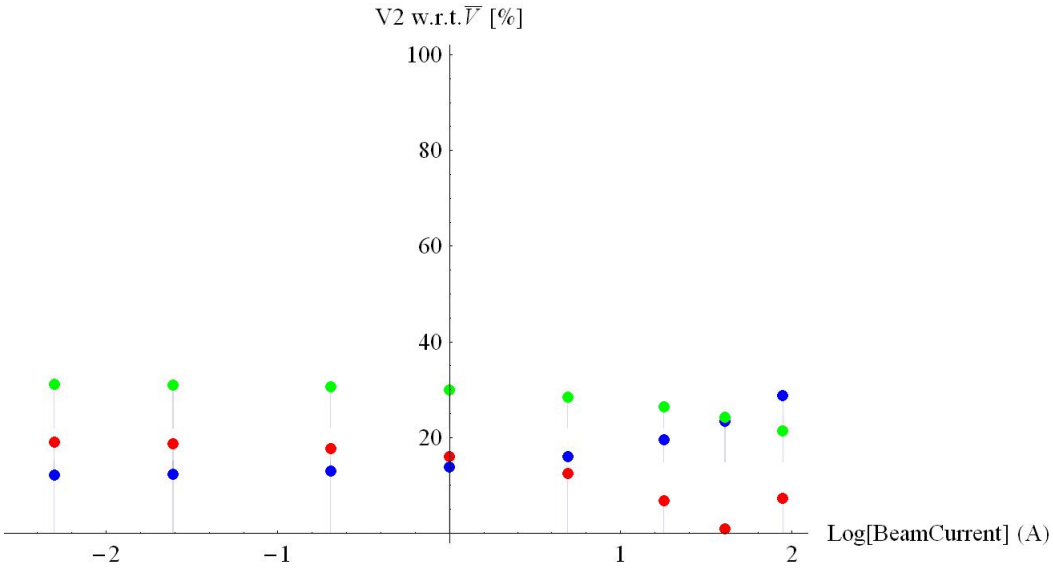

Figure 5.23: Particles v/c as a function of the beam current for a drift length of 10 cm.

It is clear that, even for very low perveance klystrons, a realistic simulation of the device requires to take in account the contribution of the space charge fields, at least in the drift tubes. This problem will be treated in the following chapter. Finally, the cavity fields analytic expression that we used so far is not appropriate anymore if the klystron cavities have a more complicated shape, as it is in the reality, expecially if we think to a multigap output cavity; in this case the cavity fundamental mode field has to be imported from an electromagnetic 2-D simulation code, such as SUPERFISH, or the 2-D FEM based code developed by Prof. S. Tantawi at SLAC.

Chapter 6

The space charge field

6.1 Introduction

The three dimensional calculation of the Coulomb repulsion between particles is one of the most complicated aspects in a particle interaction code. Since the particles are moving it requires the solution of the wave equation with boundary conditions which depend on the shape of the klystron's cavities and pipe. Besides, these calculations have to be performed many times in order to find the desired steady state solution.

An iterative method which uses the analytical expressions of the space charge potentials will be treated in the following sections; it will become soon evident that the analytical approach requires many approximations to be done if we want to preserve the simplicity and the speed of the code. However, the presented algorithm can be easily implemented also by using the fields computed with numerical electromagnetic solvers and this could definitely improve the precision and the speed of the simulations.

6.2 The space charge field

The space charge force on a test particle due to the potential generated by the distribution of all the other particles at time t depends on the position of all these particles at that instant of time. Let's start by finding an expression for the space charge potential generated by a distribution of point charges.

A convenient approach to the calculation of the space charge potential can be splitted in to three conceptual blocks: the first one is to find the potential generated by a single particle inside the beam pipe in the particle frame. This allows us to solve the static Poisson equation instead of the wave equation.

In the second block we can then calculate the electromagnetic field in the particle frame and perform a Lorentz transformation from the particle frame to the laboratory frame, obtaining both an electric field and a magnetic field.

Finally, we have to sum the fields generated by all the particles.

Unfortunately, this process is still very complicated for several reasons: first of all, the Lorentz transformation is not trivial if the domain's boundaries used to obtain the potentials are not longitudinally uniform, as it is if the beam pass from the pipe to a complicated shape cavity and again to the pipe.

The first simplification that we will do is then to consider the space charge forces only inside the drift tubes between the cavities. This approximation can be justified by observing that the cavity length in a klystron is usually small with respect to the one of the pipes. Furthermore, if the beam perveance is not too high (as we assume, if we want an high efficiency device) we can neglect the effects of the space charge forces with respect to the RF fields inside the klystron resonators. The main action of the space charge fields can then be observed while the particles are drifting.

Unfortunately, this approximation is not sufficient to fully solve the problem. The second issue is that, if we decide to solve the Poisson equation only inside the pipe (by somehow "neglecting" the discontinuity constitued by the cavities), we have to solve the problem of finding the potential due to a point charge inside an infinite conducting cylinder. This has been treated by several authors [42] [43] and it will not be discussed here.

The important result is that the expression obtained when solving the Poisson equation inside the infinite cylinder is given by an infinite sum which contains Bessel functions, as shown in the following expression:

$$G\left(\vec{r},\vec{r}'\right)=\sum_{n=0}^{\infty}\frac{\delta_n}{2\pi\epsilon_0 b}\sum_{k=1}^{\infty}\frac{J_n\left(\xi_{nk}r/b\right)J_n\left(\xi_{nk}r'/b\right)}{\xi_{nk}J_1^2\left(\xi_{nk}\right)}\cos\left[n\left(\phi-\phi'\right)\right]e^{-\xi_{nk}\frac{|z-z'|}{b}} \tag{6.1}$$

where $J_n(x)$ represents the Bessel function of order n, whose zeros are ordered as ξ_{nk}, and Neumann's symbol δ_n is defined as:

$$\delta_n=\begin{cases}1 & n=1,\\ 2 & n=2,3,4...\end{cases} \tag{6.2}$$

To make eq. (6.1) practical the summation must be performed to some finite value of k. The following picture shows the value of the amplitude of the longitudinal electric field (averaged over the transverse beam section) as a function of the number of terms of the summation [24]:

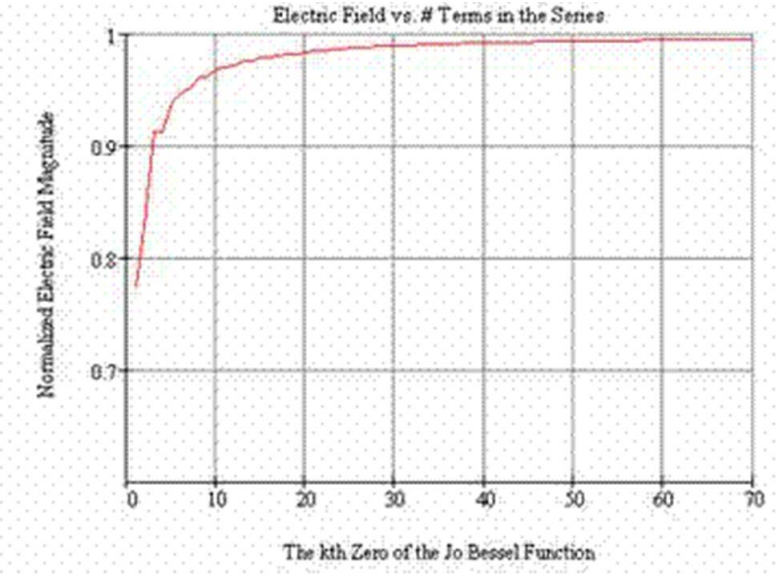

Figure 6.1: Longitudinal electric field (averaged over the transverse beam section) as a function of the number of terms of the summation over k in eq. (6.1).

The evaluation of expression (6.1) has to be performed for every particle of the beam at every iteration. This would appreciably lengthen the computing time for the simulation. Furthermore, equation (6.1) is singular on

the transverse plane. For $z = z_0$ the longitudinal electric field has to be equal to zero, but this does not come out from equation (6.1). For all these reasons we will consider, as a first step in the implementation of the space charge routine, the simple expression of the scalar potential of a point charge in the free space. This approximation will produce an error expecially on the longitudinal component of the space charge field, as it is possible to see in fig. (6.2) that shows the electric field lines between bunches in the case of: a) and infinite beam; b) a finite beam in free space; c) a finite beam in conducting cylinder. This error can be taken into account by introducing some corrective factors, and it can be still a good compromise if we want to obtain a code which is not extremely time consuming.

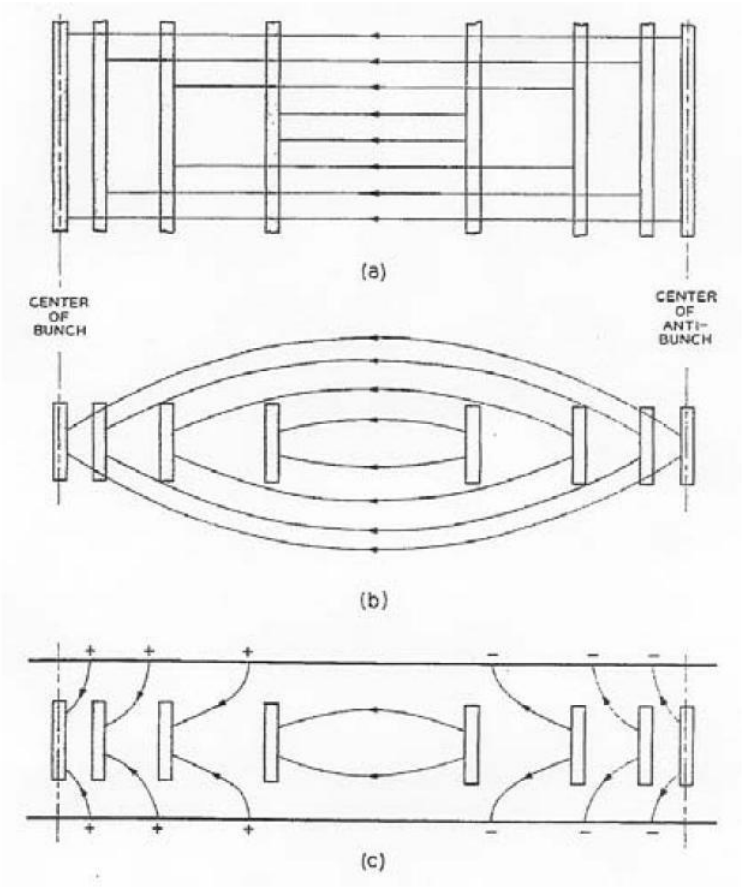

Figure 6.2: Weakening of the longitudinal fields between bunches due to the presence of the drift tube.

In the particle frame we then have that the potential generated from particle i is:

$$V_i'\left(x',y',z'\right)=\frac{q_i}{4\pi\epsilon\sqrt{\left(x'-x_i'\right)^2+\left(y'-y_i'\right)^2+\left(z'-z_i'\right)^2}} \tag{6.3}$$

$$\vec{A}_i'\left(x',y',z'\right)=0 \tag{6.4}$$

where the superscript " $'$ " indicates the particle frame quantities.

The electromagnetic field can then be obtained from:

$$\vec{E}'=-\nabla' V'-\frac{\partial\vec{A}'}{\partial t'} \tag{6.5}$$

$$\vec{B}'=\nabla'\times\vec{A}' \tag{6.6}$$

And it has then to be Lorentz transformed through [44] [45]:

$$\begin{cases}\vec{E}_{\parallel}=\left(\vec{E}'-\vec{v}\times\vec{B}'\right)_{\parallel}\\ \vec{E}_{\perp}=\gamma\left(\vec{E}'-\vec{v}\times\vec{B}'\right)_{\perp}\\ \vec{B}_{\parallel}=\left(\vec{B}'+\frac{\vec{v}}{c^2}\times\vec{E}'\right)_{\parallel}\\ \vec{B}_{\perp}=\gamma\left(\vec{B}'+\frac{\vec{v}}{c^2}\times\vec{E}'\right)_{\perp}\end{cases} \tag{6.7}$$

where $\vec{v}$ is the particle velocity.

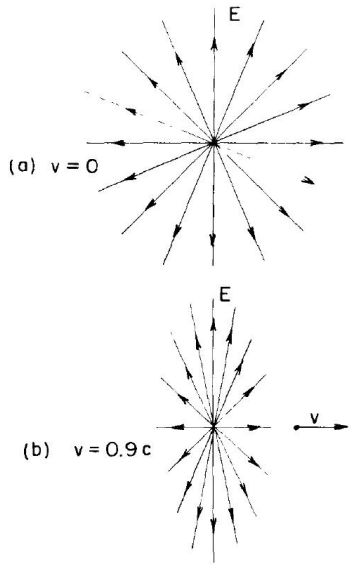

Figure 6.3: Electric field of a charge moving with the constant speed $v = 0.9c$ (b), compared with the field of a charge at rest (a).

We then get, for particle i:

$$E_{xi}(x,y,z) = \frac{\gamma q_i (x - x_i)}{4\pi\epsilon \left[(x-x_i)^2 + (y-y_i)^2 + \gamma^2 (z-z_i)^2\right]^{\frac{3}{2}}} \tag{6.8}$$

$$E_{yi}(x,y,z) = \frac{\gamma q_i (y - y_i)}{4\pi\epsilon \left[(x-x_i)^2 + (y-y_i)^2 + \gamma^2 (z-z_i)^2\right]^{\frac{3}{2}}} \tag{6.9}$$

$$E_{zi}(x,y,z) = \frac{\gamma q_i (z - z_i)}{4\pi\epsilon \left[(x-x_i)^2 + (y-y_i)^2 + \gamma^2 (z-z_i)^2\right]^{\frac{3}{2}}} \tag{6.10}$$

$$B_{xi}(x,y,z) = \frac{\beta\gamma}{c} \frac{q_i (y - y_i)}{4\pi\epsilon \left[(x-x_i)^2 + (y-y_i)^2 + \gamma^2 (z-z_i)^2\right]^{\frac{1}{2}}} \tag{6.11}$$

$$B_{yi}(x,y,z) = -\frac{\beta\gamma}{c} \frac{q_i (x - x_i)}{4\pi\epsilon \left[(x-x_i)^2 + (y-y_i)^2 + \gamma^2 (z-z_i)^2\right]^{\frac{1}{2}}} \tag{6.12}$$

$$B_{zi}(x,y,z) = 0 \tag{6.13}$$

The total field is then given by the sum of the fields generated by all the particles:

$$E_x(x,y,z) = \sum_{i=1}^{N} \frac{\gamma q_i (x - x_i)}{4\pi\epsilon \left[(x-x_i)^2 + (y-y_i)^2 + \gamma^2 (z-z_i)^2 \right]^{\frac{3}{2}}} \tag{6.14}$$

$$E_y(x,y,z) = \sum_{i=1}^{N} \frac{\gamma q_i (y - y_i)}{4\pi\epsilon \left[(x-x_i)^2 + (y-y_i)^2 + \gamma^2 (z-z_i)^2 \right]^{\frac{3}{2}}} \tag{6.15}$$

$$E_z(x,y,z) = \sum_{i=1}^{N} \frac{\gamma q_i (z - z_i)}{4\pi\epsilon \left[(x-x_i)^2 + (y-y_i)^2 + \gamma^2 (z-z_i)^2 \right]^{\frac{3}{2}}} \tag{6.16}$$

$$B_x(x,y,z) = \sum_{i=1}^{N} \frac{\beta\gamma}{c} \frac{q_i (y - y_i)}{4\pi\epsilon \left[(x-x_i)^2 + (y-y_i)^2 + \gamma^2 (z-z_i)^2 \right]^{\frac{1}{2}}} \tag{6.17}$$

$$B_y(x,y,z) = -\sum_{i=1}^{N} \frac{\beta\gamma}{c} \frac{q_i (x - x_i)}{4\pi\epsilon \left[(x-x_i)^2 + (y-y_i)^2 + \gamma^2 (z-z_i)^2 \right]^{\frac{1}{2}}} \tag{6.18}$$

$$B_z(x,y,z) = 0 \tag{6.19}$$

Once that we have the space charge field at the location of particle j due to the presence of all the other particles in the laboratory frame, we can integrate the equations of motion for the considered particle in presence of the total (space charge and focusing) field.

6.3 The algorithm

The search of a steady state solution consists of an iterative application of the two-steps routine composed by:

- the calculation of the total space charge potentials inside the drift tube as a function of time t;

- the particle tracking inside the drift tube in presence of these fields.

As we can see from the previous section, the solution of the Poisson equation gives a potential who is not explicitely dependent on time: the potential generated in a position (x, y, z) at every time t from a particle in (x_0, y_0, z_0) depends only on the distance from the two positions at that time. For this reason, the choice of z as independent variable during the integration of the equations of motion can introduce some difficulties. For example, the potential at the step z^* can depend on a particle who is in a position $z_i > z^*$. It is then evident that an addictional z to t transformation is required in order to have a z-code. The easiest approach would then be to use the t variable when calculating the space charge field, while leaving the z variable inside the cavities, since this would allow us to achieve a higher speed while integrating the equations in presence of the RF field over the same interval for all the particles.

Let's now describe the simulation algorithm more in detail. Fig. 6.4 shows a summarizing flow chart:

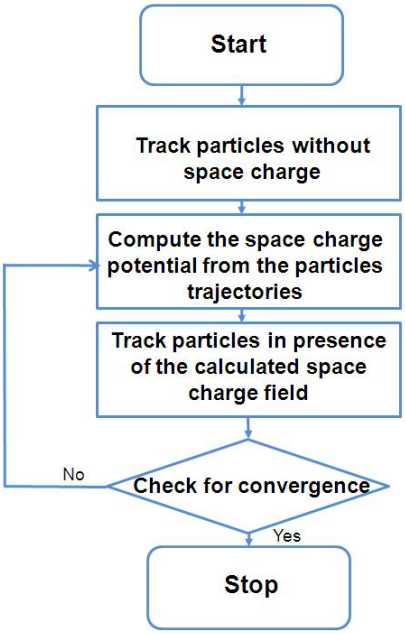

Figure 6.4: Flow chart for the steady state simulation with space charge.

The first iteration consists of a simple tracking of the electrons through the drift tube, without considering any kind of space charge field. The result of this first integration will be a complete description of the particles phase space as a function of time from the instant in which they enters into the pipe to the one in which they go out towards the next cavity. We will obtain:

$$\{x_i^0(t), y_i^0(t), z_i^0(t), p_{xi}^0, p_{yi}^0, p_{zi}^0\} \qquad i = 1, ..., N \tag{6.20}$$

where N is the number of particles emitted in a RF period.

The initial integration time can be determined for every particle by using the results of the integration of the equations of motion inside the previous cavity, while the final time can be easily determined by knowing that the particle longitudinal speed is not changing during the integration since no RF or space charge field is applied.

After the first tracking with no space charge forces taken into account, we can calculate the space charge potential generated by the previous particles distribution in every point of the pipe and for every time t. This can be done either analitically (by using the expressions reported in the previous paragraph), or numerically, by solving the Poisson's equation (in the particles frame and then Lorentz transforming) with an electromagnetic solver.

The space charge fields inside the pipe will then be:

$$\vec{E}^0(t) = \sum_{i=1}^{M} \vec{E}_i \left(x\left(t\right), y\left(t\right), z\left(t\right), x_i^0\left(t\right), y_i^0\left(t\right), z_i^0\left(t\right) \right) \tag{6.21}$$

$$\vec{B}^0(t) = \sum_{i=1}^{M} \vec{B}_i \left(x\left(t\right), y\left(t\right), z\left(t\right), x_i^0\left(t\right), y_i^0\left(t\right), z_i^0\left(t\right) \right) \tag{6.22}$$

where the summation is made over all the particles that are closer than half of the beam wavelength to (x, y, z) at time t.

These fields are then used to integrate the equations of motions during the second iteration and obtain $\{x_i^1(t), y_i^1(t), z_i^1(t), p_{xi}^1, p_{yi}^1, p_{zi}^1\}$ for all the particles. The space charge fields can then be recalculated and the procedure is iterated until it reaches the convergence. The check for convergence has

to be done at every iteration; there are many possible ways to implement it: the easiest is probably to do a control on particles phase space trajectories between two subsequent iterations:

$$\left|\xi_i^n - \xi_i^{n-1}\right| \leq \epsilon \tag{6.23}$$

where ξ_i^n is the generic normalized phase space coordinate of particle i after iteration n and ϵ depends on the desired convergence accuracy.

6.3.1 Main development issues

We are interested in klystrons *steady state* simulations: this allows us to study the evolution of only one set of particles distribuited over an RF period, because the resulting trajectory and electromagnetic field reflect the behaviour of the whole particle beam after the transient. At the same time, special attention has to be payed to the space charge potential calculation: at every time t^*, this is produced by *all* the particles that are in the considered region of space, and not only by the ones emitted in the RF period taken in account. A consequence of the steady state approach is that a particle, who has at the time $t^* \pm kT$ (with $k = 0, 1, 2, ...$) the same phase space coordinates of another particle at the time t^*, will have the same evolution. We can then simply integrate the equations of motion for every particle of the set in presence of a space charge field that is, at time t^*, the sum of the contributions of all the particles which are in the considered region of space (± 0.5 of the beam wavelength) at time t^* and belong also to sets before or after the considered one. The condition to be satisfied in order to evaluate if they are in the considered region of space or not at t^* is:

$$t_i^{in} \leq t^* \pm kT \leq t_i^{out} \qquad\qquad k = 0, 1, 2, ... \tag{6.24}$$

where t_i^{in} and t_i^{out} are respectively the entrance and the exit times of particle i into the region.

The contributions for $k \geq 3$ can be neglected, since the condition (6.24) would be, in that case, probably not satisfied. The space charge fields at

time t will then be, omitting the iteration superscript:

$$\begin{aligned}\vec{E}(t) = &\sum_{i=1}^{N} \vec{E}_i\left(x\left(t\right), y\left(t\right), z\left(t\right), x_i\left(t\right), y_i\left(t\right), z_i\left(t\right)\right) + \\ &+ \sum_{k} \left(\sum_{i=1}^{N} \sigma_{i,k}^{+}\left(t\right) \vec{E}_i\left(x\left(t\right), y\left(t\right), z\left(t\right), x_i\left(t+kT\right), y_i\left(t+kT\right), z_i\left(t+kT\right)\right) + \right. \\ &\left. + \sum_{i=1}^{N} \sigma_{i,k}^{-}\left(t\right) \vec{E}_i\left(x\left(t\right), y\left(t\right), z\left(t\right), x_i\left(t-kT\right), y_i\left(t-kT\right), z_i\left(t-kT\right)\right) \right)\end{aligned} \tag{6.25}$$

$$\begin{aligned}\vec{B}(t) = &\sum_{i=1}^{N} \vec{B}_i\left(x\left(t\right), y\left(t\right), z\left(t\right), x_i\left(t\right), y_i\left(t\right), z_i\left(t\right)\right) + \\ &+ \sum_{k} \left(\sum_{i=1}^{N} \sigma_{i,k}^{+}\left(t\right) \vec{B}_i\left(x\left(t\right), y\left(t\right), z\left(t\right), x_i\left(t+kT\right), y_i\left(t+kT\right), z_i\left(t+kT\right)\right) + \right. \\ &\left. + \sum_{i=1}^{N} \sigma_{i,k}^{-}\left(t\right) \vec{B}_i\left(x\left(t\right), y\left(t\right), z\left(t\right), x_i\left(t-kT\right), y_i\left(t-kT\right), z_i\left(t-kT\right)\right) \right)\end{aligned} \tag{6.26}$$

where:

$$\sigma_{i,k}^{+}\left(t\right) = \begin{cases} 1 & \text{if } t_i^{in} \leq t + kT \leq t_i^{out} \\ 0 & \text{if } t + kT \leq t_i^{in} \text{ or } t + kT \geq t_i^{out} \end{cases} \tag{6.27}$$

and:

$$\sigma_{i,k}^{-}\left(t\right) = \begin{cases} 1 & \text{if } t_i^{in} \leq t - kT \leq t_i^{out} \\ 0 & \text{if } t - kT \leq t_i^{in} \text{ or } t - kT \geq t_i^{out} \end{cases} \tag{6.28}$$

The other important problem that has to be solved in order to properly evaluate the space charge forces inside the klystron pipes is related to the length of the region to be considered for the contibutions of particles to the space charge field. Even if we are interested in finding the steady state

solution in presence of space charge effects only inside the drift tubes, we can't limitate the sum in equations (6.25) and (6.25) just to particles inside the pipe; in this case in fact, we will have a non physical longitudinal force directed in the $-z$ direction acting on particles at the beginning of the pipe, generated by particles ahead in the drift space, and the same but opposite problem will show up in the final part of the drift tube: particles inside the pipe will contribute to the space charge potential, while particles situated after the exit will not, and this will create a force directed in the $+z$ direction which is not real, as shown in the following picture for on-axis particles.

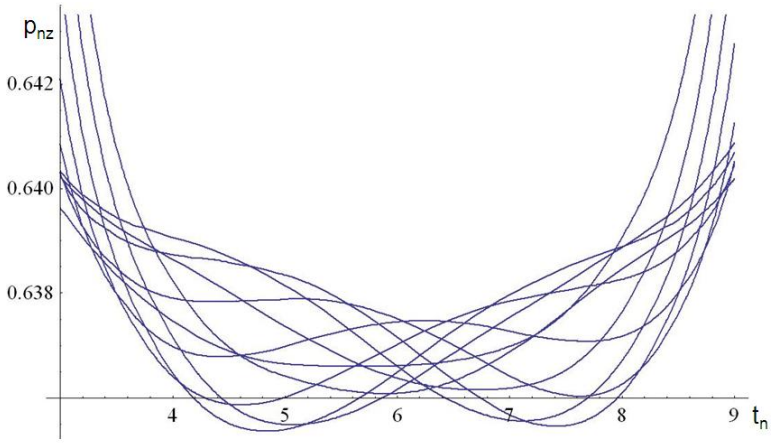

Figure 6.5: Normalized z momentum as a function of time for on-axis particles obtained considering only particles inside the drift space in the sums (6.25) and (6.25).

To solve this problem we have to extend the sums (6.25) and (6.25) to particles inside cavities and pipes before and after the drift space we are interested in finding the steady state solution for. The particles outside the considered drift tube will then be used as sources for the space charge fields but their trajectories will not be modified during the iterative procedure, since we already have the steady state solution for them. The described procedure has finally been implemented in the code for the simple case of the input klystron cavity characterized in table 5.1 followed by a 10 cm drift tube. Next figure shows then the obtained normalized z-momentum for on-

axis particles; the cavity action is shown too.

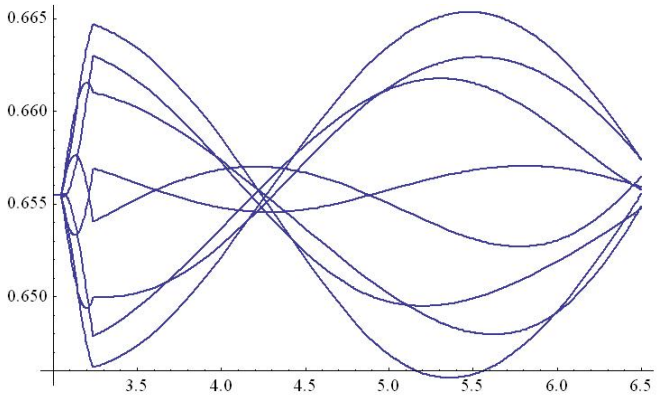

Figure 6.6: Normalized z momentum as a function of time for on-axis particles.

6.4 Final remarks

Space charge fialds play an important role in modifying the RF performance of a klystron. Even for very low perveance klystrons, a realistic simulation of the device requires to take in account the contribution of the mutual repulsion between particles, at least in the drift tubes. The described iterative method allows to evaluate the strength of these forces that cause the electrons to oscillate back and forth in the reference frame at the plasma frequency. The results we have derived apply to a finite radius beam drifting in free space, but they could be easily extended to the case of a beam inside a pipe by introducing corrective reduction coefficients for the plasma wavelength [21] [46]. The method takes in account also the transverse space charge forces and their contribution to the radial particles motion combined to the one of the magnetic focusing field.

Chapter 7

Conclusion

The design of klystron amplifiers widely lies on the intensive utilization of simulation codes. These can be 1-D codes which are based on combination of analytical formulae and electron dynamics equations and are used for a quick assessment of the power and efficiency of the new klystron design in steady state, or PIC codes, which are capable to perform very accurate simulations of the device, at the expenses of a greater complexity and a larger simulation time.

In the present work a steady state code which can self-consistently simulate the complete cavity-beam interaction has been presented. The code is based on the search of the steady state solution inside the RF cavities by iteratively solving the power balance equation; the resonators can be coupled (as it is for the klystron input and output cavities), or not. The solution determines the amplitude and phase of the electromagnetic field inside the structure starting from the cavity mode field. The latter can be the analytical pillbox field (as a first approximation), or can be imported by 2-D electromagnetic simulation codes for more complicated cavity shapes. The fundamental theory necessary to obtain the equations used to develop the simulation algorithm has been exposed in chapter 3. The cavity total field is first expanded in series of the cavity natural modes and then expressed as the product of the fundamental mode field multiplied for a complex coefficient; the equation that ties the amplitude and phase of this coefficient with

the cavity input power and with the beam current density is then obtained from the total power balance of the system. This equation depends on the beam current density that is a function of the particles velocities, and these depend on the total cavity field. It has then to be solved iteratively. The implemented solution algorithm is basically divided in two steps: the first one is to solve the equations of motion for the particles moving inside the structure; the second one is then to evaluate, from the obtained particles trajectories in phase space, the beam current density in order to calculate the complex field coefficient. This procedure is iterated until it reaches the desired convergence.

Particular attention has been payed to the integration of the electrons equations of motion. It is known that numerical integration methods such as the ordinary Runge-Kutta methods are not ideal for integrating Hamiltonian systems, because the numerical approximation to a Hamiltonian system obtained from an ordinary numerical method does introduce a non-Hamiltonian perturbation. This problem has led to the introduction of methods of symplectic integration for Hamiltonian systems, which do preserve the features of the Hamiltonian structure by arranging that each step of the integration be a canonical or symplectic transformation. The main issues related to the symplectic integration of Hamiltonian systems have been treated in Chapter 4, where the relativistic equations of motion for the particles have been written in the form suitable for numerical integration. They have been obtained from a "pseudo" time independent Hamiltonian, derived from the well known Hamiltonian of a particle in an electromagnetic field through the addiction of two more phase space variables. The dynamical system is then described by a set of eight ordinary differential equations which can finally be integrated with a symplectic implicit integration method.

The described algorithm has been implemented using *Mathematica*. The self-consistency of the code has been tested on some simple situations in absence of space charge effects; the case of presence of an external feeding (pillbox input cavity) has been treated first, followed by the case of a two

cavity klystron, where the beam itself is the power source in the output cavity. Some important simulation parameters have been discussed, such as the number of macroparticles to be simulated and their initial time and space distribution. The results have then been compared to the ones obtained with the simple calculations based on the klystron kinematic theory; these take in account only the action of the cavity field on the particles, but do not consider the effect of the beam back on the cavity. A second comparison has been made with the results from the code AJDisk. The latter is a one dimensional code that works by splitting the beam into a series of disks and allowing them to move only in the direction of propagation. The disks can be acted on by both cavity fields and space charge forces. The comparison gives a good agreement in the case of low current beams, while higher current simulations show differences due to fact that space charge effects had not been taken in account yet in the new code.

The introduction of the space charge forces has been trated in Chapter 6. The repulsion forces between particles have been evaluated in the drift tubes between cavities, where they have the more significant effects on the velocity modulation process. The search of a steady state solution in this case consists of an iterative application of the two-steps routine composed by: i) the calculation of the total space charge potentials inside the drift tube as a function of time t and ii) the particle tracking inside the considered tube in presence of these fields. The first iteration consists of a simple tracking of the electrons through the drift tube, without considering any kind of space charge field: the result of this first integration will be a complete description of the particles phase space as a function of time. The space charge potential generated by the previous particles distribution in every point of the pipe and for every time t can then be calculated and used during the next iteration to track the particles through the drift tube. The procedure is repeated until it reaches the convergence, and the check for convergence is done at every iteration. The main development issues are finally presented at the end of Chapter 6 together with their solution.

Appendix A

The *Mathematica* code

Constants

```
In[1]:= Ci = 2.99792 × 10^8; (*light speed m/s*)
        μ = 4 Pi 10^-7;    (*vacuum permeability*)
        Qe = -1.602 10^-19;  (*electron charge C*)
        Me = 9.10955 × 10^-31;  (*electron mass*)
        ϵ = 8.8541878 × 10^-12  (* vacuum permettivity *);
```

Parameters

- **Input parameters**

```
In[36]:= Pin = 250;  (*input power  - W*)
         Io = 25; (* Beam current - A *)
         Vo = 100 × 10^3;  (* Beam Voltage Volt*)

In[39]:= μP = N[Io / Vo^3/2 ] 10^6; (*microperveance*)
         f = 11.424 × 10^9;     (*driving frequency - Hz*)
         ω = 2 Pi f;      (*driving angular frequency - Hz*)

In[42]:= fo = 11.450 × 10^9 ;(*resonance frequency - Hz*)
         ωo = fo 2 Pi; (*resonant angular frequency - Hz*)

In[44]:= T = 1 / f;   (*Period - s*)
         λ = Ci / f;    (*wavelength - m*)

In[46]:= RCav = Ci / ωo 2.4048 ; (*Input Cavity Radius   -   m*)
         LCav =  0.005 (*0.00525029772329247`*) ;(*Input Cavity lenght - m *)

In[48]:= Qo = λ Sqrt[Pi fo 57.8 × 10^6 μ] 2.4048 / (1 + RCav/LCav) 2 Pi  (*Input cavity quality factor *);
         Qext = 95 ; (*Input cavity external quality factor*)
         Ql = 1 / (1/Qo) + (1/Qext);   (*First cavity loaded quality factor*)
         β = Qo / Qext; (*First cavity coupling coefficient*)

In[50]:= Kappa =  0.093 (*Focusing longitudinal B field  - T*);
```

In[51]:= RBeam = 0.00375 (*Beam Radius - m*);

$$\text{pzInit} = \sqrt{\left(\frac{\text{Qe Vo}}{\text{Ci}}\right)^2 + 2\,(-\text{Qe})\,\text{Vo Me}}\;;\quad (*\text{initial longitudinal momentum - Kg m/s} *)$$

- **Other parameters**

In[53]:=

$$\text{Qbeam} = -\frac{\text{Io}}{\text{f}};\quad (*\text{Beam charge (per Period) - C} *)$$

$$\text{GammaInit} = 1 + \frac{\text{Vo}}{511\,000};\quad (*\text{Initial relativistic factor}*)$$

$$\delta = \frac{\text{f}}{\text{fo}} - \frac{\text{fo}}{\text{f}}\quad (*\text{frequency shift}*);$$

- **Normalized Parameters**

In[56]:= ωN = ω T;

$$\text{RCavN} = \frac{\text{RCav}}{\lambda};$$

$$\text{LCavN} = \frac{\text{LCav}}{\lambda};$$

$$\text{RBeamN} = \frac{\text{RBeam}}{\lambda};$$

$$\text{pnzInit} = \frac{\text{pzInit}}{\text{Me Ci}};$$

- **Discretization setting for steady state simulation (*only one RF period simulated*)**

In[61]:= NTS = 2; (*Number of time slots in a set of particles*)

In[62]:= NSS = 1; (*Number of space slots in a set of particles*)

In[63]:= NP = NTS NSS; (*Number of particles*)

Normalized Variables

In[70]:= rn[zn_] := {xn[zn], yn[zn], tn[zn]}; (* position vector normalized to lambda *)
pn[zn_] := {pnx[zn], pny[zn], pnz[zn]} (* momentum vector normalized to mc *);

- **Integral Parameters (*used to calculate $\int \vec{J}\cdot\vec{E}\,dV$ *)**

In[72]:= NSteps = 200; (*number of steps in integral*)

$$\text{ZZ} = \text{Table}\left[\left(\frac{\text{LCavN}}{\text{NSteps}}\right) \text{i}, \{\text{i}, 0, \text{NSteps}\}\right];$$

$$\text{step} = \frac{\text{LCavN}}{\text{NSteps}};$$

Energy for TM010 mode

In[69]:=
```
(*twice the electric stored energy of the mode TM010*)
En = Integrate[ 1/2 ϵ ( BesselJ[0, 2.4048/RCav rr] )^2 rr,
   {rr, 0, RCav}, {zz, 0, LCav}, {fi, 0, 2 Pi}];
```

Normalized Cavity Fields

In[89]:=
```
αInit =
 ( 2 Sqrt[ Pin ωo En / Qext ] Exp[ i ArcTan[ ((fo/f)^2 - Qo δ) / (Qo + Qext (fo/f)^2) ] ] ) /
 ( ωo En ( 1/Qext + (fo/f)^2/Qo + i ( (fo/f)^2/Qo - δ ) ) )
(*Initial guess value for the field coefficient*)
```

Out[89]= 690 069. − 301 038. i

In[90]:=
```
(*Definition of the factor J[1,2.4048 1/RadiusAAn Sqrt[x^2+y^2] ]
   x/Sqrt[x^2+y^2]  in the potential derivative for (x,y)=(0,0) *)
PotDerivx[x_, y_] := BesselJ[1, 2.4048 1/RCavN Sqrt[x^2 + y^2] ] x/Sqrt[x^2 + y^2] /; x != 0;
PotDerivx[x_, y_] := BesselJ[1, 2.4048 1/RCavN Sqrt[x^2 + y^2] ] x/Sqrt[x^2 + y^2] /; (x == 0 && y ≠ 0);
PotDerivx[x_, y_] := 0 /; (x == 0 && y == 0);
```

In[93]:=
```
PotDerivy[x_, y_] := BesselJ[1, 2.4048 1/RCavN Sqrt[x^2 + y^2] ] y/Sqrt[x^2 + y^2] /; y != 0;
PotDerivy[x_, y_] := BesselJ[1, 2.4048 1/RCavN Sqrt[x^2 + y^2] ] y/Sqrt[x^2 + y^2] /; (y == 0 && x ≠ 0);
PotDerivy[x_, y_] := 0 /; (y == 0 && x == 0);
```

In[96]:=
```
EField[zn_] :=
  {0, 0, ( Qe λ / (Me Ci^2) ) BesselJ[0, 2.4048/RCav Sqrt[(xn[zn])^2 + (yn[zn])^2] ] Exp[i ωN (tn[zn])]};
(*electric field normalized to ( Qe lambda / (Me Ci^2) ) *)
```

In[97]:=
```
BField[zn_] := { -i ( Qe λ / (Me Ci^2) ) PotDerivy[xn[zn], yn[zn]] Exp[i ωN tn[zn]] ,
    i ( Qe λ / (Me Ci^2) ) PotDerivx[xn[zn], yn[zn]] Exp[i ωN tn[zn]] , 0 };
(*magnetic B field normalized to ( Qe lambda / (Me Ci) ) *)

Bo[zn_] := {0, 0, ( Qe λ / (Me Ci) ) Kappa}; (*focusing static B field*)
```

MacroParticles charge

In[99]:=
```
QVect = Table[0, {NP}]; (*  macro-particles charge vector   -   uniform beam *)
For[it = 0, it < NTS, it++, {
      For[is = 0, is < NSS, is++, {
        QVect[[(it) NSS + is + 1]] = ( Qbeam / (NTS NSS^2) ) (2 is + 1) }]}]
```

Initial Conditions 1

In[100]:=
```
IC = Table[0, {NP}, {6}]; (*  (Nx6) Matrix with particles initial conditions*)
For[it = 0, it < NTS, it++, {
      For[is = 1, is <= NSS, is++, {
        IC[[it NSS + is, 1]] = 0 RBeamN (2 is - 1) / (2 NSS), (*initial normalized x*)
        IC[[it NSS + is, 2]] = 0,                  (*initial normalized y*)
        IC[[it NSS + is, 3]] = it / NTS,           (*initial normalized t*)
        IC[[it NSS + is, 4]] = 0,                  (*initial normalized px*)
        IC[[it NSS + is, 5]] = 0,                  (*initial normalized py*)
        IC[[it NSS + is, 6]] = pnzInit             (*initial normalized pz*)
    }]
  }]
```

In[102]:=
```
MatrixForm[IC];
```

Drift Zero (before input cavity) -> SD0

In[105]:=
```
(*Tracking of particles (perfectly uniform beam)
  through the drift before the first cavity*)
```

In[106]:=
```
Vect1Eq[zn_] := { pnx[zn] / pnz[zn] , pny[zn] / pnz[zn] , Sqrt[1 + (pnx[zn])^2 + (pny[zn])^2 + (pnz[zn])^2] / pnz[zn] };
```

In[107]:=
```
LD0 = λ; (*Drift zero length*)
LD0N = LD0 / λ;
```

```
In[108]:= Remove[ffD0]
ffD0[aa_?MatrixQ] := Module[{},
  SD0 = Table[{xn[zn] /. (EED = NDSolve[Thread /@ {rn'[zn] == Vect1Eq[zn],
          pn'[zn] == 1/pnz[zn] pn[zn] × (Bo[zn]),
          rn[0] == {aa[[i, 1]], aa[[i, 2]], aa[[i, 3]]},
          pn[0] == {aa[[i, 4]], aa[[i, 5]], aa[[i, 6]]}},
        {xn[zn], yn[zn], tn[zn], pnx[zn], pny[zn], pnz[zn]}, {zn, 0, LD0N},
        Method → ImplicitRungeKutta, MaxStepSize → 0.005]),
    yn[zn] /. EED,
    tn[zn] /. EED,
    pnx[zn] /. EED,
    pny[zn] /. EED,
    pnz[zn] /. EED},
   {i, 1, NP}];

 ]

In[110]:= ffD0[IC]  (*Particles trajectories in Drift Zero as a function of z*)

In[111]:= T0 = Table[SD0[[i, 3]][[1]] /. zn → 0, {i, 1, NP}] ;(*entrance times in Drift Zero*)

In[112]:= T1 = Table[SD0[[i, 3]][[1]] /. zn → LD0N, {i, 1, NP}]
  (*entrance times in Input Cavity*);
```

From z to t variable in Drift Zero -> SD0t

```
In[113]:= (*Particles trajectories in Drift Zero as a function of time*)

In[114]:= SD0t = SD0; (*Initializing matrix which
  contains  the solutions in drift 0 as a function of time*)

In[115]:= ZT = Table[0, {i, NP}] (*Initializing vector which contains the functions z(t)*);

In[116]:=
InverseIF[f_, l1_, l2_] := Module[{M1, M2, nn, W},
  W = l2 - l1;
  nn = 5000;
  M1 = Table[{(l1 + i W/nn), f /. zn → (l1 + i/nn W)}, {i, 0, nn}];
  M2 = Table[0, {i, nn + 1}, {j, 2}];
  M2[[All, 1]] = M1[[All, 2]];
  M2[[All, 2]] = M1[[All, 1]];

  Interpolation[M2]]

In[117]:= For[i = 1, i ≤ NP, i++, ZT[[i]] = InverseIF[SD0[[i, 3]][[1]], 0, LD0N][tn]]
```

```
For[i = 1, i ≤ NP, i++, {
  SD0t[[i, 1]] = SD0[[i, 1]][[1]] /. zn → ZT[[i]],
  SD0t[[i, 2]] = SD0[[i, 2]][[1]] /. zn → ZT[[i]],
  SD0t[[i, 3]] = ZT[[i]],
  SD0t[[i, 4]] = SD0[[i, 4]][[1]] /. zn → ZT[[i]],
  SD0t[[i, 5]] = SD0[[i, 5]][[1]] /. zn → ZT[[i]],
  SD0t[[i, 6]] = SD0[[i, 6]][[1]] /. zn → ZT[[i]]}]
```

Steady State Solution inside the input cavity ->SC1

In[127]:=
```
(*Finding the Steady State solution inside the cavity -
 the independent variable is z *)
```

In[128]:=
```
Remove[ff]
ff[α_?NumberQ] := Module[{}, (*Print[α];*)

  SC1 = Table[{xn[zn] /. (EE = NDSolve[Thread /@ {rn'[zn] == Vect1Eq[zn],
          pn'[zn] == 1/pnz[zn] (√(1 + (pnx[zn])^2 + (pny[zn])^2 + (pnz[zn])^2))
            Re[α EField[zn]] + 1/pnz[zn] pn[zn] × (Re[α fo/f BField[zn]] + Bo[zn]),
          rn[LD0N] == {SD0[[i, 1]][[1]] /. zn → LD0N, SD0[[i, 2]][[1]] /.
              zn → LD0N, SD0[[i, 3]][[1]] /. zn → LD0N},
          pn[LD0N] == {SD0[[i, 4]][[1]] /. zn → LD0N, SD0[[i, 5]][[1]] /. zn → LD0N,
            SD0[[i, 6]][[1]] /. zn → LD0N}}, {xn[zn], yn[zn],
          tn[zn], pnx[zn], pny[zn], pnz[zn]}, {zn, LD0N, LD0N + LCavN}
          (*,Method→ImplicitRungeKutta,MaxStepSize→0.005*)])],
     yn[zn] /. EE,
     tn[zn] /. EE,
     pnx[zn] /. EE,
     pny[zn] /. EE,
     pnz[zn] /. EE},

    {i, 1, NP}];

  EzStar = Table[((Qe λ/(Me Ci^2)) BesselJ[0, 2.4048/RCavN √((SC1[[i, 1]])^2 + (SC1[[i, 2]])^2)]
      Exp[- i ωN (SC1[[i, 3]])]), {i, 1, NP}]
    (*Ez field on particles trajectories*);

  TInt =
   Table[step (2 Me Ci^2 QVect[[j]]/(T Qe)) 1/2 ((EzStar[[j]] /. zn → LD0N + ZZ[[i + 1]])[[1]] +
      (EzStar[[j]] /. zn → LD0N + ZZ[[i]])[[1]]), {j, 1, NP}, {i, 1, NSteps}];

Integ = Conjugate[ Total[Total[TInt, {2}]]];
```

```
Alpha = Conjugate[(2 Sqrt[Pin ωo En / Qext] Exp[i ArcTan[((fo/f)^2 - Qo δ) / (Qo + Qext (fo/f)^2)]] - 1/2 Integ) /
    (ωo En (1/Qext + (fo/f)^2 1/Qo + i ((fo/f)^2 1/Qo - δ)))];
Alpha]
```

```
In[130]:= FindRoot[ff[A] - A, {A, αInit},
           MaxIterations → 200, PrecisionGoal → 1, AccuracyGoal → 1]
Out[130]= {A → 651075. + 41463. i}
In[131]:= T2 = Table[SC1[[i, 3]][[1]] /. zn → LD0N + LCavN, {i, 1, NP}]
           (* exit times from first cavity*);
```

From z to t variable in the Cavity -> SC1t

```
In[132]:= (*Particles trajectories in the first Cavity as a function of time*)
In[133]:= SC1t = SC1; (*Initializing matrix which contains
           the solutions in the cavity as a function of time*)
In[134]:= ZTC = Table[0, {i, NP}] (*Initializing vector which contains the functions z(t)*);
In[135]:= For[i = 1, i ≤ NP, i++, ZTC[[i]] = InverseIF[SC1[[i, 3]][[1]], LD0N, LD0N + LCavN][tn]]
In[136]:= For[i = 1, i ≤ NP, i++, {
            SC1t[[i, 1]] = SC1[[i, 1]][[1]] /. zn → ZTC[[i]],
            SC1t[[i, 2]] = SC1[[i, 2]][[1]] /. zn → ZTC[[i]],
            SC1t[[i, 3]] = ZTC[[i]],
            SC1t[[i, 4]] = SC1[[i, 4]][[1]] /. zn → ZTC[[i]],
            SC1t[[i, 5]] = SC1[[i, 5]][[1]] /. zn → ZTC[[i]],
            SC1t[[i, 6]] = SC1[[i, 6]][[1]] /. zn → ZTC[[i]]

           }]
```

Solutions drift zero + cavity 1 (time variable) -> Ct1

```
(*Particles trajectories in Drift Zero + First cavity as a function of time*)
In[138]:= Ct1 = Table[Piecewise[{{SD0t[[i, j]] /. tn → t, t <= T1[[i]]},
                {SC1t[[i, j]] /. tn → t, t >= T1[[i]]}}], {i, NP}, {j, 6}];
```

Potentials and derivatives drift - no sp charge - focusing field only

- Potentials (*A normalized to $\frac{q}{mc}$, Φ normalized to $\frac{q}{mc^2}$*)

```
In[140]:= Ax[t_] := (- Qe / (Me Ci)) λ (Kappa / 2) yn[t]; (* longitudinal focusing B field*)
          Ay[t_] := (Qe / (Me Ci)) λ (Kappa / 2) xn[t]; (* longitudinal focusing B field*)
          Az[t_] := 0;
          Φ[t_] := 0;
```

▪ Derivatives of the potentials

In[144]:=

```
(*Vector potential derivatives*)

DerivXX[t_] := 0;   (*∂Ax/∂x*)
DerivXY[t_] := -Qe λ/(Me Ci) Kappa/2 (*∂Ax/∂y*);
DerivXZ[t_] := 0 (*∂Ax/∂z*);
DerivXT[t_] := 0 (*∂Ax/∂t*);

DerivZX[t_] := 0 (*∂Az/∂x*);
DerivZY[t_] := 0 (*∂Az/∂y*);
DerivZZ[t_] := 0 (*∂Az/∂z*);
DerivZT[t_] := 0 (*∂Az/∂t*);

DerivYX[t_] := Qe λ/(Me Ci) Kappa/2;
DerivYY[t_] := 0;
DerivYZ[t_] := 0;
DerivYT[t_] := 0;


(*Scalar potential derivatives*)

DerivΦX[t_] := 0;
DerivΦY[t_] := 0;
DerivΦZ[t_] := 0;
DerivΦT[t_] := 0;
```

▪ Fields

In[159]:=

```
Bx[t_] := 0;
By[t_] := 0;
Bz[t_] := Qe λ/(Me Ci) Kappa;
```

Drift 1 - first iteration

In[162]:=

```
(*Drift space after first cavity*)
```

In[163]:=

```
rn[t_] := {xn[t], yn[t], zn[t]};  (* unperturbed position vector   *)
pn[t_] := {pnx[t], pny[t], pnz[t]} (* unperturbed momentum vector  *);
```

In[165]:=

```
LD1 = 0.1; (*drift length*)
LD1N = LD1/λ; (* normalized drift length*)
LD1Nf = (LD1 + 3 λ)/λ; (* normalized drift length + δL *)
```

```
In[168]:= T3 = T2 + Table[LD1N / (SC1[[i, 6]][[1]] /. zn → LD0N + LCavN / Sqrt[1 + (SC1[[i, 6]][[1]] /. zn → LD0N + LCavN)^2]), {i, 1, NP}]
          (* MParticles arrival time at the end of the drift 1 *);
          T3f = T2 + Table[LD1Nf / (SC1[[i, 6]][[1]] /. zn → LD0N + LCavN / Sqrt[1 + (SC1[[i, 6]][[1]] /. zn → LD0N + LCavN)^2]), {i, 1, NP}]
          (* MParticles arrival time at the end of the drift 1 + λ *);

In[170]:= (*vectors for eq. of motions*)

          Vect1EqT[tn_] := {pnx[tn] / Sqrt[1 + pnx[tn]^2 + pny[tn]^2 + pnz[tn]^2],
            pny[tn] / Sqrt[1 + pnx[tn]^2 + pny[tn]^2 + pnz[tn]^2],
            pnz[tn] / Sqrt[1 + pnx[tn]^2 + pny[tn]^2 + pnz[tn]^2]};

          Vect2EqT[tn_] :=
            {1 / Sqrt[1 + pnx[tn]^2 + pny[tn]^2 + pnz[tn]^2] (pny[tn] (Bz[tn]) - pnz[tn] By[tn]),
             1 / Sqrt[1 + pnx[tn]^2 + pny[tn]^2 + pnz[tn]^2] (pnx[tn] (-Bz[tn]) + pnz[tn] (Bx[tn])),
             1 / Sqrt[1 + pnx[tn]^2 + pny[tn]^2 + pnz[tn]^2] (pnx[tn] By[tn] - pny[tn] Bx[tn])};


In[172]:= FIt = Table[{xn[tn] /. (EEDT = NDSolve[Thread /@ {rn'[tn] == Vect1EqT[tn],
                  pn'[tn] == Vect2EqT[tn], rn[T2[[i]]] == {SC1t[[i, 1]] /. tn → T2[[i]],
                    SC1t[[i, 2]] /. tn → T2[[i]], SC1t[[i, 3]] /. tn → T2[[i]]},
                  pn[T2[[i]]] == {SC1t[[i, 4]] /. tn → T2[[i]], SC1t[[i, 5]] /. tn → T2[[i]],
                    SC1t[[i, 6]] /. tn → T2[[i]]}}, {xn[tn], yn[tn],
                 zn[tn], pnx[tn], pny[tn], pnz[tn]}, {tn, T2[[i]], T3f[[i]]},
                Method → ImplicitRungeKutta, MaxStepSize → 0.005])[[1]],
            yn[tn] /. EEDT[[1]],
            zn[tn] /. EEDT[[1]],
            pnx[tn] /. EEDT[[1]],
            pny[tn] /. EEDT[[1]],
            pnz[tn] /. EEDT[[1]]},
           {i, 1, NP}] ; (*Particles positions and momenta in the
          pipe after first integration (NO SPACE CHARGE FIELD CONSIDERED) *)
```

Solutions drift 0 + cavity 1 + drift 1 (time variable) -> MtotT

```
          (*Particles trajectories in Drift Zero +
           First cavity + Drift 1  as a function of time*)

In[173]:= MtotT = Table[
              Piecewise[{{0, t < T0[[i]] || t > T3f[[i]]}, {Ct1[[i, j]] /. tn → t, t <= T2[[i]]},
                {FIt[[i, j]] /. tn → t, t >= T2[[i]]}}], {i, NP}, {j, 6}];
```

Space Charge Electric Field

In[175]:=
```
h[i_, t_, cc_] := Which[t + cc ≥ T0[[i]] && t + cc ≤ T3f[[i]] , 1, True, 0]
 (*condition to see if a particle has to be
  taken in account for the space charge field or not*)
```

In[176]:=
```
a = 1; b = 2; c = 0;  (*put a=1, b=0,
c=0 to consider 1 particles set before and after the considered one,
a=1, b=1, c=0 to consider 2 sets and a=1, b=1, c=1 to consider 3 sets*)
```

- **Ex**

In[177]:=
```
(*∂V/∂x  generated by particle i who is inside the pipe at the time t*)
DViDX[i_, tt_, cc_] :=
 (- Qe)/(Me Ci^2 λ) QVect[[i]] √(1 + (MtotT[[i, 4]] /. t → tt + cc)^2 + (MtotT[[i, 5]] /. t → tt + cc)^2 +
     (MtotT[[i, 6]] /. t → tt + cc)^2) (xxn[tt] - MtotT[[i, 1]] /. t → tt + cc) /
   (4 Pi ϵ ((xxn[tt] - (MtotT[[i, 1]] /. t → tt + cc))^2 +
       (yyn[tt] - (MtotT[[i, 2]] /. t → tt + cc))^2 + (1 + (MtotT[[i, 4]] /. t → tt + cc)^2 +
          (MtotT[[i, 5]] /. t → tt + cc)^2 + (MtotT[[i, 6]] /. t → tt + cc)^2)
        (zzn[tt] - (MtotT[[i, 3]] /. t → tt + cc))^2)^(3/2))
```

In[178]:=
```
(*Ex space charge field for particle j at time t *)
EX[j_, t_] := -(Sum[ h[i, t, 0] DViDX[i, t, 0] , {i, 1, j - 1}] +
    Sum[ h[i, t, 0] DViDX[i, t, 0], {i, j + 1, NP}] +
    a Sum[ h[i, t, 1] DViDX[i, t, 1] + h[i, t, -1] DViDX[i, t, -1] , {i, 1, NP}] +
    b Sum[ h[i, t, 2] DViDX[i, t, 2] + h[i, t, -2] DViDX[i, t, -2] , {i, 1, NP}] +
    c Sum[ h[i, t, 3] DViDX[i, t, 3] + h[i, t, -3] DViDX[i, t, -3] , {i, 1, NP}])
```

- **Ey**

In[179]:=
```
DViDY[i_, tt_, cc_] :=
 (- Qe)/(Me Ci^2 λ) QVect[[i]] √(1 + (MtotT[[i, 4]] /. t → tt + cc)^2 + (MtotT[[i, 5]] /. t → tt + cc)^2 +
     (MtotT[[i, 6]] /. t → tt + cc)^2) (yyn[tt] - (MtotT[[i, 2]] /. t → tt + cc)) /
   (4 Pi ϵ ((xxn[tt] - (MtotT[[i, 1]] /. t → tt + cc))^2 +
       (yyn[tt] - (MtotT[[i, 2]] /. t → tt + cc))^2 + (1 + (MtotT[[i, 4]] /. t → tt + cc)^2 +
          (MtotT[[i, 5]] /. t → tt + cc)^2 + (MtotT[[i, 6]] /. t → tt + cc)^2)
        (zzn[tt] - (MtotT[[i, 3]] /. t → tt + cc))^2)^(3/2))
```

In[180]:=
```
(*Ey space charge field for particle j at time t *)
EY[j_, t_] := -(Sum[ h[i, t, 0] DViDY[i, t, 0] , {i, 1, j - 1}] +
    Sum[ h[i, t, 0] DViDY[i, t, 0], {i, j + 1, NP}] +
    a Sum[ h[i, t, 1] DViDY[i, t, 1] + h[i, t, -1] DViDY[i, t, -1] , {i, 1, NP}] +
    b Sum[ h[i, t, 2] DViDY[i, t, 2] + h[i, t, -2] DViDY[i, t, -2] , {i, 1, NP}] +
    c Sum[ h[i, t, 3] DViDY[i, t, 3] + h[i, t, -3] DViDY[i, t, -3] , {i, 1, NP}])
```

- **Ez**

In[181]:=
```
DViDZ[i_, tt_, cc_] := (- Qe)/(Me Ci^2 λ) QVect[[i]]
  (√(1 + (MtotT[[i, 4]] /. t → tt + cc)^2 + (MtotT[[i, 5]] /. t → tt + cc)^2 +
      (MtotT[[i, 6]] /. t → tt + cc)^2)) (zzn[tt] - (MtotT[[i, 3]] /. t → tt + cc)) /
  (4 Pi ϵ ((xxn[tt] - (MtotT[[i, 1]] /. t → tt + cc))^2 +
      (yyn[tt] - (MtotT[[i, 2]] /. t → tt + cc))^2 +
      (1 + (MtotT[[i, 4]] /. t → tt + cc)^2 + (MtotT[[i, 5]] /. t → tt + cc)^2 + (MtotT[[i,
          6]] /. t → tt + cc)^2) (zzn[tt] - (MtotT[[i, 3]] /. t → tt + cc))^2)^(3/2));
```

In[182]:=
```
(*Ez space charge field for particle j at time t *)
EZ[j_, t_] := -(Sum[ h[i, t, 0] DViDZ[i, t, 0] , {i, 1, j - 1}] +
    Sum[ h[i, t, 0] DViDZ[i, t, 0], {i, j + 1, NP}] +
    a Sum[ h[i, t, 1] DViDZ[i, t, 1] + h[i, t, -1] DViDZ[i, t, -1] , {i, 1, NP}] +
    b Sum[ h[i, t, 2] DViDZ[i, t, 2] + h[i, t, -2] DViDZ[i, t, -2] , {i, 1, NP}] +
    c Sum[ h[i, t, 3] DViDZ[i, t, 3] + h[i, t, -3] DViDZ[i, t, -3] , {i, 1, NP}] )
```

Space Charge Magnetic Field

- $\frac{\partial Az}{\partial x} = -By = -\frac{\gamma\beta}{Ci}\ (Ex')$

In[183]:=
```
DAziDX[i_, tt_, cc_] := (MtotT[[i, 6]] /. t → tt + cc)/Ci (- Qe)/(Me Ci λ 4 Pi ϵ) QVect[[i]]
  (xxn[tt] - (MtotT[[i, 1]] /. t → tt + cc)) / ((xxn[tt] - (MtotT[[i, 1]] /. t → tt + cc))^2 +
      (yyn[tt] - (MtotT[[i, 2]] /. t → tt + cc))^2 +
      (1 + (MtotT[[i, 4]] /. t → tt + cc)^2 + (MtotT[[i, 5]] /. t → tt + cc)^2 +
        (MtotT[[i, 6]] /. t → tt + cc)^2) (zzn[tt] - (MtotT[[i, 3]] /. t → tt + cc))^2)^(3/2)
```

- $\frac{\partial Az}{\partial y} = Bx = \frac{\gamma\beta}{Ci}\ (-Ey')$

In[184]:=
```
DAziDY[i_, tt_, cc_] := (MtotT[[i, 6]] /. t → tt + cc)/Ci (- Qe)/(Me Ci λ 4 Pi ϵ) QVect[[i]]
  (yyn[tt] - (MtotT[[i, 2]] /. t → tt + cc)) / ((xxn[tt] - (MtotT[[i, 1]] /. t → tt + cc))^2 +
      (yyn[tt] - (MtotT[[i, 2]] /. t → tt + cc))^2 +
      (1 + (MtotT[[i, 4]] /. t → tt + cc)^2 + (MtotT[[i, 5]] /. t → tt + cc)^2 +
        (MtotT[[i, 6]] /. t → tt + cc)^2) (zzn[tt] - (MtotT[[i, 3]] /. t → tt + cc))^2)^(3/2)
```

- $\frac{\partial Az}{\partial z}$

In[185]:=
```
DAziDZ[i_, tt_, cc_] :=
 MtotT[[i, 6]] /. t → tt + cc / Ci  - Qe / Me Ci λ 4 Pi ϵ  QVect[[i]] (1 + (MtotT[[i, 4]] /. t → tt + c)^2 +
    (MtotT[[i, 5]] /. t → tt + c)^2 + (MtotT[[i, 6]] /. t → tt + c)^2)
  (zzn[tt] - (MtotT[[i, 3]] /. t → tt + cc)) / ((xxn[tt] - (MtotT[[i, 1]] /. t → tt + cc))^2 +
      (yyn[tt] - (MtotT[[i, 2]] /. t → tt + cc))^2 +
      (1 + (MtotT[[i, 4]] /. t → tt + cc)^2 + (MtotT[[i, 5]] /. t → tt + cc)^2 +
         (MtotT[[i, 6]] /. t → tt + cc)^2) (zzn[tt] - (MtotT[[i, 3]] /. t → tt + cc))^2)^(3/2)
```

- **Bx Space Charge**

In[186]:=
```
(*Bx space charge field for particle j at time t *)
BxSC[j_, t_] := Sum[ h[i, t, 0] DAziDY[i, t, 0] , {i, 1, j - 1}] +
  Sum[ h[i, t, 0] DAziDY[i, t, 0], {i, j + 1, NP}] +
  a Sum[ h[i, t, 1] DAziDY[i, t, 1] + h[i, t, -1] DAziDY[i, t, -1] , {i, 1, NP}] +
  b Sum[ h[i, t, 2] DAziDY[i, t, 2] + h[i, t, -2] DAziDY[i, t, -2] , {i, 1, NP}] +
  c Sum[ h[i, t, 3] DAziDY[i, t, 3] + h[i, t, -3] DAziDY[i, t, -3] , {i, 1, NP}]
```

- **By Space Charge**

In[187]:=
```
(*By space charge field for particle j at time t *)
BySC[j_, t_] := - (Sum[ h[i, t, 0] DAziDX[i, t, 0] , {i, 1, j - 1}] +
     Sum[ h[i, t, 0] DAziDX[i, t, 0], {i, j + 1, NP}] +
     a Sum[ h[i, t, 1] DAziDX[i, t, 1] + h[i, t, -1] DAziDX[i, t, -1] , {i, 1, NP}] +
     b Sum[ h[i, t, 2] DAziDX[i, t, 2] + h[i, t, -2] DAziDX[i, t, -2] , {i, 1, NP}] +
     c Sum[ h[i, t, 3] DAziDX[i, t, 3] + h[i, t, -3] DAziDX[i, t, -3] , {i, 1, NP}])
```

- **Bz Space Charge**

In[188]:=
```
(*Bz space charge field for particle j at time t *)
BzSC[j_, t_] := 0
```

In[189]:=

Eq motion ->SSIter

In[190]:=
```
rrn[t_] := {xxn[t], yyn[t], zzn[t]};
(* unperturbed position vector  -  drift space 1 *)
ppn[t_] := {ppnx[t], ppny[t], ppnz[t]}
 (* unperturbed momentum vector  -  drift space 1  *);
```

In[192]:=

```
V1EqSC[tt_] := {ppnx[tt]/Sqrt[1 + ppnx[tt]^2 + ppny[tt]^2 + ppnz[tt]^2],
  ppny[tt]/Sqrt[1 + ppnx[tt]^2 + ppny[tt]^2 + ppnz[tt]^2],
  ppnz[tt]/Sqrt[1 + ppnx[tt]^2 + ppny[tt]^2 + ppnz[tt]^2]};

V2EqSC[s_, tt_] := {1/Sqrt[1 + ppnx[tt]^2 + ppny[tt]^2 + ppnz[tt]^2]
    (ppny[tt] (Bz[tt] + BzSC[s, tt]) - ppnz[tt] (By[tt] + BySC[s, tt])) +
   EX[s, tt], 1/Sqrt[1 + ppnx[tt]^2 + ppny[tt]^2 + ppnz[tt]^2]
    (ppnz[tt] (Bx[tt] + BxSC[s, tt]) - ppnx[tt] (Bz[tt] + BzSC[s, tt])) +
   EY[s, tt], 1/Sqrt[1 + ppnx[tt]^2 + ppny[tt]^2 + ppnz[tt]^2]
    (ppnx[tt] (By[tt] + BySC[s, tt]) - ppny[tt] (Bx[tt] + BxSC[s, tt])) + EZ[s, tt]};

SSIter = Table[{xxn[tt] /. (EEIter = NDSolve[Thread /@ {rrn'[tt] == V1EqSC[tt],
            ppn'[tt] == V2EqSC[i, tt], rrn[T2[[i]]] == {SC1t[[i, 1]] /. tn → T2[[i]],
              SC1t[[i, 2]] /. tn → T2[[i]], SC1t[[i, 3]] /. tn → T2[[i]]},
            ppn[T2[[i]]] == {SC1t[[i, 4]] /. tn → T2[[i]],
              SC1t[[i, 5]] /. tn → T2[[i]], SC1t[[i, 6]] /. tn → T2[[i]]}},
          {xxn[tt], yyn[tt], zzn[tt], ppnx[tt], ppny[tt], ppnz[tt]},
          {tt, T2[[i]], T3f[[i]]}, Method → ImplicitRungeKutta(*,
          MaxStepSize→Infinity,MaxSteps→50000*)])[[1]],
    yyn[tt] /. EEIter[[1]],
    zzn[tt] /. EEIter[[1]],
    ppnx[tt] /. EEIter[[1]],
    ppny[tt] /. EEIter[[1]],
    ppnz[tt] /. EEIter[[1]]},
   {i, 1, NP}] ; (* Second Iteration WITH THE SPACE CHARGE FIELD generated
  from the particles distribution obtained from the first Iteration*)


MtotT = Table[Piecewise[
     {{0, tn < T0[[i]] || tn > T3f[[i]]}, {MtotT[[i, j]] /. t → tn, tn <= T2[[i]]},
      {SSIter[[i, j]] /. tt → tn, tn >= T2[[i]]}}], {i, NP}, {j, 6}];

MtotT = Table[MtotT[[i, j]] /. tn → t, {i, NP}, {j, 6}];
(*Particles trajectories in Drift Zero +
 First cavity + Drift 1  as a function of time*)
```

```
Funct[aaa_?MatrixQ] := Module[{},
  SSIter = Table[{xxn[tt] /. (EEIter = NDSolve[Thread /@ {rrn'[tt] == V1EqSC[tt],
             ppn'[tt] == V2EqSC[i, tt], rrn[T2[[i]]] == {SC1t[[i, 1]] /. tn → T2[[i]],
               SC1t[[i, 2]] /. tn → T2[[i]], SC1t[[i, 3]] /. tn → T2[[i]]},
             ppn[T2[[i]]] == {SC1t[[i, 4]] /. tn → T2[[i]],
               SC1t[[i, 5]] /. tn → T2[[i]], SC1t[[i, 6]] /. tn → T2[[i]]}},
           {xxn[tt], yyn[tt], zzn[tt], ppnx[tt], ppny[tt], ppnz[tt]},
           {tt, T2[[i]], T3f[[i]]}, Method → ImplicitRungeKutta])[[1]],
     yyn[tt] /. EEIter[[1]],
     zzn[tt] /. EEIter[[1]],
     ppnx[tt] /. EEIter[[1]],
     ppny[tt] /. EEIter[[1]],
     ppnz[tt] /. EEIter[[1]]},
    {i, 1, NP}](*Integrates the eq. of motion with space charge field *);

  Mprev = MtotT;

  MtotT = Table[Piecewise[{{0, tn < T0[[i]] || tn > T3f[[i]]}, {MtotT[[i, j]] /. t → tn,
       tn <= T2[[i]]}, {SSIter[[i, j]] /. tt → tn, tn >= T2[[i]]}}], {i, NP}, {j, 6}];

MtotT = Table[MtotT[[i, j]] /. tn → t, {i, NP}, {j, 6}];
  Print[1]
 ](*Matrix which contains the difference between the positions and the
  momenta calculated during this iteration (SSIter) and the last one (),
 divided by the medium value of the function in this iteration  *)
For[r = 1, r ≤ 4, r++,
 Funct[MtotT]]
MtotT = Table[Piecewise[
    {{0, tn < T0[[i]] || tn > T3f[[i]]}, {MtotT[[i, j]] /. t → tn, tn <= T2[[i]]},
     {SSIter[[i, j]] /. tt → tn, tn >= T2[[i]]}}], {i, NP}, {j, 6}];

MtotT = Table[MtotT[[i, j]] /. tn → t, {i, NP}, {j, 6}];
```

From t to z variable ->MtotZ

```
MtotZ = MtotT; (*Initializing matrix which
 contains  the total solutions as a function of time*)
TZD = Table[0, {i, NP}] (*Initializing vector which contains the functions z(t)*);


InverseIFt[f_, l1_, l2_] := Module[{M1, M2, nn, W},
  W = l2 - l1;
  nn = 5000;
  M1 = Table[{{l1 + i W/nn}, f /. t → (l1 + i/nn W)}, {i, 0, nn}];
  M2 = Table[0, {i, nn + 1}, {j, 2}];
  M2[[All, 1]] = M1[[All, 2]];
  M2[[All, 2]] = M1[[All, 1]];

  Interpolation[M2]]


For[i = 1, i ≤ NP, i++, TZD[[i]] = InverseIFt[MtotT[[i, 3]], T0[[i]], T3f[[i]]][zn]]
```

```
For[i = 1, i ≤ NP, i++, {
  MtotZ[[i, 1]] = MtotT[[i, 1]] /. t → TZD[[i]],
  MtotZ[[i, 2]] = MtotT[[i, 2]] /. t → TZD[[i]],
  MtotZ[[i, 3]] = TZD[[i]],
  MtotZ[[i, 4]] = MtotT[[i, 4]] /. t → TZD[[i]],
  MtotZ[[i, 5]] = MtotT[[i, 5]] /. t → TZD[[i]],
  MtotZ[[i, 6]] = MtotT[[i, 6]] /. t → TZD[[i]]

 }]
```

Bibliography

[1] A.A. Heil, O. Heil, "Eine neue Methode zur Erzeugung kurzer, ungedämpfter, elektromagnetischer Wellen grober Intensität", Zietschrift Für Physik, Verlag Von Julius Springer, Berlin, (1935).

[2] W.W. Hansen, R.D. Richtmyer, "On Resonators Suitable for Klystron Oscillators", Journal. Of Appl. Physics, 10, p. 189-199, 1939.

[3] R.H. Varian and S.F. Varian, "A High Frequancy Oscillator and Amplifier", J. Appl. Phys., Vol. 10, 1939, p. 321.

[4] M.J. Smith, G. Phillips, "Power Klystrons Today", John Wiley & Sons Inc., 1994.

[5] G. Caryotakis, "High Power Klystrons: Theory and Practice at the Stanford Linear Accelerator Center", SLAC-PUB-10620, 2004.

[6] E.L. Lien, "High Efficiency Klystron Amplifiers", Conv. Record, MOGA-70, 8th Int. Conf. on Microwave and Optical Generation and Amplification, Amsterdam, September 1970.

[7] E.L. Lien, "Advances in Klystron Amplifiers - A Tutorial Treatment Emphasising Efficiency, Bandwidth and Applications", Microwave Journal, Microwave Tube Series No. 9 Technical Feature, December 1973.

[8] P.J. Tallerico, "Design Considerations for the High Power Multicavity Klystron", IEEE Trans. Electron Devices, Vol. ED-18,1971,p. 374.

[9] T.G. Mihran, "The Effect of Drift Length, Beam Radius and Perveance on Klystron Power Conversion Efficiency, IEEE Trans. on Electron Devices, Vol. ED-14, No. 4, April 1967.

[10] D.L. Webster, "Cathode-Ray Bunching", J. Appl. Phys., Vol. 10, p. 501, 1939.

[11] E. Feenberg, "Notes on Velocity Modulation" , Sperry Gyroscope Lab. Report 5521-1043, Sperry Gyroscope Co.,Inc., Garden City, NY, September 1945.

[12] D.L. Webster, "Theory of Klystron Oscillations", J. Appl. Phys., Vol. 10, p. 864, December 1939.

[13] W.C. Hahn, "Small Signal Theory of Velocity Modulated Electron Beams", Gen. Electr. Rev., Vol. 42, p. 258, 1939.

[14] W.C. Hahn and G.F. Metcalf, "Velocity Modulated Tubes", Proc. IRE, Vol. 27, p. 106, 1939.

[15] S. Ramo, "Space-Charge and Field Waves in an Electron Beam", Phys. Rev., Vol. 56, p. 276, 1939.

[16] T. Wessel Berg, "A General Theory of Klystrons with Arbitrary, Extended Interaction Fields", Technical Report, Stanford Microwave Laboratory Report No. 376, March, 1957.

[17] T. Wessel Berg, "Space-Charge Wave Theory of Interaction Gaps and Multi-Cavity Klystrons with Extended Fields", Norwegian Defense Research Establishment, Kjeller-Lillestrøm, Norway, NDRE Rept. 32, September 1960.

[18] M. Chodorow and T. Wessel-Berg, "A High Efficiency Klystron with Distribuited Interaction", IRE Trans. Electron Devices, Vol. ED-8, 1961

[19] J.-Y. Raguin, Private Communication, April 2010.

[20] J.-Y. Raguin, "Le Klystron à Interaction Etendue: Etude Théorique et Experimentale", PhD Thesis, Université Paris VI, November 1995.

[21] G.M. Branch, T. G. Mihran, "Plasma Frequency Reduction Factors in Electron Beams", IRE Trans. On Elec. Dev. ED-2, p. 3, 1955.

[22] H. Yonezawa, Y. Okazaki, "A One-Dimensional Disk Model Simulation for Klystron Design", SLAC-TN-84-5, May 1984.

[23] T. Kageyama, Y. Morizumi and E. Watanabe, "A Large-Signal Analysis of Broad-Band Klystrons with Design Applications", IEEE Trans. Electron Devices, Vol. ED-24, 1977, p. 3.

[24] A. Jensen, "AJDisk manual", vers. 9.0, 2002-2008.

[25] ATK Mission Research, "MAGIC User's Manual", 2004-2005.

[26] Computer Simulation Technology, "CST Studio Suite User's Manual",2010.

[27] The Michelle Code, SAIC website, `http://www.saic.com/products/software/michelle/`.

[28] J. Petillo et al., "The MICHELLE Three-Dimensional Electron Gun and Collector Modeling Tool: Theory and Design", IEEE Trans. on Plasma Science, Vol. 30, no. 3, June 2002.

[29] Los Alamos Accelerator Group, "User's Guide for the POISSON/SUPERFISH Group of Codes", Los Alamos National Laboratory Report LA-UR-87-115.

[30] S.G. Tantawi, Private Communication, March 2010.

[31] G. Gerosa and P. Lampariello, "Lezioni di campi elettromagnetici", Edizioni Ingegneria 2000, 1995.

[32] R.E. Collin, "Foundation For Microwave Engineering", McGraw Hill, 1992.

[33] M.A. Leontovich, "Investigations on Radiowave Propagation, Part II", Printing House of the Academy of Sciences, Moscow, p. 5-12, 1948.

[34] J.D. Jackson, "Classical Electrodynamics", Wiley NY, 1975.

[35] G. Franceschetti, "Campi elettromagnetici", Bollati Boringhieri, Torino, 1988.

[36] S.G. Tantawi, private communication, September 2009.

[37] B. Leimkuhler and S. Reich, "Simulating Hamiltonian Dynamics", Cambridge University Press, 2005.

[38] R.D. Ruth, "A Canonical Integration Technique", IEEE Trans. on Nuclear Science, Vol. NS-30, No. 4, p. 2669-2671, August 1983.

[39] E. Forest and R.D. Ruth, "Fourth-Order Symplectic Integration", Physica D 43, p. 105-117, 1990.

[40] H. Goldstein, "Classical Mechanics", Addison-Wesley, 1973.

[41] J.E. Rowe, "Nonlinear Electron-Wave Interaction Phenomena", New York Academic Press, 1965.

[42] M. de Magistris, V.G. Vaccaro and L. Verolino, "Bunched Beam in Axisymmetric Systems", Il Nuovo Cimento, Vol. 109 A, No. 11, November 1996.

[43] C.J. Bouwkamp and N.G. de Bruijm, "The Electrostatic Field of a Point Charge Inside a Cylinder, in Connection with Wave Guide Theory", Journal of Applied Physics, Vol. 18, p. 562-577, (1947).

[44] L. Palumbo and M. Migliorati, "Lezioni del Corso di Fisica Moderna, I Modulo", Università di Roma La Sapienza, A.A. 2008-2009.

[45] R.P. Feynman, "The Feynman Lectures on Physics: The Definitive and Extended Edition", vol. 1, Addison Wesley, 2005.

[46] J.W. Gewartowski, H. A. Watson, "Principles of Electron Tubes", D. Van Nostrand Company, Inc., 1965.

[47] B. Spataro, private communication, 2008.

[48] T.P. Wangler, "Principles of RF Linear Accelerators", J. Wiley and sons, Inc., Canada, 1998.

[49] P.B. Wilson, "High-Energy Electron Linacs: applications to storage ring RF Systems and Linear Collider", SLAC PUB-2884, 1982.

[50] J.C. Slater, "Microwave Electronics", Van Nostrand, Princeton, NJ, 1950.

[51] S. Ramo, "The Electronic-Wave Theory of Velocity-Modulation Tubes", Proceedings of the I.R.E., Pg. 757-763, December 1939.

[52] R. Warnecke and P. Guenard, "Les Tubes Electroniques à Commande par Modulation de Vitesse", Paris: Gauthier-Villars, 1951.

[53] M. Chodorow, C. Susskind, "Fundamentals of Microwave Electronics", McGraw-Hill Book Company, New York, 1964.